Screening of heavy quarks and hadrons at finite temperature and density

Dissertation

zur Erlangung des Doktorgrades
der Fakultät für Physik
der Universität Bielefeld

vorgelegt von
Matthias Döring

22. September 2006

Contents

Chapter 1

Introduction

1.1 Hot and dense strongly interacting matter

The exploration and prediction of the behavior of nuclear matter under extreme conditions is presumably one of the most challenging problems in particle physics today.
At moderate temperatures the strong interaction confines the quarks and gluons to form hadrons. However, at temperatures of the order of $10^{12}K$ hadronic matter dissolves into a quark-gluon plasma (QGP), in which quarks and gluons do no longer exist as colorless bound states only. At asymptotically large temperatures they can be considered as a weakly interacting gas.
On the experimental side the formation of a QGP can be accomplished in the collision of heavy nuclei. It is expected that a thermally equilibrated plasma is formed after the collision, before hadronization sets in. Basing on the AGS and SPS experiments heavy ion collisions are currently under investigation with the relativistic heavy ion collider (RHIC) at BNL and will in future be studied with the large hadron collider (LHC) at CERN [1, 2, 3]. Furthermore a QGP existed in the early universe, a few microseconds after the big bang and it may also exist at lower temperatures but higher quark densities in the interior of compact stars.
In an experimental scenario like heavy ion collisions there is not only a finite temperature T, but there is also a finite baryon chemical potential μ_b (or quark chemical potential $\mu = \mu_b/3$) which is provoked through the presence of the heavy nuclei. For example in an $Au - Au$ collision at RHIC with an CMS-energy of $\sqrt{s} = 130\,GeV$ the hadronic freeze-out occurs at a baryon chemical potential of $\mu_b \approx 45MeV$ [4]. This is much smaller than the corresponding freeze-out temperature of $T_{freeze} \approx 170MeV$ [5, 6] and hence $\mu/T << 1$.
With increasing beam energy the transition temperature as well as the freeze out temperature increases and the corresponding baryon chemical potential decreases. Fig. 1.1 shows a qualitative sketch of the corresponding QCD

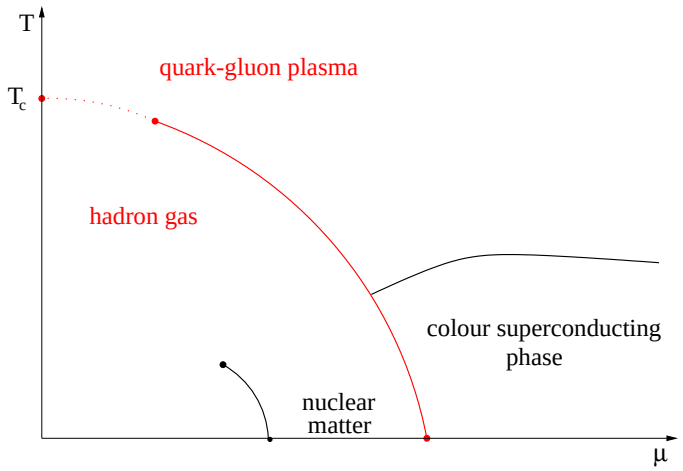

Figure 1.1: Qualitative picture of the phase diagram of QCD.

phase diagram. The 1st order phase transition line (red) ends in a 2nd order phase transition point at a positive value of μ_b. For smaller or vanishing baryon chemical potentials the transition between hadron gas and QGP is only a crossover (dashed red line). At $\mu_b = 0$ the transition temperature of 2-flavor continuum QCD in the chiral limit can be calculated to be $T_c \approx 170 - 190\, MeV$ [7, 8, 9], where typical errors are of the order of 10% of the value.
The other phases of QCD like ordinary nuclear matter or color superconducting phases will not be discussed in this work.

1.2 Thermodynamics and screening

In this work we examine some of the fundamental properties of strongly interacting matter at finite temperature and small baryon chemical potentials, i.e. we will consider the properties of matter like those generated by RHIC in heavy ion collisions.
The emphasis will lie on the change of bulk thermodynamical quantities which is caused through the switch-on of a baryon or quark chemical potential μ. The quantities of interest are related to the screening properties of heavy quarks and hadrons inside the quark gluonic medium.
We will study QCD as a quantum field theory with gluons and $N_f = 2$ flavors of dynamical quarks. All our calculations are done in thermal and baryon chemical equilibrium. Our approach to study the μ-dependence is based on a Taylor expansion method in μ/T.
The temperatures T under investigation range from $0.76T_c$ to $4T_c$. The

range of quark chemical potentials μ is not known exactly since there are no serious estimates of the radius of convergence ρ of the Taylor expansion in μ/T. Rough estimates from the equation of state suggest that $\rho \sim \mathcal{O}(1)$ [10].
In chapter 2 I give a brief summary of the theoretical fundamentals of QCD at finite temperature and density and describe the framework used for the numerical evaluation. Especially I will give a description of the Taylor expansion method. This method is used up to the 6th order in μ in the subsequent chapters.
In chapter 3 we discuss the equation of state of the pure quantum fields at finite temperature and baryon density which is the most simple quantity to be handled with the Taylor expansion method. Because most of the work for this project was accomplished by my colleagues, we will concentrate on the main results only. These form the basis for the other chapters. In chapter 4 we change the scenario. Namely we introduce a number of heavy test quarks and/or anti-quarks separated by a fixed distance r into the medium. We study the thermodynamics of this system by calculating the free energy with respect to the vacuum case.
The free energy contains the whole thermodynamical information about the heavy quarks/anti-quarks. We will concentrate on the screening properties of the intermediate quantum fields. In particular we will calculate the screening masses $m(T, \mu)$.
In chapter 5 we then discuss the screening of hadrons instead of heavy quarks.
Finally a summary with conclusions and an outlook is given in chapter 6.
Some of the technical details about the Taylor expansion method are presented in the appendix.

Chapter 2

Quantum chromodynamics on the lattice

2.1 QCD at finite temperature and finite baryon chemical potential

Quantum chromodynamics is formulated as a non-Abelian $SU(3)$ gauge theory containing a set of N_f quark fermion fields $\Psi_1, \cdots, \Psi_{N_f}$ with masses $m_1, \cdots, m_{N_f}$. The interaction with the gluonic gauge fields $A^a_\nu, a = 1, \cdots, 8$ as well as self interactions of the gluons are governed by an overall gauge coupling g. In the continuum the action is written as

$$S_E^{(cont.)} = \int d^4x \, \mathcal{L}_E, \tag{2.1}$$

where in the Euclidean formulation the Lagrangian density adopts the form

$$\mathcal{L}_E = \frac{1}{4} F^a_{\mu\nu} F^a_{\mu\nu} + \sum_{j=1}^{N_f} \bar{\Psi}_j \left(\not{D} + m_j \right) \Psi_j. \tag{2.2}$$

$F^a_{\mu\nu} = \partial_\mu A^a_\nu - \partial_\nu A^a_\mu + g f^{abc} A^b_\mu A^c_\nu$ is the field strength tensor of the gluon fields and $\not{D} = \gamma_\mu D_\mu$ is the covariant derivative

$$D_\mu = \partial_\mu + ig\mathcal{A}_\mu, \tag{2.3}$$

where $\mathcal{A}_\mu = A^a_\mu \lambda^a / 2$. Here γ_μ are the Euclidean Dirac matrices and λ^a the Gell-Mann matrices which are the generators of the gauge group.
We now consider the system of quantum fields to be in thermal and baryon-chemical equilibrium. A finite temperature $T = 1/\beta$ and chemical potentials $\boldsymbol{\mu} = (\mu_1, \cdots, \mu_{N_f})$ are introduced by considering the grand canonical partition function

$$Z(T, \boldsymbol{\mu}) = \mathrm{Tr} \left[e^{-\beta \left(H - \sum_{j=1}^{N_f} \mu_j N_{q,j} \right)} \right], \tag{2.4}$$

where the Hamiltonian $H = \int d^3x\ \mathcal{H}$ is related to the Minkowskian QCD Lagrangian $L_M = \int d^3x\ \mathcal{L}_M$ via Legendre transformation. The $N_{q,j}$ are conserved charges which in our case are the quark numbers of the corresponding flavor

$$N_{q,j} = \int d^3x\ J_0^{(j)}(x) = \int d^3x\ \bar{\Psi}_j \gamma_0 \Psi_j. \tag{2.5}$$

The trace in (2.4) is performed over all possible quantum states of the fields. The partition function (2.4) is then translated into the path integral expression

$$Z(T, \boldsymbol{\mu}) = \int \mathcal{D}A\mathcal{D}\bar{\Psi}\mathcal{D}\Psi\ e^{-S_E}, \tag{2.6}$$

where the action S_E has got the same structure as in the Euclidean continuum case apart from the fact that the temporal integral is shrinked to the finite interval $[0, \beta]$, namely

$$S_E = \int_0^\beta d\tau \int_V d^3x \left(\mathcal{L}_E - \sum_{j=1}^{N_f} \mu_i \bar{\Psi}_j \gamma_0 \Psi_j \right). \tag{2.7}$$

The (anti-) commutation relations for the bosonic and fermionic fields imply that all field configurations covered by the path integral in (2.6) have to fulfil periodic boundary conditions for the gluons and anti-periodic boundary conditions for the fermions in the temporal direction. In order to keep numerical expressions finite we also consider the case of a finite spatial volume V instead of integrating over infinite intervals. There are no restrictions on the boundary conditions in the spatial directions. We always choose them to be periodic.
Inserting (2.2) into (2.7) we see that we can also write

$$S_E = \int_0^\beta d\tau \int_V d^3x\ \mathcal{L}_E(\boldsymbol{\mu})\ , \tag{2.8}$$

where $\mathcal{L}_E(\boldsymbol{\mu})$ has the same functional form as $\mathcal{L}_E$ but we have to make the replacement

$$igA_0 \to igA_0 - \mu_j, \tag{2.9}$$

in the flavor j. Bulk thermodynamical quantities $O(V, T, \boldsymbol{\mu})$ can now be calculated as ensemble averages

$$O(V, T, \boldsymbol{\mu}) = \langle \mathcal{O} \rangle_{V,T,\boldsymbol{\mu}} = \frac{1}{Z} \int \mathcal{D}A\mathcal{D}\bar{\Psi}\mathcal{D}\Psi\ \mathcal{O}(A, \bar{\psi}, \psi, V, T, \boldsymbol{\mu}) e^{-S_E}\ . \tag{2.10}$$

Because we are not studying any volume dependence in this work we will occasionally suppress the dependence on V. In addition in most cases there is no explicit dependence of the quantity $\mathcal{O}$ on the macroscopic parameters V, T and $\boldsymbol{\mu}$. Quantities like the energy density ϵ, the pressure p or particle number densities n_i are related to derivatives of the grand canonical potential

$$\Omega = -T \ln Z \,, \tag{2.11}$$

with respect to the macroscopic parameters, i.e. we have for the pressure p and particle numbers n_i

$$\frac{p}{T^4} = -\frac{1}{T^4}\frac{\partial \Omega}{\partial V} = -\frac{1}{VT^4}\Omega(T, \boldsymbol{\mu}) \,, \tag{2.12a}$$

$$\frac{n_i}{T^3} = -\frac{1}{VT^3}\frac{\partial \Omega}{\partial \mu_i} \,. \tag{2.12b}$$

We will also refer to the grand canonical potential as the free energy F of the system.
For a more detailed discussion about the fundamentals of QCD and field theory at finite temperature and density we refer to standard textbooks such as [11, 12, 13].

2.2 The lattice regularization

In QCD, path integral expressions like (2.6) or (2.10) are suffering from ultraviolet divergencies which have to be properly regularized and renormalized. One way to do this is to discretize space-time by using a finite four dimensional hypercubic lattice with lattice spacing a. Each lattice point x is labeled by an integer array $n = (n_1, n_2, n_3, n_4)$ such that $x = n \cdot a$. Thereby all momenta are cut off because they can be chosen from the 1st Brillouin zone $[-\pi/a, \pi/a]$ and the ultraviolet divergencies do not appear anymore. We choose to take the same number N_σ of lattice points in every spatial direction. In the timelike direction a smaller number N_τ is chosen in order to accommodate the finite temperatures. For $N_\sigma/N_\tau \gtrsim 4$ corrections to the infinite volume limit get small. Therefore we take $N_\sigma/N_\tau = TV^{1/3} = 4$ here. The absolute sizes of N_σ and N_τ are chosen as large as allowed by the available computational power. Temperature and volume can then be obtained from N_σ and N_τ

$$T = \frac{1}{\beta} = \frac{1}{N_\tau a} \,, \tag{2.13a}$$

$$V = (N_\sigma a)^3 \,. \tag{2.13b}$$

The continuum expressions of the preceding section are translated into the lattice regularized formulation by replacing space-time integrals and derivatives by discrete sums and differential quotients such that in the limit $a \to 0$

the continuum physics is obtained. Dimensionless fields are introduced by multiplying the fields with appropriate powers of a. The gauge fields are represented by the link variables

$$U_\mu(n) = \exp\left[iga\mathcal{A}_\mu(x)\right]. \tag{2.14}$$

$U_\mu(n)$ connects the site n to the nearest neighbor $n+\hat{\mu}$ in the μ-direction. The QCD lattice action can then be written as

$$S_E = S_G + S_F\ , \tag{2.15}$$

where the Wilson gauge action S_G is the discretized gluonic action

$$S_G = \beta \sum_{n,\mu<\nu} \left(1 - \frac{1}{N_c}\mathrm{Re\ Tr}\ \right) \ , \tag{2.16}$$

with $\beta = 2N_c/g^2$ and the number of colors is $N_c = 3$ here. The sum extends over all elementary plaquettes of the lattice and the symbol

$$= U_\mu(n)U_\nu(n+\mu)U_\mu^\dagger(n+\nu)U_\nu^\dagger(n) \tag{2.17}$$

represents the product of the four consecutive links of the plaquette, starting at the lattice point n. In the following we denote products of consecutive links as diagrams where the order of the factors is indicated by the direction of the links.
The fermionic part of the action is written as

$$S_F = \sum_{n,m} \bar{\Psi}_n K_{n,m} \Psi_m\ , \tag{2.18}$$

where the sum extends over all lattice sites n and m. The choice of the lattice action is not unique, i.e. we are allowed to add arbitrary terms, which are vanishing in the continuum limit. For vanishing chemical potentials the most naive way of discretization leads to

$$K_{n,m} = \frac{1}{2}\sum_\mu \gamma_\mu \left(\delta_{n+\hat{\mu},m}U_\mu(n) - \delta_{n-\hat{\mu},m}U_\mu^\dagger(n-\hat{\mu})\right) + M\delta_{n,m}\ , \tag{2.19}$$

where $M = a \cdot m$ is the dimensionless bare mass parameter. In the free case ($g = 0$) the fermion propagator calculated from this action is

$$\left\langle \Psi_n \otimes \bar{\Psi}_m \right\rangle = K^{-1}_{n,m} = \int_{-\pi}^{\pi} \frac{d^4p}{(2\pi)^4} \frac{-i\sum_\mu \gamma_\mu \tilde{p}_\mu + M}{\sum_\mu \tilde{p}_\mu^2 + M^2} e^{ip(n-m)}\ , \tag{2.20}$$

where $\tilde{p}_\mu = \sin(p_\mu)$ and '$\otimes$' denotes the tensor product in Dirac space. While in the continuum this propagator has got poles at $p_\mu \sim \pm im$ only

there are now two poles in every direction μ at the corners of the Brillouin zone. Therefore in the continuum limit this action describes $2^{\dim} = 2^4 = 16$ independent quarks instead of only one. There are several ways to deal with this doubling problem one of which is introduced in the next section.
Finally we note that the replacement rule (2.9) for the introduction of a quark chemical potential μ can be transfered to the lattice gauge links [14]. In the action the gauge links in the temporal direction have to be replaced by

$$U_4(n) = e^{+igA_4(x)} \quad \rightarrow \quad e^{+igaA_4(x)-a\mu} = e^{-a\mu}\, U_4(n), \tag{2.21a}$$
$$U_4^\dagger(n) = e^{-igA_4(x)} \quad \rightarrow \quad e^{-igaA_4(x)+a\mu} = e^{+a\mu}\, U_4^\dagger(n). \tag{2.21b}$$

2.3 Staggered fermions

The starting point of the staggered fermion formulation [15] is to apply a unitary transformation in spinor space $\Gamma(n)$ to the fermion fields at every lattice point n

$$\begin{aligned} \Psi_n &= \Gamma(n)\chi_n \,, \\ \bar{\Psi}_n &= \bar{\chi}_n\Gamma^\dagger(n) \,, \end{aligned} \tag{2.22}$$

such that the Dirac matrices γ_μ become diagonal

$$\Gamma^\dagger(n)\gamma_\mu\Gamma(n+\mu) = \eta_\mu(n)\cdot\mathbf{1} \,, \tag{2.23}$$

where the $\eta_\mu(n)$ are numbers. One possible solution of this task is

$$\Gamma(n) = \gamma_1^{n_1}\gamma_2^{n_2}\gamma_3^{n_3}\gamma_4^{n_4}, \tag{2.24}$$
$$\eta_\mu(n) = (-1)^{n_1+\cdots+n_{\mu-1}}, \tag{2.25}$$

where $\eta_\mu(n)$ are called the staggered phases. The fermion action now consists of four equivalent terms. Leaving away three of them and keeping only one we can reduce the number of fermion doublers by a factor of 4. The staggered action can then be written as

$$S_F = \sum_{n,m} \bar{\chi}_n K_{n,m}\chi_m \,, \tag{2.26}$$

where the fermion matrix (for quark chemical potential $\mu = 0$) now has got the form

$$K_{n,m} = \frac{1}{2}\left[\sum_\mu \eta_\mu(n)\left(\delta_{n+\hat{\mu},m}U_\mu(n) - \delta_{n-\hat{\mu},m}U_\mu^\dagger(n-\hat{\mu})\right)\right] + M\delta_{n,m}. \tag{2.27}$$

Insight in the continuum limit is gained by defining the fermion fields on the corners of a hypercubic lattice with lattice spacing $2a$ and lattice points at $N_\mu = 2n_\mu + \rho_\mu$ where ρ_μ is either 0 or 1.

$$\Psi^f_\alpha(n) = \frac{1}{2\sqrt{2}} \sum_\rho \Gamma(2n+\rho)_{\alpha f} \bar{U}_\rho(n) \chi(2n+\rho) \,, \tag{2.28a}$$

$$\bar{\Psi}^f_\alpha(n) = \frac{1}{2\sqrt{2}} \sum_\rho \bar{\chi}(2n+\rho) \bar{U}^\dagger_\rho(n) \Gamma^\dagger(2n+\rho)_{f\alpha} \,. \tag{2.28b}$$

In the limit $m \to 0$ there remains a $U(1) \otimes U(1)$ chiral symmetry in the staggered action which is a remnant of the original $SU(4) \otimes SU(4)$ symmetry in the continuum. Due to the Nielsen-Ninomiya no-go theorem there does not exist a local lattice action in four space-time dimensions having the full chiral symmetry without including any doublers. The staggered formulation is a compromise in this respect. While keeping 3 doublers we have got a remnant chiral symmetry.
Carrying out the integration over the Grassmann valued fields Ψ_n and $\bar{\Psi}_n$ in (2.6) or (2.10) one is left with the determinant of the fermion matrix and the integration measure is proportional to

$$\mathcal{D}U \; P(U) \sim \mathcal{D}U \; \det(K) \; e^{-S_E}. \tag{2.29}$$

For N_f degenerated fermion flavors $\det(K)$ is the N_f-th power of the fermion determinant for one single flavor. Therefore in order to compensate for the fourfold staggered fermion degeneracy we take the fourth root of $\det(K)$.

$$\mathcal{D}U \; P(U) \sim \mathcal{D}U \; \left(\det(K)\right)^{N_f/4} \; e^{-S_E}. \tag{2.30}$$

We admit that this "fourth root trick" is still a matter of discussion and that there is no rigorous proof for the correctness of this procedure so far.
Due to the γ_5-hermiticity at $\mu = 0$

$$\gamma_5 K \gamma_5 = K^\dagger \tag{2.31}$$

the fermion determinant is real. Furthermore it can be shown that the eigenvalues of K are pairwise complex conjugated and therefore $\det(K)$ is even positive.
Because in our numerical simulations we will have to compute the inverse of the fermion matrix it is furthermore useful to rewrite $\det(K)$ as the determinant of a symmetric matrix which can be inverted by conjugate gradient methods. Dividing the lattice into even and odd sites[1] and writing the fermion fields in the corresponding representation

$$\boldsymbol{\chi} = \begin{pmatrix} \boldsymbol{\chi}_e \\ \boldsymbol{\chi}_o \end{pmatrix}, \quad \bar{\boldsymbol{\chi}} = (\bar{\boldsymbol{\chi}}_e, \bar{\boldsymbol{\chi}}_o) \,, \tag{2.32}$$

[1] A site n is called even if $n_1 + n_2 + n_3 + n_4$ is even and it is called odd otherwise.

we see that the fermion matrix has got the form

$$K = \begin{pmatrix} M & D_{eo} \\ D_{oe} & M \end{pmatrix}, \tag{2.33}$$

where for $\mu = 0$ we have $D_{eo}^{\dagger} = -D_{oe}$ and therefore

$$K^{\dagger}K = \begin{pmatrix} M^2 - D_{eo}D_{oe} & 0 \\ 0 & M^2 - D_{oe}D_{eo} \end{pmatrix} \equiv \begin{pmatrix} (K^{\dagger}K)_{ee} & 0 \\ 0 & (K^{\dagger}K)_{oo} \end{pmatrix} \tag{2.34}$$

Because the determinants of $(K^{\dagger}K)_{ee}$ and $(K^{\dagger}K)_{oo}$ are equal we have

$$\det(K) = \det(K^{\dagger}K)^{1/2} = \det((K^{\dagger}K)_{ee}) \; . \tag{2.35}$$

We see that if we make the replacement

$$\det(K) \rightarrow \det((K^{\dagger}K)_{ee}) \; , \tag{2.36}$$

in (2.30) we still describe a system with N_f fermion flavors but the fermion matrix is symmetric.
The lattice regularization method and a detailed description of the staggered fermion formulation can be found in textbooks like [16, 17].

2.4 Improved actions

The lattice actions (2.16) and (2.18) are not unique. I.e. we are allowed to add arbitrary terms to the actions as long as the continuum limit is not changed. This can be used to construct improved actions that show reduced cut-off dependencies. On the other hand including additional terms increases the computational effort. Therefore improving the action is always a compromise between numerical accuracy and computing power.
The original Wilson action (2.16) represents the continuum action up to $\mathcal{O}(a^2)$. In the Symanzik improvement program [18, 19] we make an ansatz for the action including not only 1×1-plaquettes but also higher loops of gauge links. In this work we use the following Symanzik improved action containing planar 1×2- and 2×1-loops which represent the continuum limit up to $\mathcal{O}(a^4)$,

$$\begin{aligned} S_G^{(1,2)} &= \beta \sum_{n,\mu<\nu} \frac{5}{3} \left(1 - \frac{1}{N_c} \mathrm{Re\ Tr} \right. \\ &- \frac{1}{6} \left(1 - \frac{1}{2N_c} \mathrm{Re\ Tr} \right. \end{aligned} \tag{2.37}$$

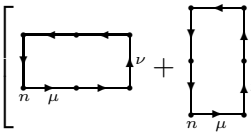

In the fermionic sector we use the following way of improvement. First we replace the gauge links $U_\mu(n)$ in the fermion matrix by so-called fat links [20]

$$U_\mu^{fat}(n) = \frac{1}{1+6\omega}\left(\; + \omega \sum_{\nu\neq\mu} \; \right) . \qquad (2.38)$$

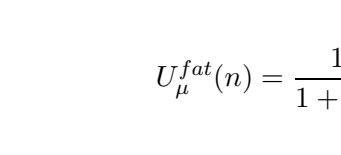

This is a weighted sum of the ordinary gauge link and all three link paths connecting the same nearest neighbor sites. These paths are called "staples". The fat links improve the flavor symmetry that is reduced to a $U(1)\otimes U(1)$ symmetry in the staggered formulation. I.e. a reduced pion mass splitting is observed for non-zero values of ω. In our simulations we use $\omega = 0.2$.
In a second step we improve the rotational symmetry of the free fermion propagator in momentum space, which is a function of p^2 in the continuum. This is accomplished by including not only paths which connect nearest neighbor sites but also paths connecting sites which are separated by three links [21]. The following general ansatz is appropriate for the staggered fermion matrix

$$K_{n,m} = \sum_\mu \eta_\mu(n)\left(c_{10}A_{nm} + c_{30}B_{1,nm} + c_{12}B_{2,nm}\right) + M\delta_{n,m} \; , \qquad (2.39)$$

where A is the fat link part connecting nearest neighbor sites.

$$A_{nm} = \left(\delta_{n+\hat{\mu},m}U_\mu^{fat}(n) - \delta_{n-\hat{\mu},m}U_\mu^{fat\,\dagger}(n-\hat{\mu})\right) . \qquad (2.40)$$

B_1 consists of three successive links in the μ-direction

$$B_{1,nm} = \delta_{n+3\hat{\mu},m} \; - \delta_{n-3\hat{\mu},m} \left(\; \right)^\dagger , \qquad (2.41)$$

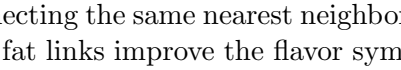

and B_2 connects sites along L-shaped paths.

$$B_{2,nm} = \tfrac{1}{2}\sum_{\nu\neq\mu}$$

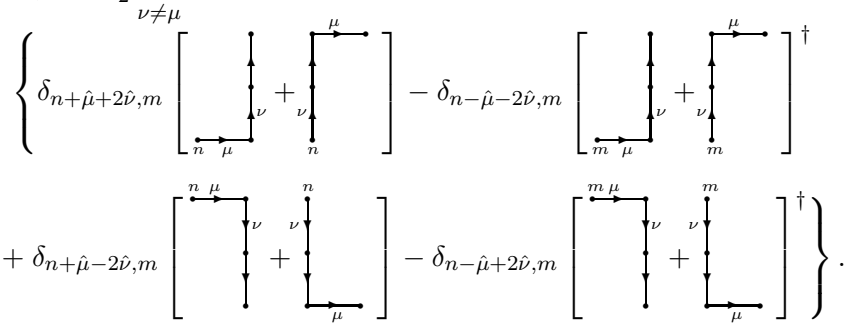

$$\left\{ \delta_{n+\hat{\mu}+2\hat{\nu},m} \left[\; + \; \right] - \delta_{n-\hat{\mu}-2\hat{\nu},m} \left[\; + \; \right]^\dagger \right.$$

$$\left. + \, \delta_{n+\hat{\mu}-2\hat{\nu},m} \left[\; + \; \right] - \delta_{n-\hat{\mu}+2\hat{\nu},m} \left[\; + \; \right]^\dagger \right\} .$$

If we neglect $\mathcal{O}(g^2)$ contributions to the coefficients the relation

$$c_{10} + 3c_{30} + 6c_{12} = \frac{1}{2} \qquad (2.42)$$

guarantees the correct continuum limit. If we furthermore demand that

$$c_{10} + 24c_{30} + 6c_{12} = 24c_{12} \ , \tag{2.43}$$

then the free lattice fermion propagator is rotationally invariant up to order p^4. In order to reduce the computational effort there are basically two competing possibilities to solve these two equations. Namely we either demand c_{30} or c_{12} to vanish. The advantage is that we do not have to calculate B_1 or B_2 respectively. The choice $c_{12} = 0$ leads to the Naik action [22]. Because of a better high temperature behavior of the pressure (see [23]) we choose $c_{30} = 0$ which leads to the p4-action [21]. Then the remainder of the coefficients are

$$c_{10} = 3/8 \tag{2.44a}$$
$$c_{12} = 1/48 \tag{2.44b}$$

2.5 Simulation of dynamical staggered fermions

The main task of lattice QCD is the numerical computation of the expectation value of an observable $\mathcal{O}[A, \bar{\psi}, \psi]$. Assuming that the dependence on the fermion fields is such that the fermionic path integral can be performed we have

$$O(T, V, \mu) = \langle \mathcal{O} \rangle = \frac{1}{Z} \int \mathcal{D}U \ \mathcal{O}[U] \det\left(K[U]\right)^{N_f/4} e^{-S_G[U]}, \tag{2.45}$$

where the integral is to be done over the set of all $SU(3)$ matrix configurations on the lattice. Because this range is very high dimensional simple numerical integration techniques are not applicable. Fortunately the weight factor

$$P[U] = \frac{1}{Z} \det\left(K[U]\right)^{N_f/4} e^{-S_G} \tag{2.46}$$

possesses only one large peak at U_{cl}, the solution of the classical equation of motion. Therefore a configuration U contributes the more to the integral the closer it is to U_{cl}. In a numerical simulation we generate a Markov chain of configurations such that the obtained ensemble $\{U_i\}_{i=1,\cdots,n}$ is distributed according to the probability measure $\mathcal{D}U \, P[U]$ around the peak. The mean value (2.45) can then be estimated by the sample average of the corresponding observable values $\{O_i\}_{i=1,\cdots,n}$.
In order to take $\mathcal{D}U \, P[U]$ as a probability measure $P[U]$ has to be real and positive. In fact this is only true for vanishing or imaginary quark chemical potentials. Therefore we will restrict the discussion to the case $\mu = 0$ here and comment on the treatment of $\mu \neq 0$ in section 2.7.
In order to sample the configuration according to the probability distribution (2.46) the following procedure is adequate. Starting from an arbitrary

configuration, we generate a configuration U_{i+1} from U_i such that the transition probability $P(U_i \to U_{i+1})$ fulfills the detailed balance condition

$$P(U_i)P(U_i \to U_{i+1}) = P(U_{i+1})P(U_{i+1} \to U_i), \tag{2.47}$$

and such that the Markov chain is ergodic. Then the averages in Markov time are equal to the corresponding ensemble averages. If N_f is a multiple of 4 we can make use of (2.36) and rewrite the fermion determinant in (2.46) as a Gaussian path integral over so-called pseudo-fermionic bosonic fields ϕ_e, ϕ_e^* on the even lattice sites. In addition we need momenta $H_\mu(n) \in SU(3)$ conjugated to the gauge links $U_\mu(n)$ for the updating procedure. We then consider the probability density

$$P_\Phi[H, U, \phi_e^*, \phi_e] = \frac{1}{Z_\phi} e^{-\frac{1}{2}\mathrm{tr}H^2 - \phi_e^*(K^\dagger K)^{-1}_{ee}\phi_e - S_G} \tag{2.48}$$

where

$$Z_\phi = \int \mathcal{D}H\mathcal{D}U\mathcal{D}\phi_e^*\mathcal{D}\phi_e \; e^{-\frac{1}{2}\mathrm{tr}H^2 - \phi_e^*(K^\dagger K)^{-1}_{ee}\phi_e - S_G} \tag{2.49}$$

and the trace is done over space-time and color indices. We consider the substitution

$$\phi = \begin{pmatrix} \phi_e \\ 0 \end{pmatrix} = K^\dagger \eta\,, \quad \phi^\dagger = (\phi_e^*, 0) = \eta^\dagger K. \tag{2.50}$$

Then η is Gaussian distributed. In order to generate a new configuration U_{i+1} from U_i we take the exponent in (2.48) as the Hamiltonian of a classical system in four spatial dimensions

$$\mathcal{H} = \frac{1}{2}\mathrm{tr}H^2 + \phi_e^*(K^\dagger K)^{-1}_{ee}\phi_e + S_G. \tag{2.51}$$

We introduce an artifical time τ and evolve U and a H according to the classical equations of motion

$$\frac{\partial U}{\partial \tau} = iHU, \quad \frac{\partial H}{\partial \tau} = -\frac{\partial H}{\partial U}, \tag{2.52}$$

where H and η are taken from a Gaussian heatbath at the beginning of each trajectory. ϕ_e is calculated from (2.50). Basically the discretized versions of (2.52) are then solved numerically using the leapfrog algorithm with a finite time step size $\delta\tau$ and a total trajectory length $\Delta\tau = N_l\delta\tau$. In the limit $\delta\tau \to 0$ the leapfrog algorithm is energy conserving and the detailed balance condition is fulfilled. For $\delta\tau \neq 0$ there is a systematic error of order $\delta\tau^2$. This error can be corrected using an additional Metropolis step at the end of each trajectory, namely the final configuration is only accepted as a new configuration with a probability

$$p = \min\left(1, e^{-H(\tau+\Delta\tau)+H(\tau)}\right). \tag{2.53}$$

We keep the old configuration if the acceptance test fails.
Unfortunately this so-called ϕ-algorithm [24] only works if N_f is a multiple of 4. For other values of N_f the standard way of updating is the R algorithm [24]. Instead of introducing pseudo-fermionic fields ϕ we write

$$\det\left[\left(K^\dagger K\right)_{ee}\right]^{\frac{N_f}{4}} = \exp\left[\frac{N_f}{4}\mathrm{tr}\left(\ln(K^\dagger K)_{ee}\right)\right], \tag{2.54}$$

and we have a Hamiltonian

$$\mathcal{H} = \frac{1}{2}\mathrm{tr}P^2 + \frac{N_f}{4}\mathrm{tr}\left(\ln(K^\dagger K)_{ee} + S_G\right). \tag{2.55}$$

The equation of motion for the momentum then has got the form

$$\frac{\partial H}{\partial \tau} = -\frac{\partial S_G}{\partial U} + \frac{N_f}{4}\,\mathrm{tr}\left[\frac{1}{(K^\dagger K)_{ee}}\frac{\partial (K^\dagger K)_{ee}}{\partial U}\right]. \tag{2.56}$$

During the update procedure the trace is now approximated using a noisy estimator

$$\mathrm{tr}\left[\frac{1}{(K^\dagger K)_{ee}}\frac{\partial (K^\dagger K)_{ee}}{\partial U}\right] \approx X_e^\dagger \frac{\partial (K^\dagger K)_{ee}}{\partial U} X_e. \tag{2.57}$$

where

$$X_e = \frac{1}{(K^\dagger K)_{ee}}\left(K^\dagger R\right)_e, \tag{2.58}$$

and R is a Gaussian random noise vector, which is held fixed during the leapfrog steps. The inversions of the fermion matrix are done using conjugate gradient algorithms. Due to the introduction of a stochastic term in the equations of motion the R algorithm is not time reversible and cannot be made exact using a Metropolis step.
Recently there have been some ideas [25, 26] for exact algorithms which base on approximating the function $x^{-N_f/4}$ by rational or polynomial functions.

$$x^{-N_f/4} \approx r(x)^2. \tag{2.59}$$

Introducing pseudo-fermionic fields the Hamiltonian can then be written as

$$\mathcal{H} = \frac{1}{2}\mathrm{tr}H^2 + \phi_e^*\, r((K^\dagger K)_{ee})\, \phi_e + S_G\,. \tag{2.60}$$

While these ideas will most likely be relevant for future simulations of staggered fermions, all the simulations for this work were still done using the R-algorithm. The simulation parameters are shown in table 2.1. The pseudo-critical coupling on a 16×4 lattice was determined in [27] from the peak position of the chiral susceptibility. We take

$$\beta_c = 3.649 \tag{2.61}$$

as the numerical value here. Several thousands of configurations were produced for 18 different values of the coupling β listed in table 2.2.

N_f	2
ma	0.1
$\delta\tau$	0.025
N_l	20
$\Delta\tau$	0.5

Table 2.1: *Simulation parameters.*

β	3.52	3.55	3.58	3.60	3.63	3.65	3.66	3.68	3.70
T/T_c	0.81	0.87	0.90	0.96	1.00	1.02	1.06	1.11	1.16
$N_{conf.}$	3000	3000	3500	3800	3000	4000	4000	3600	2000
β	3.72	3.75	3.80	3.85	3.90	3.95	4.00	4.245	4.43
T/T_c	1.23	1.36	1.36	1.50	1.65	1.81	1.98	3.00	4.01
$N_{conf.}$	2000	1000	1000	1000	1000	1000	1000	1000	1600

Table 2.2: Number of configurations per β-value/temperature.

2.6 Setting the scale

Because in a lattice simulation all parameters and fields in the action are replaced by dimensionless quantities, all computed quantities are dimensionless, too. Observables carrying dimension can only be obtained as dimensionless ratios including an appropriate power of the lattice spacing a. A physical scale can then be introduced by fixing the value of some quantity to its physical value. Best suited for this purpose is the string tension σ at zero temperature, because it can easily and accurately be calculated on the lattice and it is indirectly accessible in experiment through the study of heavy quark spectra. At zero temperature the physical value of the string tension is $\sqrt{\sigma} \approx 460\, MeV$ [28, 29, 30].
The string tension is the proportionality constant describing the linear rise of the potential between a heavy quark Q and a heavy anti-quark $\bar{Q}$ in a range of large distances r

$$V_{Q\bar{Q}}(r) = -\frac{4}{3}\frac{\alpha_s}{r} + \sigma r \ . \tag{2.62}$$

In full QCD a heavy quark-anti-quark pair splits into two mesons if the distance r becomes very large. This string breaking results in a finite value of $V_{Q\bar{Q}}(r)$ for $r \to \infty$ and (2.62) no longer holds. Fortunately at $T = 0$ and $\mu = 0$ this string breaking does not occur within the accessible ranges under consideration due to the use of smeared Wilson loop operators. Therefore there are no restrictions to fit $V_{Q\bar{Q}}(r)$ to the form (2.62) using the strong coupling α_s and the string tension σ as fit parameters. For 2-flavor QCD and a relatively large quark mass of $M = 0.1$ this has been done in [31],

leading to

$$\alpha_s = 0.212(3) \ . \tag{2.63}$$

The string tension $\sigma(\beta)$ at $T = 0$ as a function of the coupling β can be fitted to the form [32]

$$a\sqrt{\sigma} = \bar{a}\frac{1 + \bar{c}_2\bar{a}^2 + \bar{c}_4\bar{a}^4}{\bar{c}_0} \ , \tag{2.64}$$

where

$$\bar{a} = a\Lambda_L = \left(\frac{6\beta_0}{\beta}\right)^{-\frac{\beta_1}{2\beta_0}} e^{-\frac{\beta}{12\beta_0}} \tag{2.65}$$

is the solution of the two loop renormalization group equation

$$a\frac{dg}{da} = \beta_0 g^3 + \beta_1 g^5 + \mathcal{O}(g^7) \ , \tag{2.66}$$

with

$$\beta_0 = \frac{1}{16\pi^2}\left(11 - \frac{2N_f}{3}\right) \ , \tag{2.67a}$$

$$\beta_1 = \frac{1}{(16\pi^2)^2}\left(102 - \frac{38N_f}{3}\right) \ . \tag{2.67b}$$

The fit parameters in (2.64) have been determined in [33, 34].

2.7 The Taylor expansion method for finite quark chemical potentials

In order to treat $\mathcal{D}U\, P[U]$ as a probability measure the fermion determinant has to be positive definite. Unfortunately this is in general only true for $\mu = 0$ because for non-vanishing chemical potential the γ_5-hermiticity is changed into

$$\gamma_5 K(\mu)\gamma_5 = K(-\mu)^\dagger, \tag{2.68}$$

and therefore $\det(K)$ is in general not even real because

$$\det(K(\mu))^* = \det(K(-\mu)). \tag{2.69}$$

One consequence of this relation is that for non-real gluonic observables $\mathcal{O}$ we have

$$\langle \mathcal{O}^* \rangle_\mu = \langle \mathcal{O} \rangle^*_{-\mu} \tag{2.70}$$

There are several approaches to circumvent this so-called "sign" problem, i.e. there are multi-parameter reweighting techniques [35], where the simulation is done at vanishing μ and results are reweighted to finite μ. Then there is the possibility of simulating at imaginary μ where the fermion determinant is real and positive as can be seen from (2.68). The results are analytically continued to real values of μ afterwards [36]. A recent overview on these methods can be found in [37].
In this work we use the Taylor expansion technique [38], where the fermion determinant and if necessary also the operator of an observable are expanded in powers of μ or μ/T. This results in an expansion of our observable

$$\langle \mathcal{O} \rangle_\mu = o_0 + o_1\mu + o_2\mu^2 + \cdots \ . \tag{2.71}$$

On a finite lattice $\langle \mathcal{O} \rangle_\mu$ is an analytic function in μ and the series on the right hand side is convergent for every value of μ. In the thermodynamic limit the radius of convergence ρ may be finite and the observable $\langle \mathcal{O} \rangle_\mu$ becomes singular at $\mu = \rho$. If $\mathcal{O}$ is a susceptibility then the phase transition line should give an upper bound for the radius of convergence.
The explicit expressions for the expansion coefficients are discussed in appendix A. They contain traces of matrices of the form

$$A = K^{-1}\frac{\partial^{n_1} K}{\partial \mu^{n_1}} \cdots K^{-1}\frac{\partial^{n_m} K}{\partial \mu^{n_m}} \ . \tag{2.72}$$

We evaluate these traces on every gauge link configuration by means of the random noise vector method. Given a set of independent equally distributed random unit vectors $\eta_1, \eta_2, \eta_3, \cdots$ we have

$$\mathrm{Tr}\,(A) = \lim_{n\to\infty} \frac{1}{n} \sum_{i=1}^{n} \eta_i^\dagger A \eta_i \tag{2.73}$$

In this work we always use $n = 50$ Z2-vectors with components $\sim \pm 1$ to get reliable estimates of $\mathrm{Tr}\,(A)$. Because in our estimates we use the same random vectors for all the traces, the correct unbiased estimate for a product of traces is

$$\prod_{i=1}^{m} \mathrm{Tr}\,(A_i) \approx \frac{(n-m)!}{n!} \sum_{\substack{n_1,\cdots,n_m \\ n_i \neq n_j}} \eta_{n_1}^\dagger A_1 \eta_{n_1} \cdots \eta_{n_m}^\dagger A_m \eta_{n_m} \ . \tag{2.74}$$

We note that the sum on the right can contain a large number of terms. Approximately there are n^m terms, where in this work m is equal to 6 at maximum. We therefore have to be very careful when executing the sum numerically. This gets even worse if we consider correlations of observables in which connected and disconnected parts almost cancel like for the 6th order expansion coefficient of the equation of state.

Chapter 3

The equation of state

3.1 The equation of state at finite density

The equation of state of QCD at finite temperature and also at finite density has been extensively studied and received more and more attention in recent years. This is due to both the advances in theoretical predictions and the possibility of comparison to experimental data, collected nowadays and in future colliders.
The derived quantities like the pressure p, energy density ε and quark number density n_q are just the derivatives of the grand canonical potential, eq. (2.12), with respect to volume V, temperature T and quark chemical potential μ

$$\frac{p}{T^4} = -\frac{1}{T^4}\frac{\partial\Omega}{\partial V} = -\frac{1}{VT^4}\Omega(T,\mu)\ , \tag{3.1a}$$

$$\frac{\varepsilon}{T^4} = 3\frac{p}{T^4} + T\frac{\partial}{\partial T}\left(\frac{p}{T^4}\right)\ , \tag{3.1b}$$

$$\frac{n_q}{T^3} = -\frac{1}{VT^3}\frac{\partial\Omega}{\partial\mu}\ . \tag{3.1c}$$

We will only discuss the pressure and the relation to the quark number density here. At $\mu = 0$ the equation for the pressure can be calculated up to an additive integration constant, which is unknown since in MC simulations we never calculate the value of the partition function itself. The common choice is to put $p = 0$ at $T = 0$. For $T \neq 0$ the value of p is then obtained by integrating the derivative of p along a line of constant physics [39].
For $\mu \neq 0$ we have to differentiate (3.1) with respect to μ. We then obtain p/T^4 as a Taylor series

$$\frac{p}{T^4} = \sum_{n=0}^{\infty} c_n(T)\left(\frac{\mu}{T}\right)^n\ , \tag{3.2a}$$

where

$$c_n(T) = \frac{1}{n!}\frac{1}{VT^3}\frac{\partial^n \ln Z}{\partial\left(\mu/T\right)^n}\bigg|_{\mu=0} \ . \tag{3.3}$$

The $c_n(T)$ for $n > 0$ will be the simplest quantities to be presented in this work. Namely, apart from a multiplicative factor, they are just the expansion coefficients of $\langle\mathcal{O}\rangle_\mu$ with $\mathcal{O} = 1$.
In appendix A we show that the odd order derivatives of the partition function vanish and thus $c_n(T) = 0$ for odd n. Because the quark number density is related to the pressure via

$$\frac{n_q}{T^3} = \frac{\partial}{\partial\left(\mu/T\right)}\left(\frac{p}{T^4}\right) \ , \tag{3.4}$$

the μ-expansion coefficients are related to those of the pressure

$$\frac{n_q}{T^3} = \sum_{n=0}^{\infty}(n+1)\ c_{n+1}(T)\left(\frac{\mu}{T}\right)^n \ , \tag{3.5}$$

and finally the coefficients $c_n(T)$ also occur in the expansion of susceptibilities

$$\begin{aligned}\frac{\chi}{T^2} &= \frac{1}{VT^4}\frac{\partial\Omega}{\partial\left(\mu/T\right)^2} \ , \\ &= \sum_{n=0}^{\infty}(n+1)(n+2)\ c_{n+2}(T)\left(\frac{\mu}{T}\right)^n \ .\end{aligned} \tag{3.6}$$

Another related quantity of interest is the isovector susceptibility which is defined as

$$\frac{\chi^I}{T^2} = \frac{1}{VT^4}\frac{\partial\Omega}{\partial\left(\mu_I/T\right)^2} \ , \tag{3.7}$$

where $\mu_I = (\mu_u - \mu_d)/2$. After taking the derivatives with respect to μ_I, we set $\mu_u = \mu_d = \mu$ such that the isovector chemical potential μ_I vanishes. Then χ^I can be expanded in powers of the remaining quark chemical potential μ leading to a series

$$\frac{\chi^I}{T^2} = \sum_{n=0}^{\infty}(n+1)(n+2)\ c^I_{n+2}(T)\left(\frac{\mu}{T}\right)^n \ . \tag{3.8}$$

Details on the calculation of c^I_n can be found in [10]. In fig. 3.1 we show the coefficients $c_n(T)$ and $c^I_n(T)$. Due to the use of improved actions the

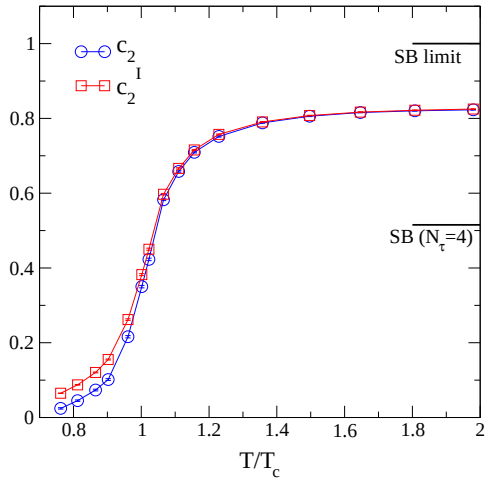

(a)

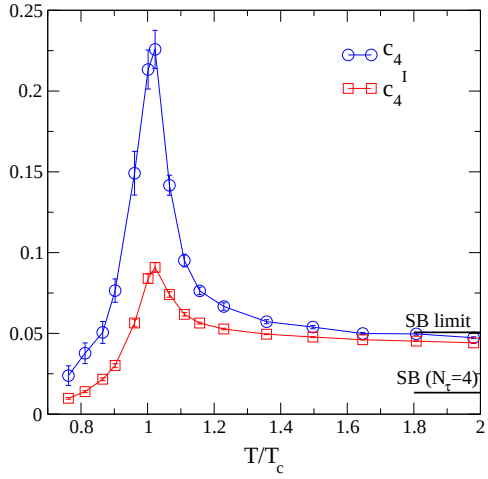

(b)

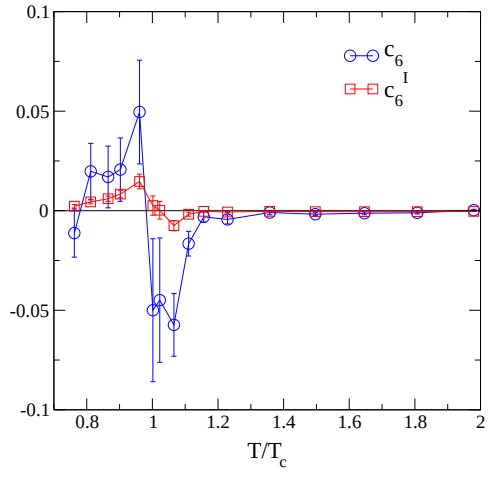

(c)

Figure 3.1: μ-expansion coefficients of the pressure c_2, c_4, c_6 and c_2^I, c_4^I, c_6^I versus temperature.

high temperature limits agree better with the continuum Stefan-Boltzmann limits

$$\lim_{T\to\infty} c_2 = N_f/2 \quad \lim_{T\to\infty} c_4 = N_f/4\pi^2 \quad \lim_{T\to\infty} c_6 = 0 \,, \tag{3.9}$$

than with the corresponding limits calculated from the free unimproved lattice action [40].
The μ-expansion coefficients of the equation of state show some of the typical features shared by most of the expansion coefficients discussed in the next chapters. The greatest changes in the values of the coefficients occur around T_c. I.e. for c_2 we have got the largest slope, c_4 has got a strong peak and c_6 shows an abrupt change of sign. At high temperatures all coefficients converge to the corresponding Stefan-Boltzmann value, which for the 4th and 6th order coefficient is reached within a range of $T \sim 1.2T_c$ and $T \sim 1.8T_c$.
Finally at low temperatures $T < T_c$ the coefficients c_2, c_4, c_6 are compatible with predictions of a hadron resonance gas model [41].
Further details like pictures of the susceptibilities and estimates of the radius of convergence of the power expansions can be found in [10, 40].

Chapter 4

Heavy quarks

4.1 Heavy quark free energies

Consider the grand canonical ensemble of QCD including a set of static (or heavy) quarks placed at positions $\boldsymbol{r}_1, \boldsymbol{r}_2, \cdots, \boldsymbol{r}_n$ and anti-quarks at positions $\boldsymbol{r}'_1, \boldsymbol{r}'_2, \cdots, \boldsymbol{r}'_m$ which form a color state x. The corresponding free energy $F^{\mathrm{x}}_{n,m} = F^{\mathrm{x}}_{n,m}(\boldsymbol{r}_1, \cdots, \boldsymbol{r}'_m, T, \mu)$ is defined via

$$\exp\left(-\beta F^{\mathrm{x}}_{n,m}\right) = Z = \mathcal{N} \sum_{|s\rangle} \langle s| \, e^{-\beta(H-\mu N_q)} \, |s\rangle \ , \tag{4.1}$$

where $\mathcal{N}$ depends on the normalization of the states and the sum extends over all states $|s\rangle$ of the quantum fields in a fixed gauge such that the set of static quarks and anti-quarks at the given positions form the color state x. Let $\Delta F^{\mathrm{x}}_{n,m} = F^{\mathrm{x}}_{n,m} - F_{0,0}$ the difference of the free energies of our thermodynamical system with and without heavy quarks and anti-quarks. For example we average over all color states of every single quark and anti-quark. We call this the color averaged state (x=av).
Using the common anti-commutation relations for the quark creation and annihilation operators and their static time evolution equation it can be shown [42] that (4.1) can be written as

$$\exp\left(-\beta \Delta F^{\mathrm{av}}_{n,m}\right) = \left\langle \mathrm{tr}L(\boldsymbol{r}_1) \cdots \mathrm{tr}L(\boldsymbol{r}_n) \mathrm{tr}L^\dagger(\boldsymbol{r}'_1) \cdots \mathrm{tr}L^\dagger(\boldsymbol{r}'_m) \right\rangle \ , \tag{4.2}$$

where the "small" trace is the "real" trace divided by $N_c = 3$

$$\mathrm{tr} = \frac{1}{N_c}\mathrm{Tr} \ , \tag{4.3}$$

and $L(\boldsymbol{r})$ is the so-called Polyakov loop

$$L(\boldsymbol{r}) = \mathrm{T} \, e^{ig \int_0^\beta dt \mathcal{A}_4(\boldsymbol{r},t)} \ . \tag{4.4}$$

T is the time ordering operator. On the lattice $L(\boldsymbol{r})$ is the ordered product of all gauge links in the temporal direction at the spatial point $\boldsymbol{r} = a\boldsymbol{n}$

$$L(\boldsymbol{n}) = \prod_{n_4=1}^{N_\tau} U_4(\boldsymbol{n}, n_4) \; . \tag{4.5}$$

From (4.2) we see that the Polyakov loop represents a static, heavy test quark. Heavy anti-quarks are described by the hermitian conjugate matrix. In color space single quark and anti-quark states are represented as triplets transforming according to the fundamental representations **3** and $\mathbf{3}^*$ of $SU(3)$ respectively. For compound states $|s\rangle$ as in (4.1) the corresponding product representations can be decomposed into irreducible representations; i.e. for a quark anti-quark pair we have

$$\mathbf{3} \otimes \mathbf{3}^* \;\; = \;\; \mathbf{1} \oplus \mathbf{8} \, , \tag{4.6}$$

or for a system of two and three quarks we have

$$\mathbf{3} \otimes \mathbf{3} \;\; = \;\; \mathbf{3}^* \oplus \mathbf{6} \, , \tag{4.7}$$

$$\mathbf{3} \otimes \mathbf{3} \otimes \mathbf{3} \;\; = \;\; \mathbf{1} \oplus \mathbf{8} \oplus \mathbf{8}' \oplus \mathbf{10} \, . \tag{4.8}$$

Every state $|s\rangle$ of quarks and anti-quarks decomposes into multiplets weighted with the associated Clebsch-Gordon coefficients. Inserting this into (4.1) it can be shown [43, 44] that for the color averaged free energies we have

$$\exp\left(-\beta F^{\mathrm{av}}_{Q\bar{Q}}\right) \;\; = \;\; \frac{1}{9}\exp\left(-\beta F^{1}_{Q\bar{Q}}\right) + \frac{8}{9}\exp\left(-\beta F^{8}_{Q\bar{Q}}\right) \; , \tag{4.9}$$

$$\exp\left(-\beta F^{\mathrm{av}}_{QQ}\right) \;\; = \;\; \frac{1}{3}\exp\left(-\beta F^{3}_{QQ}\right) + \frac{2}{3}\exp\left(-\beta F^{6}_{QQ}\right) \; , \tag{4.10}$$

$$\begin{aligned} \exp\left(-\beta F^{\mathrm{av}}_{QQQ}\right) \;\; = \;\; & \frac{1}{27}\exp\left(-\beta F^{1}_{QQQ}\right) + \frac{8}{27}\exp\left(-\beta F^{8}_{QQQ}\right) \\ & + \frac{8}{27}\exp\left(-\beta F^{8'}_{QQQ}\right) + \frac{10}{27}\exp\left(-\beta F^{10}_{QQQ}\right) \; , \end{aligned} \tag{4.11}$$

where i.e. $F^{1}_{Q\bar{Q}}$ and $F^{8}_{Q\bar{Q}}$ are the free energies of the system with a heavy quark-anti-quark pair in a color singlet and color octet state respectively. They are defined in analogy to (4.1), where the sum extends over those states which contain a heavy $Q\bar{Q}$ pair in the singlet and octet state.
In what follows we will always write "F..." instead of "ΔF..." for simplicity. Then "F..." contains only that part of the free energy which is provoked by the presence of the heavy test quarks and anti-quarks. Therefore we will occasionally call "F..." the free energy of the heavy quark-anti-quark part. The free energies are related to the correlation functions of the Polyakov

loops; i.e.

$$\exp\left(-\beta F^1_{Q\bar{Q}}\right) = \left\langle \mathrm{tr}\left[L_1 L_2^\dagger\right]\right\rangle \tag{4.12a}$$

$$\begin{aligned}\exp\left(-\beta F^1_{QQQ}\right) = \frac{1}{2}\langle & 9\ \mathrm{tr}L_1\mathrm{tr}L_2\mathrm{tr}L_3 - 3\ \mathrm{tr}L_1\mathrm{tr}\left[L_2L_3\right] \\ & -3\mathrm{tr}L_2\mathrm{tr}\left[L_1L_3\right] - 3\mathrm{tr}L_3\mathrm{tr}\left[L_1L_2\right] \\ & +\mathrm{tr}\left[L_1L_2L_3\right] + \mathrm{tr}\left[L_1L_3L_2\right]\rangle\ ,\end{aligned} \tag{4.12b}$$

where $L_i = L(\boldsymbol{r}_i)$.
Although the lattice gauge action is invariant under local gauge transformations $G(n) \in SU(3)$

$$\chi_n \rightarrow G(n)\chi_n\ , \tag{4.13a}$$

$$\bar{\chi}_n \rightarrow \bar{\chi}_n G^{-1}(n)\ , \tag{4.13b}$$

$$U_\mu(n) \rightarrow G(n)U_\mu(n)G^{-1}(n+\hat{\mu})\ , \tag{4.13c}$$

the Polyakov loop $L(\boldsymbol{n})$ is gauge dependent but $\mathrm{tr}\,L(\boldsymbol{n})$ is not. Therefore only the color averaged free energies are gauge invariant because they are calculated from traces of the Polyakov loop only. Because we are also interested in results for the singlet free energy we have to fix the gauge. We choose to transform our gauge link configurations to Coulomb gauge using the overrelaxation algorithm [45] before calculating our Polyakov loop correlations.

4.2 The renormalized Polyakov loop

In the quenched limit (i.e. quark mass $M \rightarrow \infty$) the action is invariant under transformations

$$U_4(n) \rightarrow zU_4(n)\ , \tag{4.14}$$

where z is an element of the group $Z(N_c) = \{\exp(2\pi i n/N_c)\,|n = 0, \cdots, N_c\}$ which is the center of $SU(N_c)$. The Polyakov loop serves as an order parameter for the spontaneous breaking of this symmetry. In the thermodynamic limit it is vanishing below and non-vanishing above the transition temperature. For finite M this symmetry is broken explicitly.
The free energy of a single quark inside a medium contains the self energy of the quark which is a divergent quantity in the continuum limit. A consequence is that the continuum limit of the Polyakov loop is vanishing even in the non-symmetric phase. It is therefore necessary to renormalize the Polyakov loop with some renormalization constant Z before taking the continuum limit.

$$L_{ren} = Z(g^2)\cdot L\ . \tag{4.15}$$

In general we may assume that Z depends not only on the coupling g^2 but also on the value of the chemical potential μ. In fact we will see later that there is no necessity for the assumption of a μ-dependence so far.
We now briefly summarize how to determine the value of Z, more details can be found in [46]. Consider a quark Q and an anti-quark $\bar{Q}$ with a spatial distance $r = |\boldsymbol{r}|$ and the color averaged free energy

$$F^{\mathrm{av}}_{Q\bar{Q}}(r,T,\mu) = -T \ln \left\langle \mathrm{tr}\, L_{ren}(\boldsymbol{r})\ \mathrm{tr}\, L^{\dagger}_{ren}(\boldsymbol{0}) \right\rangle_{\mu} . \tag{4.16}$$

We note that we replace our distances r on the lattice by improved distances to accommodate for lattice artefacts in the rotational symmetry of the heavy quark potential [47].
$F^{\mathrm{av}}_{Q\bar{Q}}$ stays finite in the continuum limit. For infinite separations the quark Q and the anti-quark $\bar{Q}$ are uncorrelated and $F^{\mathrm{av}}_{Q\bar{Q}}(r,T,\mu)$ can be written as

$$F^{\mathrm{av}}_{Q\bar{Q}}(\infty,T,\mu) = -2T \ln \left| \langle \mathrm{tr}\, L_{ren} \rangle_{\mu} \right| , \tag{4.17}$$

where the Polyakov loop is calculated at some arbitrary spatial position. We see that the multiplication of L with the renormalization constant Z can be obtained by adding a constant to $F^{\mathrm{av}}_{Q\bar{Q}}/T$.

$$\frac{F_{Q\bar{Q}}(r,T,\mu)}{T} = -2 \ln \left| \langle \mathrm{tr}\, L \rangle_{\mu} \right| + c(g^2) . \tag{4.18}$$

Now for small distances r the temperature and density of the medium should have no influence on the free energy. Therefore we choose c such that $F^{1}_{Q\bar{Q}}(r,T,0)$ matches the zero temperature heavy quark potential $V_{Q\bar{Q}}(r)$ at the smallest available distance r_0. For the simulations in this work we have $N_\tau = 4$ such that $r_0 = 1/(4T)$. $V_{Q\bar{Q}}(r)$ is given in the Cornell form

$$V_{Q\bar{Q}}(r) = -\frac{4}{3} \cdot \frac{\alpha_s}{r} + \sigma r , \tag{4.19}$$

After having determined $c(g^2)$ in this way the renormalization constant $Z(g^2)$ can be calculated. Then the Polyakov loop as well as all the values of the corresponding free energies are fixed. All numerical results presented in this chapter are renormalized following this procedure.

4.3 Singlet and color averaged free energies of a heavy quark-anti-quark pair

A purely gluonic observable $\mathcal{O}$ like the Polyakov loop $L(\boldsymbol{r})$ or a corresponding correlation function does not explicitly depend on the quark chemical potential; it is calculated in terms of link variables $U_\rho(x)$ of the gauge field

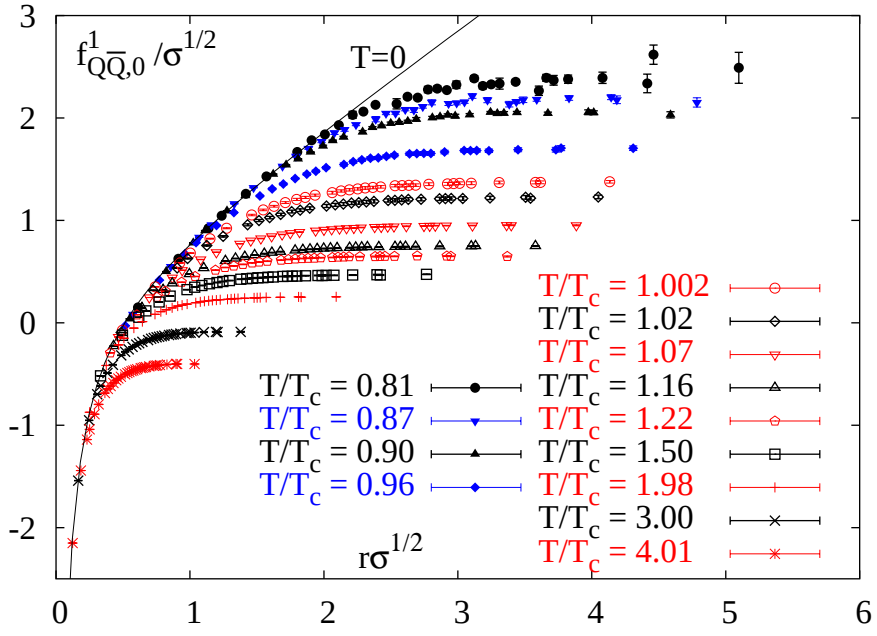

(a)

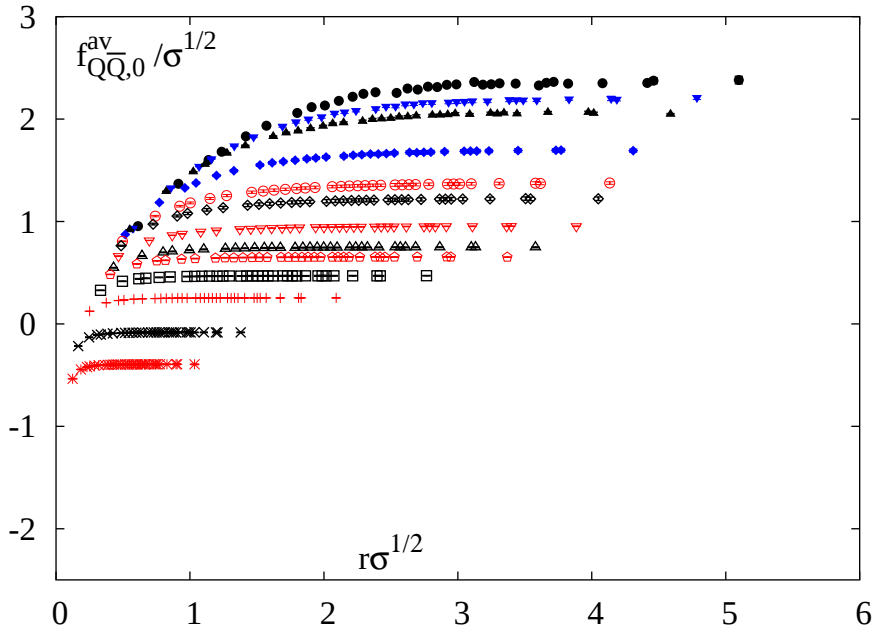

(b)

Figure 4.1: The 0^{th} order coefficients $f^1_{Q\bar{Q},0}$ and $f^{av}_{Q\bar{Q},0}$ in units of the square root of the string tension for the singlet and color averaged free energy in the vicinity of T_c. $f^1_{Q\bar{Q},0}$ is matched to the $T = 0$ heavy quark potential at small distances (a).

configuration which do not explicitly depend on μ. Any μ-dependence of the expectation value $\langle \mathcal{O} \rangle_\mu$ thus arises from the μ-dependence of the Boltzmann weights in the QCD partition function, i.e. the μ-dependence of the fermion determinant.
On the lattice we average the values of the Polyakov loop and the corresponding correlation functions over all sites, i.e. for the color averaged and singlet correlation function we have

$$\mathcal{C}^{\mathrm{av}}(r) = \frac{1}{\mathcal{N}} \sum_{\boldsymbol{x},\boldsymbol{y}} \mathrm{tr} L(\boldsymbol{x}) \ \mathrm{tr} L^\dagger(\boldsymbol{y}) \ , \tag{4.20a}$$

$$\mathcal{C}^{1}(r) = \frac{1}{\mathcal{N}} \sum_{\boldsymbol{x},\boldsymbol{y}} \mathrm{tr} \left[L(\boldsymbol{x}) L^\dagger(\boldsymbol{y}) \right] \ , \tag{4.20b}$$

where the sums refer to all sites $\boldsymbol{x}, \boldsymbol{y}$ with $\|\boldsymbol{x} - \boldsymbol{y}\| = r$ and $\mathcal{N}$ is the number of these $\boldsymbol{x}, \boldsymbol{y}$-pairs. $\mathcal{C}^{\mathrm{av},1}$ and the corresponding expectation values are strictly real for every single gauge field configuration. For this reason the odd orders in the μ-expansion vanish as is argued in appendix A. The same is true for the corresponding free energies

$$F^{\mathrm{av}}_{Q\bar{Q}}(r,T,\mu) = -T \ \ln \left\langle \mathcal{C}^{\mathrm{av}}(r) \right\rangle_\mu \ , \tag{4.21a}$$

$$F^{1}_{Q\bar{Q}}(r,T,\mu) = -T \ \ln \left\langle \mathcal{C}^{1}(r) \right\rangle_\mu \ . \tag{4.21b}$$

In order to determine the expansion coefficients of the color averaged and singlet free energies,

$$\begin{aligned} F^{x}_{Q\bar{Q}}(r,T,\mu) \ &= \ f^{x}_{Q\bar{Q},0}(r,T) + f^{x}_{Q\bar{Q},2}(r,T) \left(\frac{\mu}{T}\right)^2 + f^{x}_{Q\bar{Q},4}(r,T) \left(\frac{\mu}{T}\right)^4 \\ &\quad + f^{x}_{Q\bar{Q},6}(r,T) \left(\frac{\mu}{T}\right)^6 + \mathcal{O}\left(\left(\frac{\mu}{T}\right)^8 \right) \ , \end{aligned} \tag{4.22}$$

with $x = \mathrm{av}$ and 1, we apply (A.13) to the corresponding Polyakov loop correlation functions.

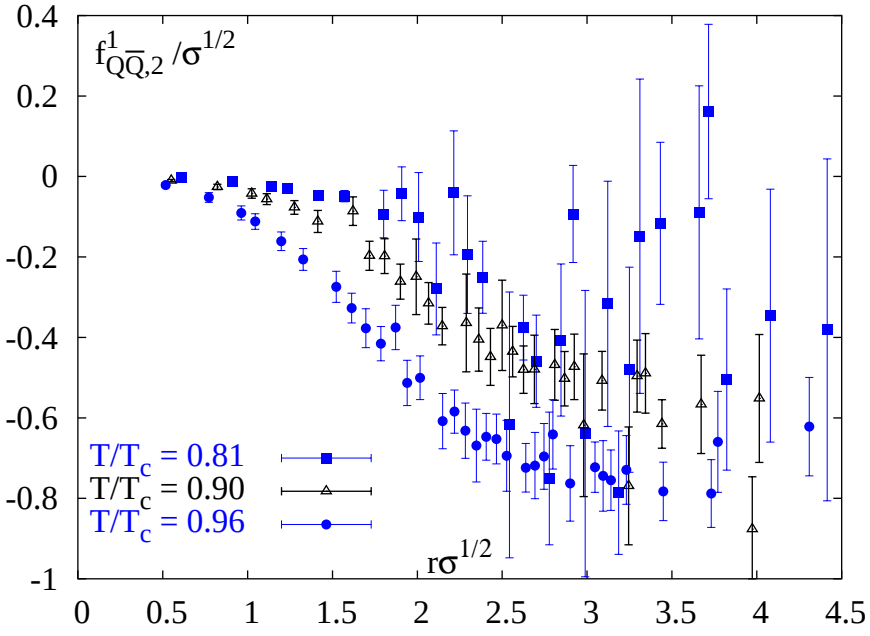

(a)

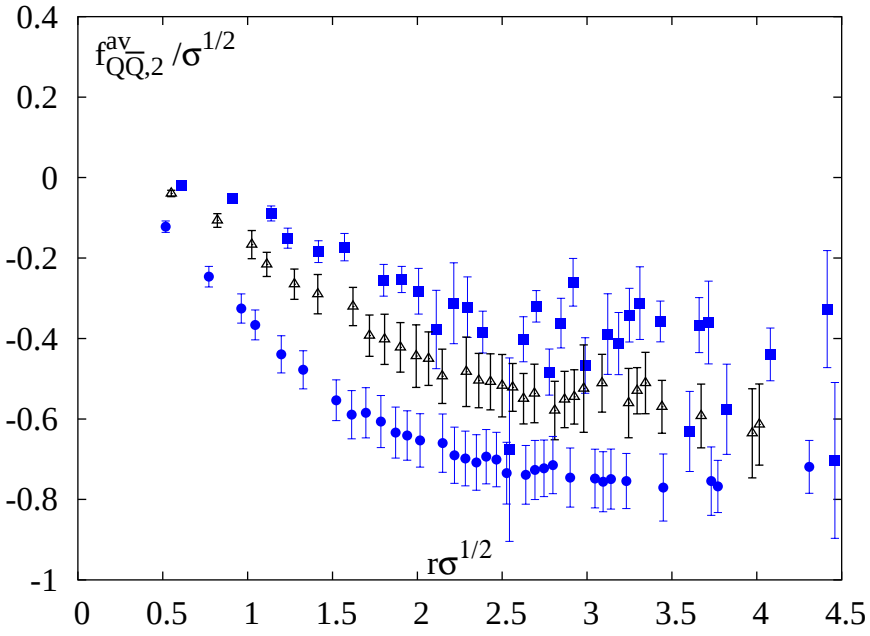

(b)

Figure 4.2: The 2^{nd} order coefficients of the singlet (a) and color averaged (b) free energies for some selected temperatures below T_c.

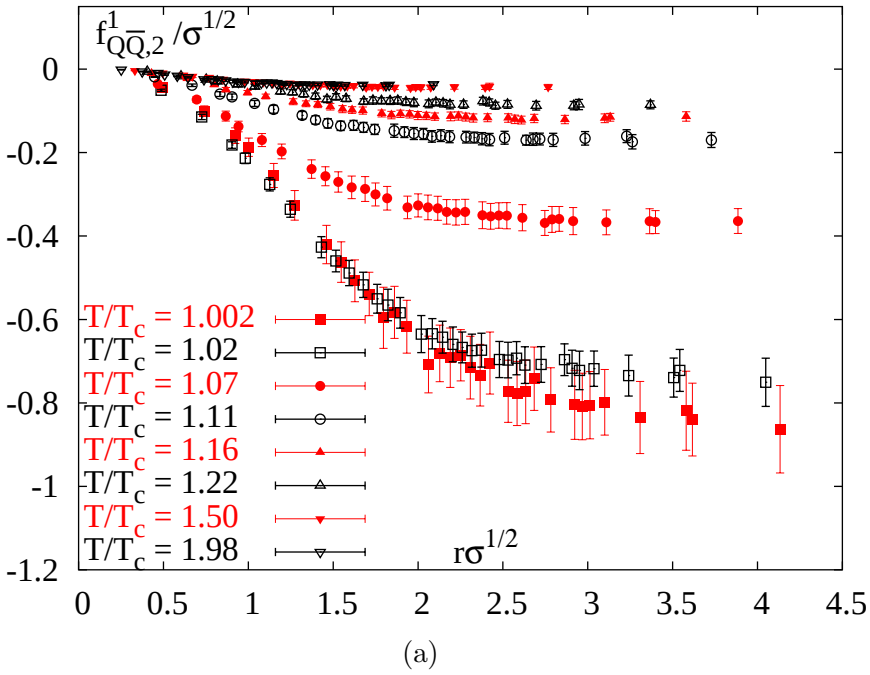

(a)

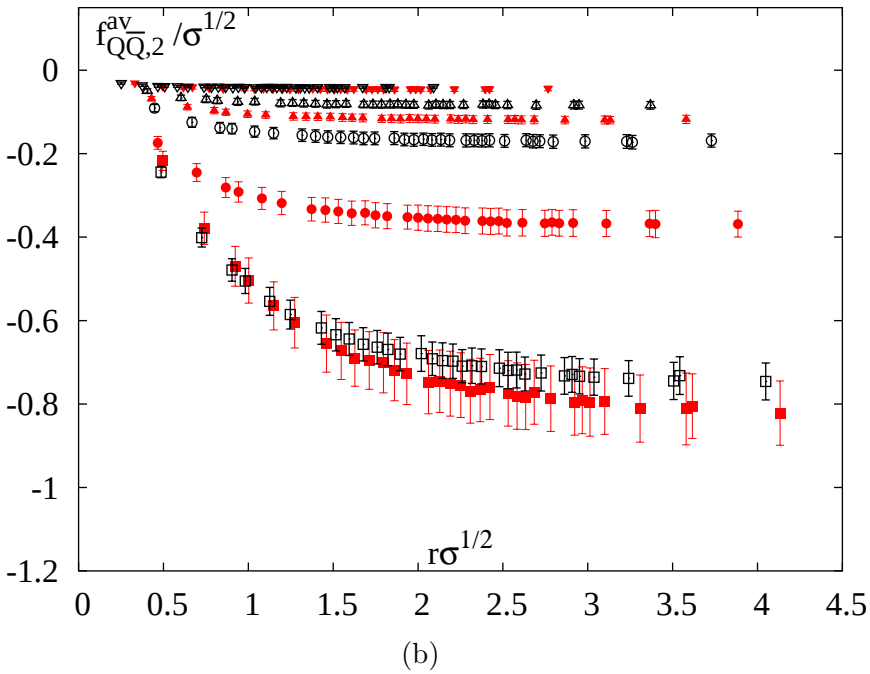

(b)

Figure 4.3: The 2^{nd} order coefficients of the singlet (a) and color averaged (b) free energies for some selected temperatures above T_c.

From the Polyakov loop correlations we obtain the free energies in units of the inverse lattice spacing F/a^{-1}. These results can be transformed into units of temperature or the string tension via

$$aF = N_\tau \frac{F}{T} = a\sqrt{\sigma}\frac{F}{\sqrt{\sigma}} \,, \tag{4.23}$$

where the factor $a\sqrt{\sigma}$ is known from (2.64). In fig. 4.1-4.5 we show the leading and higher order expansion coefficients up to sixth order in μ/T expressed in units of the square root of the string tension. The figures do not contain all the analyzed data because for $T \gg T_c$ the absolute values are very small and for $T < T_c$ the statistical errors are sometimes very large. The 0th order results show the expected string breaking behavior due to the screening of the quarks in the surrounding medium. The screening sets in at smaller distances the more the temperature is increased. In [31] the 0th order data presented here have been used to calculate a screening radius, defined in [46], separating the Coulomb part of the potential from the exponentially screened part.
For the second order expansion coefficients we display separately results below (fig. 4.2) and above (fig. 4.3) the $\mu = 0$ transition temperature T_c. As can be seen the second order expansion coefficients are always negative and increase in magnitude in the vicinity of T_c. Therefore for small values of $\mu \neq 0$ the free energies get lowered compared to the $\mu = 0$ case. The strongest reduction can be seen directly at the transition temperature.
The corresponding results for the 4^{th} and 6^{th} order expansion coefficients are shown in fig. 4.4 and fig. 4.5, respectively. Here we only show results above T_c; below T_c the expansion coefficients are consistent with being zero within errors even at rather short distances and errors grow large for $rT \geq 1$.
We note that all expansion coefficients shown in figs. 4.2 to 4.5 vanish at small distances. This shows that a quark anti-quark pair is not affected by the surrounding medium if its size becomes small. This observation also justifies our procedure to renormalize the Polyakov loop by matching the $\mu = 0$ singlet free energy to the $T = 0$ heavy quark potential, namely that the renormalization constant is independent of μ and T.
Also close to T_c, where the μ-dependence of the free energies is strongest, the absolute values of the fourth and sixth order expansion coefficients are of the same order as or smaller than the second order expansion coefficient. Therefore the 4^{th} and 6^{th} order contributions rapidly become negligible for $\mu/T < 1$.
Although the errors are large for the higher order expansion coefficients they show that at high temperature the 2^{nd} and 4^{th} order expansion coefficients are opposite in sign, $f^{\text{av},1}_{Q\bar{Q},2}(r,T) < 0$ and $f^{\text{av},1}_{Q\bar{Q},4}(r,T) > 0$. This is consistent with the expectation that at high temperature the asymptotic large distance value of the heavy quark free energy is proportional to the value of the Debye mass. In this limit one obtains alternating signs of the expansion coefficients

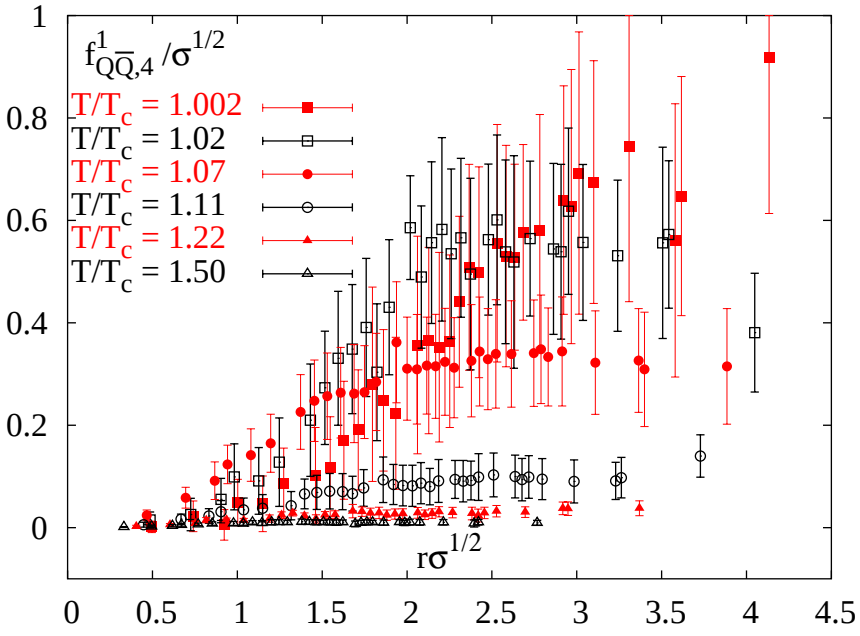

(a)

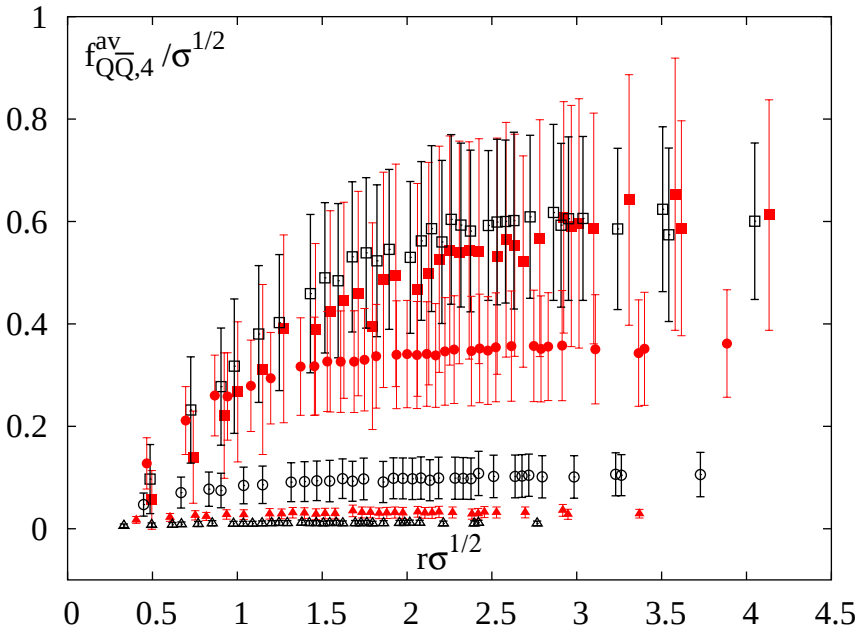

(b)

Figure 4.4: The 4^{th} order coefficients of the singlet (a) and color averaged (b) free energies for temperatures above T_c.

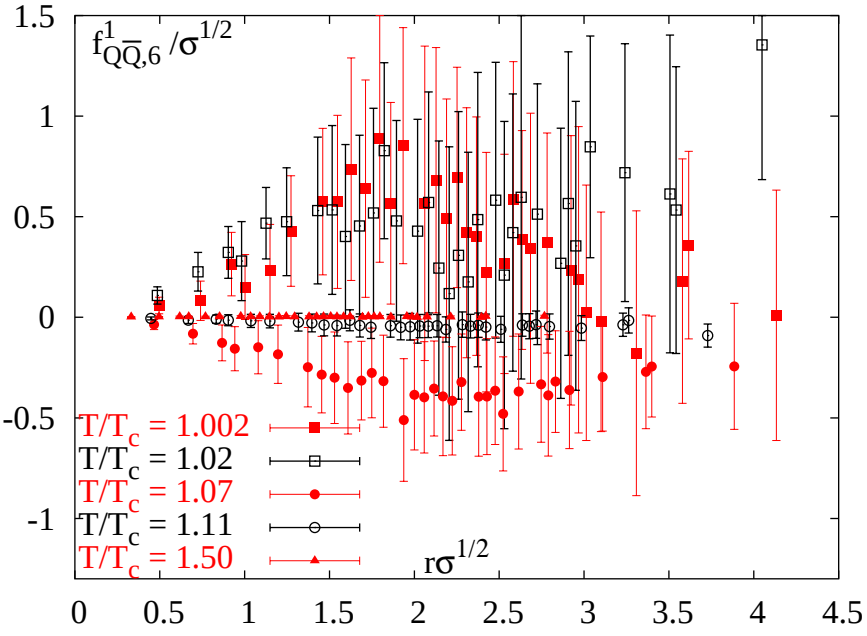

(a)

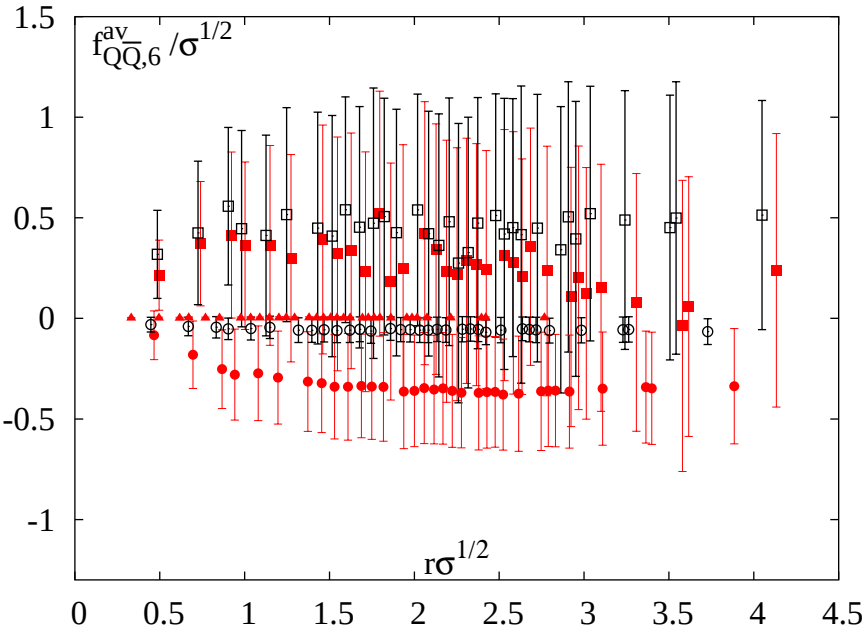

(b)

Figure 4.5: The 6^{th} order coefficients of the singlet (a) and color averaged (b) free energies for temperatures above T_c.

of the heavy quark free energies when one expands the perturbative Debye mass [13],

$$\frac{m_D(T,\mu)}{g(T)T} = \frac{m_{D,0}(T)}{g(T)T}\sqrt{1+\frac{3N_f}{(2N_c+N_f)\pi^2}\left(\frac{\mu}{T}\right)^2}\,, \tag{4.24}$$

with $m_{D,0}(T) = g(T)T\sqrt{\frac{N_c}{3}+\frac{N_f}{6}}$ denoting the Debye mass for vanishing baryon chemical potential. Although the statistical significance of our results for $f^{\mathrm{av},1}_{Q\bar{Q},6}(r,T)$ rapidly drops with increasing temperature this pattern of alternating signs seems to be valid also at sixth order at least for temperatures $T\gtrsim 1.05T_c$.

Except for temperatures close to the transition temperature the asymptotic behavior of the free energies is reached at distances $rT\gtrsim 1.5$. We determine their large distance value by taking the weighted average of the values at the five largest distances. The results are shown in fig. 4.6 and 4.7. We note that $|f^{\mathrm{av},1}_{Q\bar{Q},2}(\infty,T)|$ have a pronounced peak at T_c. This also holds for $|f^{\mathrm{av},1}_{Q\bar{Q},2}(r,T)|$ evaluated at any fixed distance r as indicated by fig. 4.8. The peak height is maximum for $r\to\infty$. In fact, $f^{\mathrm{av},1}_{Q\bar{Q},2}(r,T)$ is proportional to the second derivative of a partition function including a pair of static sources, $Q\bar{Q}$. I.e. from appendix A we have

$$\begin{aligned} f_2^{\mathrm{av},1}(r,T) &= -\left.\frac{\partial^2 T\ln\left\langle \mathcal{C}^{\mathrm{av},1}(r)\right\rangle_\mu}{\partial(\mu/T)^2}\right|_{\mu=0}\,, \\ &= -T^3\frac{\left\langle \mathcal{C}^{\mathrm{av},1}(r)D_2\right\rangle - \left\langle \mathcal{C}^{\mathrm{av},1}(r)\right\rangle\langle D_2\rangle}{\left\langle \mathcal{C}^{\mathrm{av},1}(r)\right\rangle}\,. \end{aligned} \tag{4.25}$$

It thus shows the characteristic properties of a susceptibility in the vicinity of a (phase) transition point.
Fig. 4.6 and 4.7 also show that at large distances, within the statistical errors of our analysis, the expansion coefficients for the color averaged and singlet free energies approach identical values,

$$f^{\mathrm{av}}_{Q\bar{Q},n}(\infty,T) = f^{1}_{Q\bar{Q},n}(\infty,T)\,, \tag{4.26}$$

where

$$f^{x}_{Q\bar{Q},n}(\infty,T) = \lim_{r\to\infty} f^{x}_{Q\bar{Q},n}(r,T)\,, \quad \text{with } x=\mathrm{av},\ 1\,. \tag{4.27}$$

This suggests that at large distances, e.g. for $rT\gtrsim 1.5$, the quark anti-quark sources are screened independently from each other; their relative color orientation thus becomes irrelevant.
Including all terms up to sixth order we calculated the singlet and color averaged free energies in the range from $\mu/T = 0.0$ up to 0.8. Results for

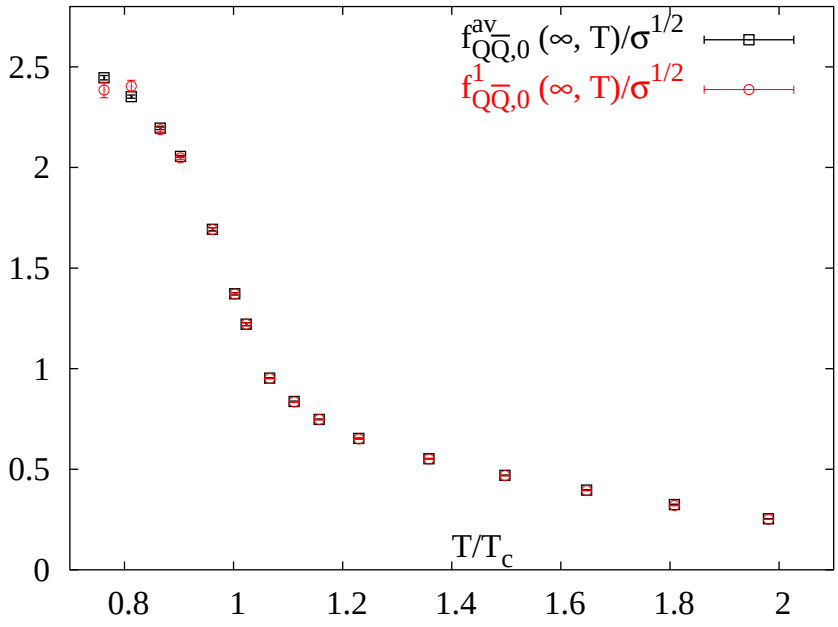

(a)

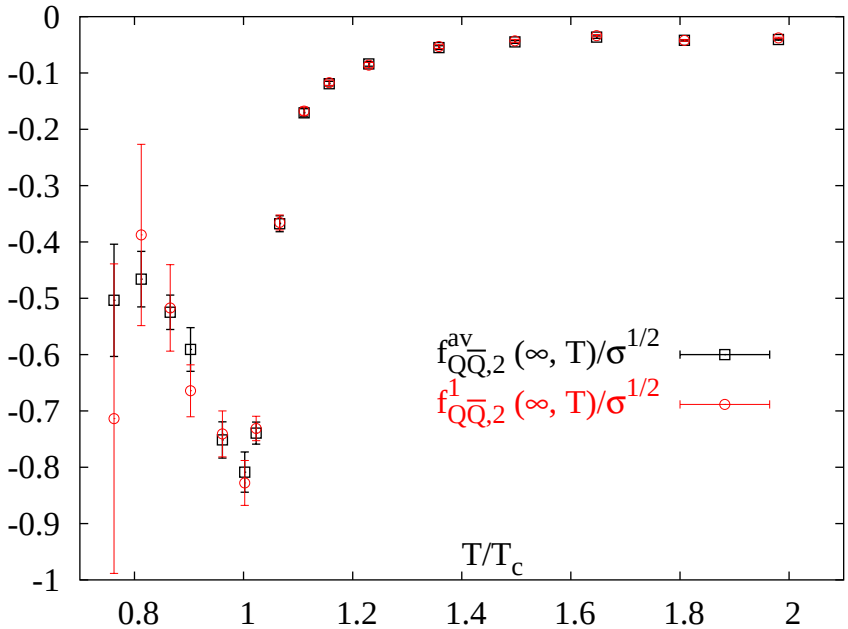

(b)

Figure 4.6: The 0^{th} and 2^{nd} order coefficients for the singlet and color averaged free energies at infinite distance rT versus temperature. They have been obtained from a weighted average of $f^{\rm av}_{Q\bar{Q},n}(r,T)$ and $f^{1}_{Q\bar{Q},n}(r,T)$ at the five largest distances.

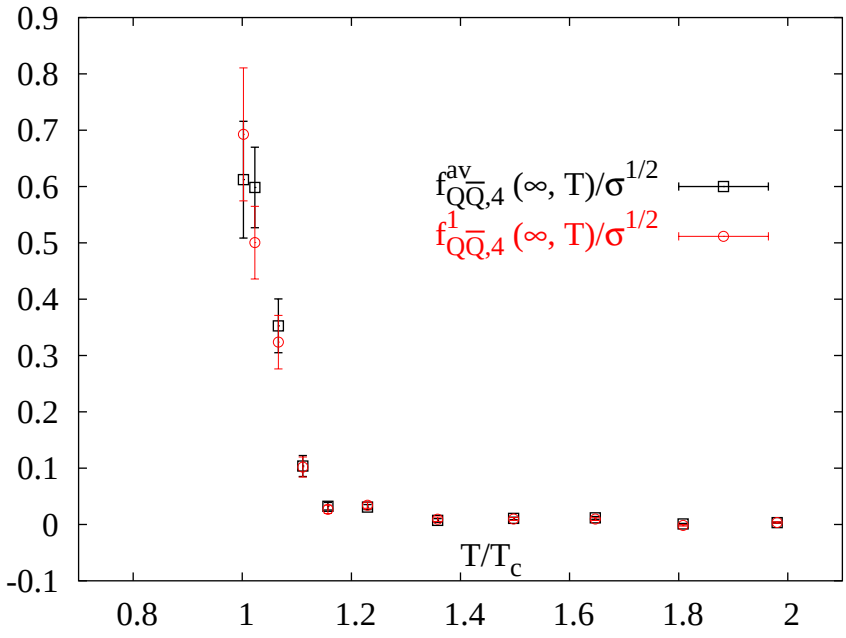

(a)

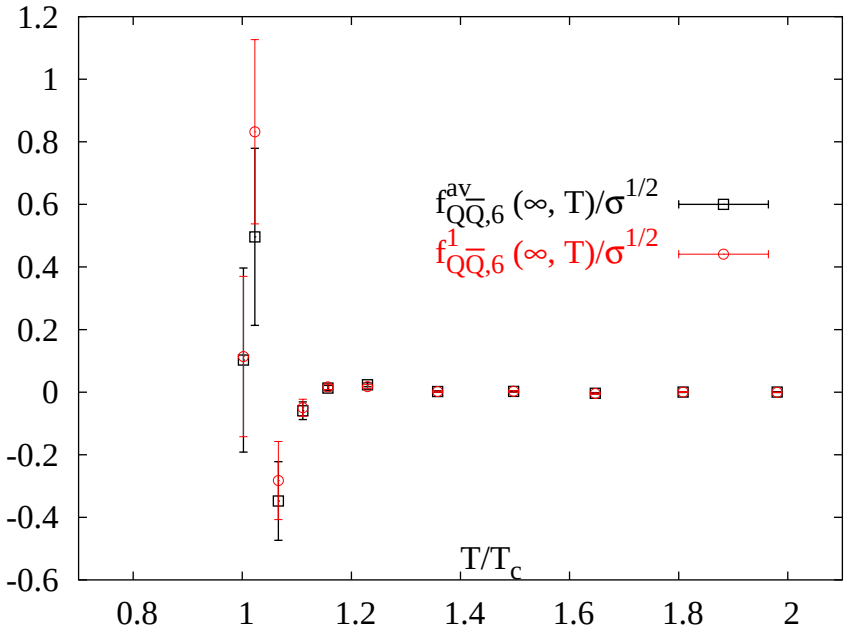

(b)

Figure 4.7: The 4^{th} and 6^{th} order coefficients for the singlet and color averaged free energies at infinite distance rT versus temperature. They have been obtained from a weighted average of $f^{\rm av}_{Q\bar{Q},n}(r,T)$ and $f^{1}_{Q\bar{Q},n}(r,T)$ at the five largest distances.

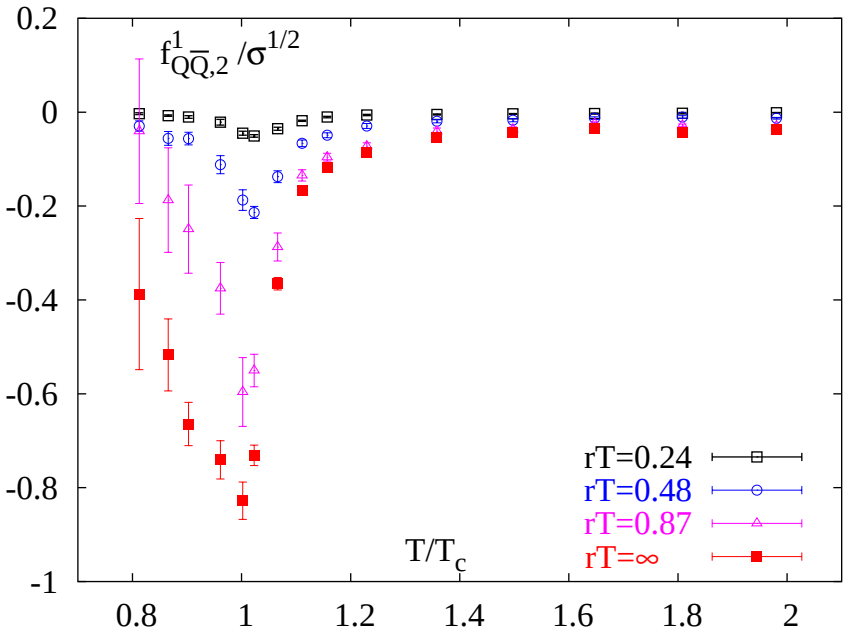

Figure 4.8: 2nd order coefficients for the singlet free energy for several fixed values of rT.

the color singlet free energies evaluated at a few values of temperature are shown in fig. 4.9. Similar results hold for the color averaged free energies. The free energies decrease relative to their values at $\mu/T = 0$ for all temperatures above and below T_c. At small distances the curves always agree within errors. With increasing distance a gap opens up which reflects the decrease in free energy at non zero μ. As indicated by the asymptotic values $f^{\mathrm{av},1}_{Q\bar{Q},2}(\infty, T)$, which give the dominant μ-dependent contribution at large distances, the medium effects are largest close to the transition temperature and become smaller with increasing temperature.

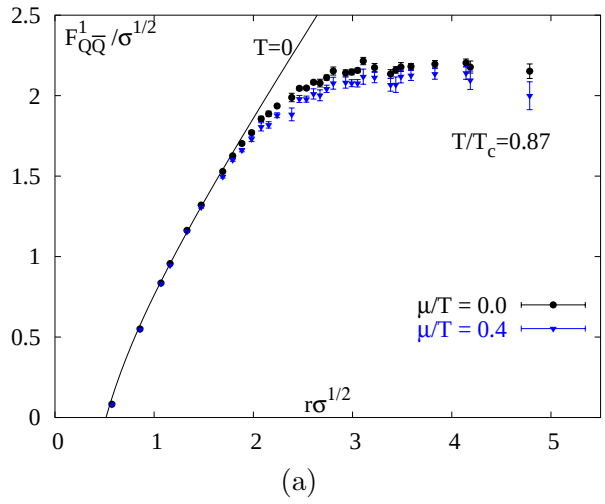

(a)

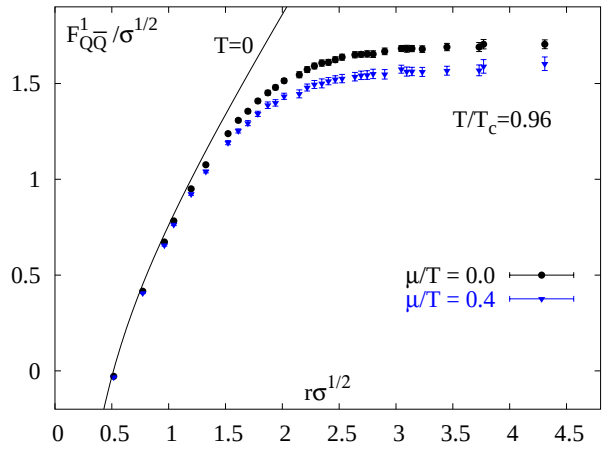

(b)

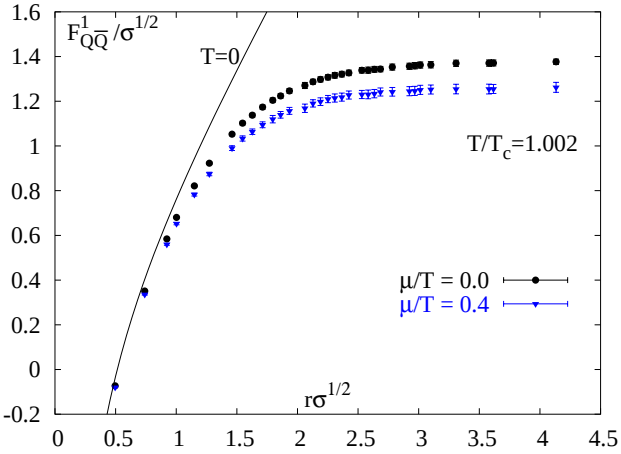

(c)

Figure 4.9: The singlet free energies $F^1_{Q\bar{Q}}$ as function of distance for finite chemical potential and for various temperatures.

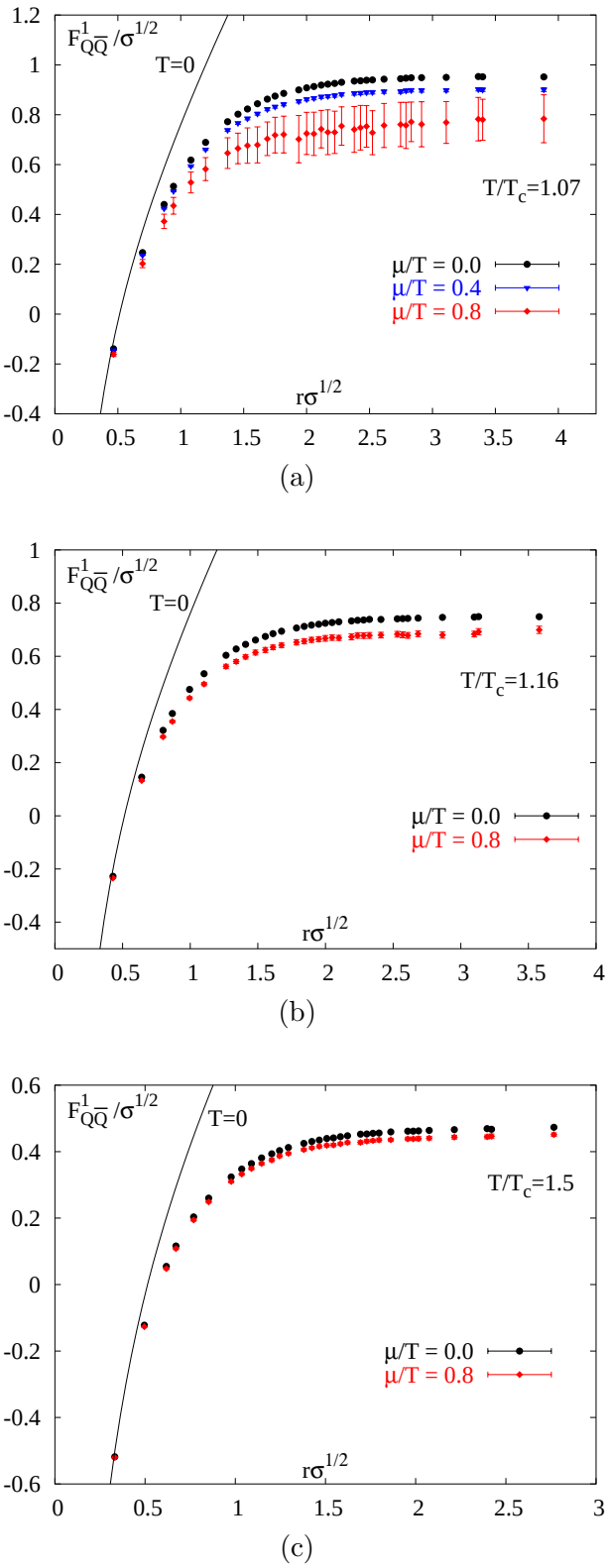

Figure 4.10: The singlet free energies $F^1_{Q\bar{Q}}$ as function of distance for finite chemical potential and for various temperatures.

4.4 Screening masses

For temperatures above T_c and large distances r the heavy quark free energies are expected to be screened,

$$\begin{aligned} \Delta F^{\mathrm{av},1}_{Q\bar{Q}}(r,T,\mu) &= F^{\mathrm{av},1}_{Q\bar{Q}}(\infty,T,\mu) - F^{\mathrm{av},1}_{Q\bar{Q}}(r,T,\mu) \ , \\ &\sim \frac{1}{r^n} e^{-m^{\mathrm{av},1}(T,\mu) r} \end{aligned} \tag{4.28}$$

with $n = 1, 2$ for the singlet and color averaged free energies respectively. In the infinite distance limit we thus can extract the screening masses,

$$m^{\mathrm{av},1}(T,\mu) = -\lim_{r\to\infty} \frac{1}{r} \ln\left(\Delta F^{\mathrm{av},1}_{Q\bar{Q}}(r,T,\mu)\right) \ . \tag{4.29}$$

We use this as our starting point to derive a Taylor expansion for the screening masses. Expanding the logarithm in (4.29) in powers of μ/T it is obvious that also the screening masses are even functions in μ/T,

$$\begin{aligned} m^{\mathrm{av},1}(T,\mu) &= m^{\mathrm{av},1}_0(T) + m^{\mathrm{av},1}_2(T)\left(\frac{\mu}{T}\right)^2 + m^{\mathrm{av},1}_4(T)\left(\frac{\mu}{T}\right)^4 \\ &\quad + m^{\mathrm{av},1}_6(T)\left(\frac{\mu}{T}\right)^6 + \mathcal{O}\left(\left(\frac{\mu}{T}\right)^8\right) \ . \end{aligned} \tag{4.30}$$

To analyze the approach of the various expansion coefficients to the large distance limits we introduce effective masses, $m^x_{\mathrm{eff},n}(r,T)$, with $x = \mathrm{av}, 1$,

$$m^x_{\mathrm{eff},2}(r,T) = -\frac{1}{r}\frac{\Delta f^x_{Q\bar{Q},2}(r,T)}{\Delta f^x_{Q\bar{Q},0}(r,T)} \ , \tag{4.31a}$$

$$m^x_{\mathrm{eff},4}(r,T) = -\frac{1}{r}\left[\frac{\Delta f^x_{Q\bar{Q},4}(r,T)}{\Delta f^x_{Q\bar{Q},0}(r,T)} - \frac{1}{2}\left(\frac{\Delta f^x_{Q\bar{Q},2}(r,T)}{\Delta f^x_{Q\bar{Q},0}(r,T)}\right)^2\right] \ , \tag{4.31b}$$

$$\begin{aligned} m^x_{\mathrm{eff},6}(r,T) &= -\frac{1}{r}\left[\frac{\Delta f^x_{Q\bar{Q},6}(r,T)}{\Delta f^x_{Q\bar{Q},0}(r,T)} - \frac{\Delta f^x_{Q\bar{Q},4}(r,T)\Delta f^x_{Q\bar{Q},2}(r,T)}{\Delta f^x_{Q\bar{Q},0}(r,T)^2}\right. \\ &\quad \left. + \frac{1}{3}\left(\frac{\Delta f^x_{Q\bar{Q},2}(r,T)}{\Delta f^x_{Q\bar{Q},0}(r,T)}\right)^3\right] \ . \end{aligned} \tag{4.31c}$$

In the limit of large distances these relations define the expansion coefficients of the color averaged and singlet screening masses,

$$m^{\mathrm{av},1}_n(T) = \lim_{r\to\infty} m^{\mathrm{av},1}_{\mathrm{eff},n}(r,T) \ . \tag{4.32}$$

As will become obvious in the following the effective masses defined above show only little r-dependence. They are thus suitable for a determination

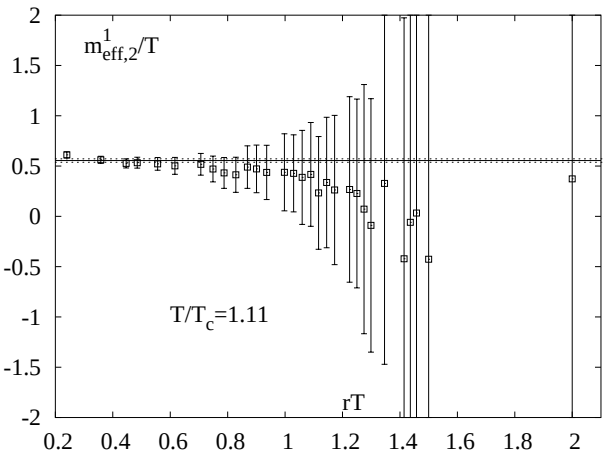

(a)

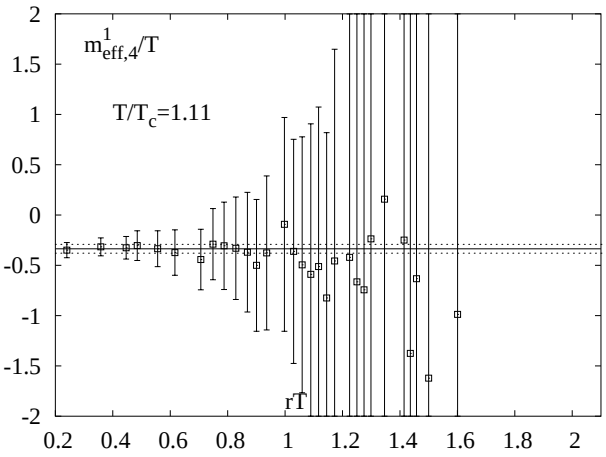

(b)

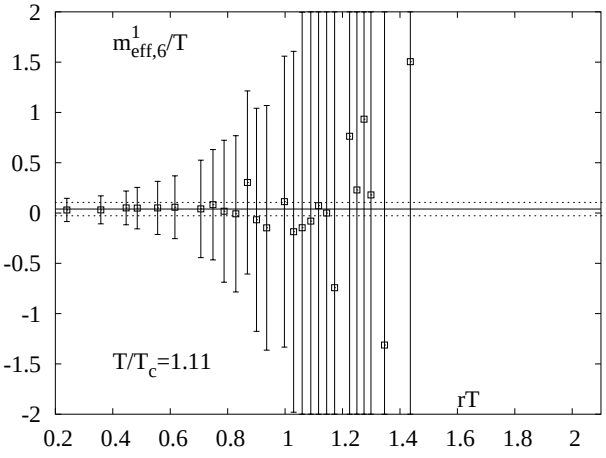

(c)

Figure 4.11: Example for the distance dependent effective masses converging at large distance to the expansion coefficients for the screening mass which are represented by the horizontal lines.

of the μ-dependent corrections to the screening masses. This is not the case for the leading order, μ-independent, contribution. In order to determine $m_0^1(T)$ we use an ansatz for the large distance behavior of the singlet free energy motivated by leading order high temperature perturbation theory,

$$f^1_{Q\bar{Q},0}(r,T) = f^1_{Q\bar{Q},0}(\infty,T) - \frac{4}{3}\frac{\alpha_0(T)}{r}e^{-m_0^1(T)r}. \tag{4.33}$$

We fit our data to this ansatz using $\alpha_0(T)$ and $m_0^1(T)$ as fit parameters where $f^1_{Q\bar{Q},0}(\infty,T)$ is determined as described in the previous section. We average results received from five fit windows with left borders between $rT = 0.8$ and $rT = 1.0$ and right border at $rT = 1.73$. While the above ansatz is known to describe rather well the large distance behavior of the color singlet free energy, it also is known [44, 48] that the sub-leading power-like corrections are much more difficult to control in the case of the color averaged free energy. For this reason we will analyze here only the leading order contribution to the singlet screening mass. Results for effective masses in the singlet channel are shown in fig. 4.11 as function of rT for one value of the temperature. As can be seen the asymptotic value is indeed reached quickly before the errors grow large at distances $rT \gtrsim 1$. The expansion coefficients $m_2^{\mathrm{av},1}(T)$, $m_4^{\mathrm{av},1}(T)$ and $m_6^{\mathrm{av},1}(T)$ are thus well determined from the plateau values of these ratios. Similar results hold in the color averaged channel. We found the left border of the plateau to lie between $rT = 0.48$ close to T_c and $rT = 0.23$ for $T > 1.15T_c$. Results for the various expansion coefficients are shown in fig. 4.12. This figure shows that at high temperatures the μ-dependent corrections to the screening mass of the color averaged free energies $m^{\mathrm{av}}(T,\mu)$ are twice as large as those of the (Debye) screening mass in the singlet channel, $m^1(T,\mu)$. This is expected from high temperature perturbation theory [48] , which suggests that the leading order contribution to the color singlet free energy is given by one gluon exchange while the color averaged free energy is dominated by two gluon exchange. Using resummed gluon propagators then leads to screening masses that differ by a factor of 2,

$$m_n^1(T) = \frac{1}{2}m_n^{\mathrm{av}}(T)\ , \quad n = 2,4,6\ , \tag{4.34}$$

Our results suggest that this relation holds already close to T_c (fig. 4.12). We thus have no evidence for large contributions from the magnetic sector, which is expected to dominate the screening in the color averaged channel at asymptotically large temperatures [49] and which would violate the simple relation given in (4.34).

In order to compare the expansion coefficients with perturbation theory we need to specify the running coupling $g(T)$. We use the next-to-leading order perturbative result for the running of the coupling with temperature but

allow for a free overall scale factor. We thus fit our data on the T-dependence of the leading order ($\mu = 0$) screening mass by the ansatz,

$$m_0^1(T) = A \cdot \frac{2}{\sqrt{3}} g(T) T \ , \tag{4.35}$$

with the 2nd order perturbative running coupling,

$$g(T)^2 = \left[\frac{29}{24\pi^2} \ln\left(\frac{\widetilde{\mu} T}{\Lambda_{\overline{MS}}} \right) + \frac{115}{232\pi^2} \ln\left(\ln\left(\frac{\widetilde{\mu} T}{\Lambda_{\overline{MS}}} \right) \right) \right]^{-1} \ , \tag{4.36}$$

where we use $T_c/\Lambda_{\overline{MS}} = 0.77(21)$ and the scale $\widetilde{\mu} = 2\pi$. Fitting our data to (4.35) with fit parameter A, yields

$$A \ = \ 1.397(18) \ . \tag{4.37a}$$

Our fit result is included in fig. 4.12. We also compare the temperature dependence of $m_2^1(T)$, $m_4^1(T)$ and $m_6^1(T)$ with corresponding expansion coefficients of the perturbative Debye mass which result from an expansion of (4.24) using (4.35) as the 0th order. These expansion coefficients are alternating in sign,

$$m_{D,2}(T) \ = \ \frac{\sqrt{3}}{4\pi^2} \cdot A g(T) \ , \tag{4.38a}$$

$$m_{D,4}(T) \ = \ -\frac{3\sqrt{3}}{64\pi^4} \cdot A g(T) \ , \tag{4.38b}$$

$$m_{D,6}(T) \ = \ \frac{9\sqrt{3}}{512\pi^6} \cdot A g(T) \ . \tag{4.38c}$$

At least for the second order coefficient $m_2^1(T)$ we find that this yields a satisfactory description of the numerical results for $T \gtrsim 2T_c$. (4.38) shows that subsequent terms differ by about an order of magnitude, which explains why our signal for a non-zero contribution $m_n^1(T)$ is rather poor for $n > 2$. From (4.38) we find $m_{D,2}(T)/m_{D,0}(T) = 3/8\pi^2$ which is independent of A and $g(T)$ and is compared with our numerical results in fig. 4.14(a). We note that the perturbative value for this ratio is already reached for $T/T_c \gtrsim 2$. In fig. 4.14(b) we show the μ-dependence of the singlet screening mass for a small values of μ/T. Here we included only contributions from the 0th and 2nd order expansion in the calculation of $m^1(\mu, T)/T$.

In order to further justify the procedure to extract the screening masses from our effective masses, which mainly are based on fractions of the free energies at rather short distances, we additionally performed fits over the full range of distances. Using an ansatz

$$\alpha(T, \mu) \ = \ \alpha_0(T) + \alpha_2(T) \left(\frac{\mu}{T} \right)^2 + \cdots + \alpha_6(T) \left(\frac{\mu}{T} \right)^6 + \mathcal{O}\left(\left(\frac{\mu}{T} \right)^8 \right) \ ,$$

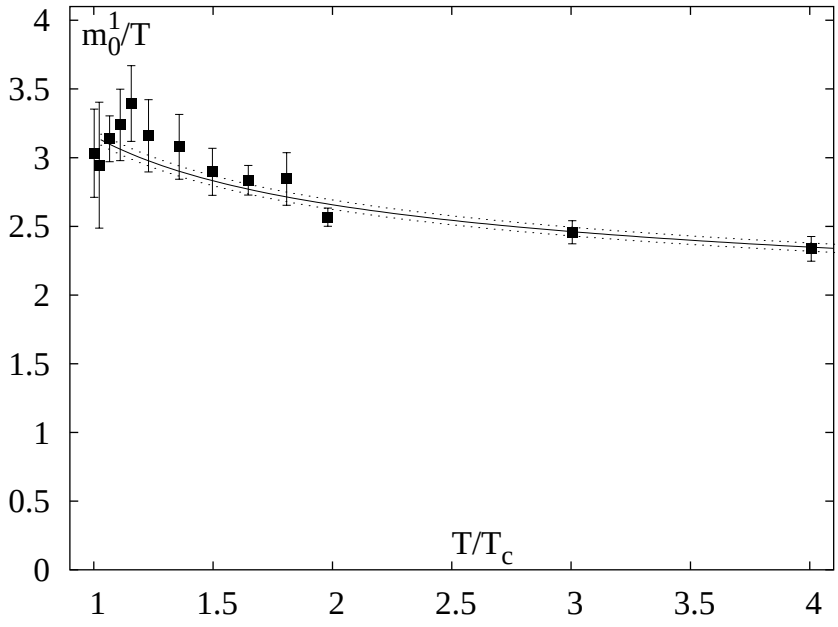

(a)

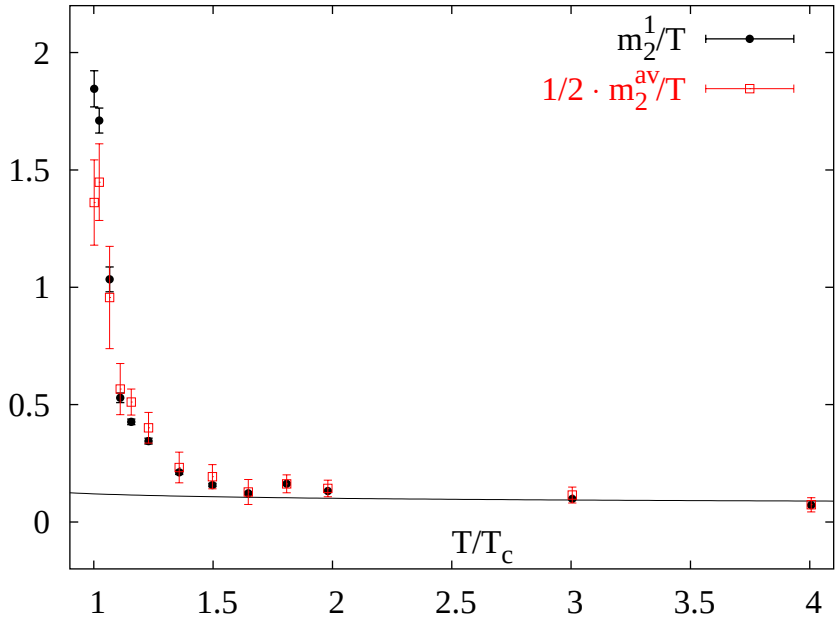

(b)

Figure 4.12: 0th and 2nd order expansion coefficients of screening masses in the color singlet (m^1) and color averaged (m^{av}) channels. $m_2^x(T)$ is determined from the $r \to \infty$ limit of (4.31). The lines are the first order perturbative predictions according to (4.38). The dotted lines in (a) show the 1σ-range of the χ^2-fit with parameter A.

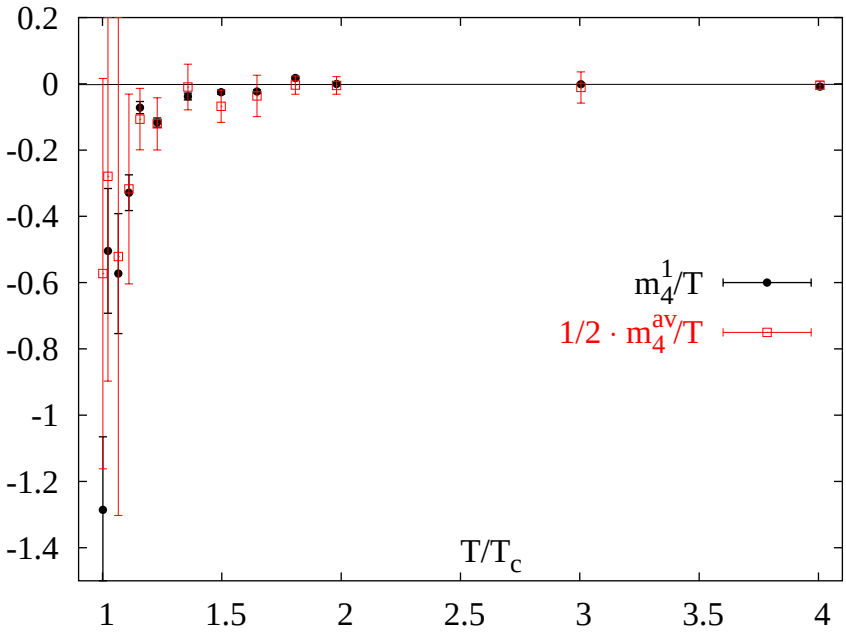

(a)

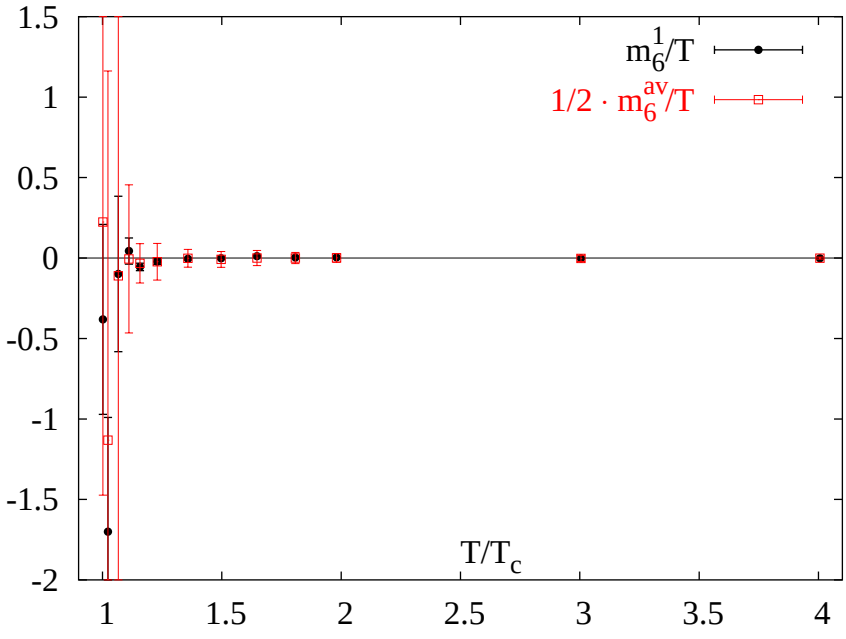

(b)

Figure 4.13: 4th and 6th order expansion coefficients of screening masses in the color singlet (m^1) and color averaged ($m^{\rm av}$) channels. $m_n^x(T)$ is determined from the $r \to \infty$ limit of (4.31). The lines are the first order perturbative predictions according to (4.38).

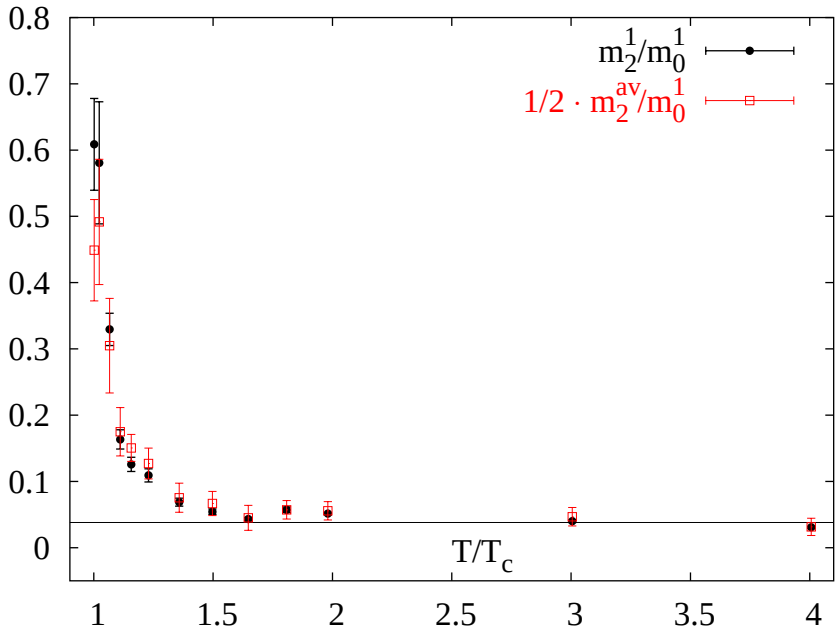

(a)

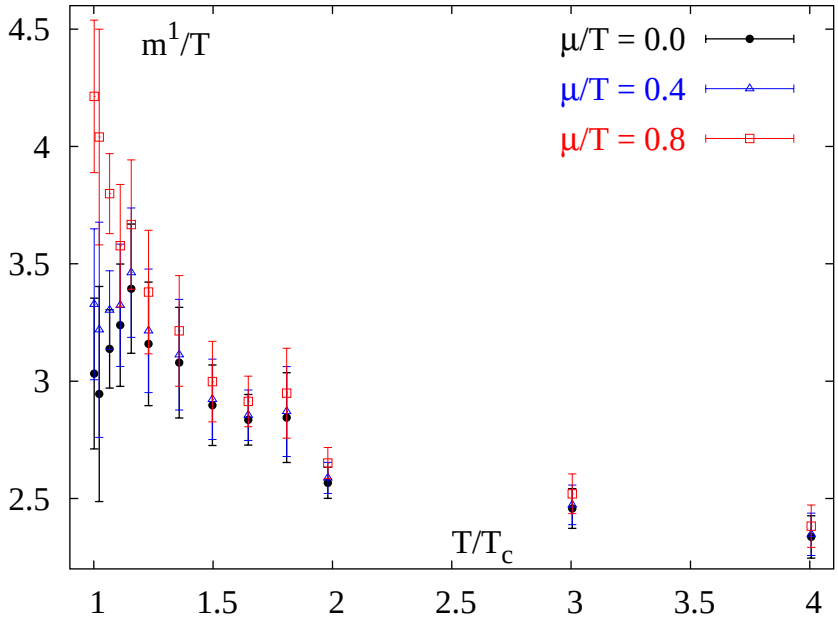

(b)

Figure 4.14: The ratio $m_2^x(T)/m_0^1(T)$ (a) and the screening mass $m^1(T)$ evaluated for $\mu/T = 0.0, 0.4$ and 0.8 including the 0^{th} and 2^{nd} order expansion coefficients in μ (b). The line in (a) shows the leading order perturbative prediction, which is $3/8\pi^2$.

and expanding (4.28) in powers of μ we get expressions for the higher order coefficients, i.e. for the second order

$$m_2^1(T) - \frac{c_2(T)}{r} = -\frac{1}{r}\frac{\Delta f^1_{Q\bar{Q},2}(r,T)}{\Delta f^1_{Q\bar{Q},0}(r,T)} ,$$

where

$$c_2(T) = \frac{\alpha_2(T)}{\alpha_0(T)} . \tag{4.39}$$

We use $m_2(T)$ and $c_2(T)$ as fit parameters. We choose to vary the left border of our fit window between the first and 9th value of the available distances where we find smooth plateaus. We compare the results obtained in this way (open squares in fig.4.15 (b)) to those of our previous analysis (closed circles). In fact there are almost no significant differences. Only close to the transition the results from the fits are slightly smaller. Unfortunately the fitting procedure suffers from large errors. Results for m_4 and m_6 remain consistent with zero.

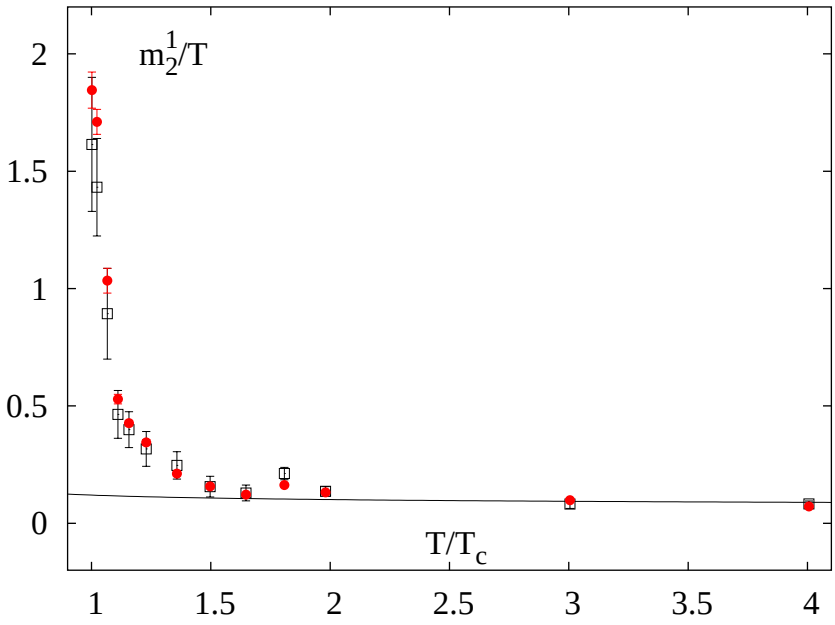

Figure 4.15: Comparison of the 2nd order coefficients obtained with the effective mass limit (closed circles) and with the fitting procedure (open squares).

4.5 The μ, T-dependence of the Polyakov loop

In contrast to the free energies discussed so far the trace of the Polyakov loop

$$\operatorname{tr} L \equiv \frac{1}{N_\sigma^3 N_\tau} \sum_{\boldsymbol{x}} \operatorname{tr} L(\boldsymbol{x}) \tag{4.40}$$

is not exclusively real but is in general a complex quantity. Anyhow in full QCD the expectation value $P_0 = \langle \operatorname{tr} L \rangle$ at $\mu = 0$ is real. In fact we find the imaginary parts of all the μ-expansion coefficients to be non-uniform and vanishing within statistical errors.
We write the expansion of the renormalized Polyakov loop as

$$\langle \operatorname{tr} L \rangle_\mu = P_0 + P_1 \frac{\mu}{T} + P_2 \left(\frac{\mu}{T}\right)^2 + P_3 \left(\frac{\mu}{T}\right)^3 + \cdots \,, \tag{4.41}$$

where we assume $P_0, P_1, \cdots$ to be real. The results are shown in fig. 4.16 to 4.18.
The 0th order P_0 in fig. 4.16 is the $\mu = 0$ Polyakov loop, which is an order parameter for the deconfining phase transition in the quenched approximation. We note that $\langle \operatorname{tr} L \rangle$ is not restricted to values below 1 due to the multiplication with the renormalization constant $Z(g^2)$. The higher orders are multiplied with the same constant.
All the higher order coefficients show large peaks close to or at T_c and tend quickly towards zero or at least to comparatively small values for $T > T_c$. At least for the coefficients of order 0,1,2 and maybe 3 we find specific algebraic signs.

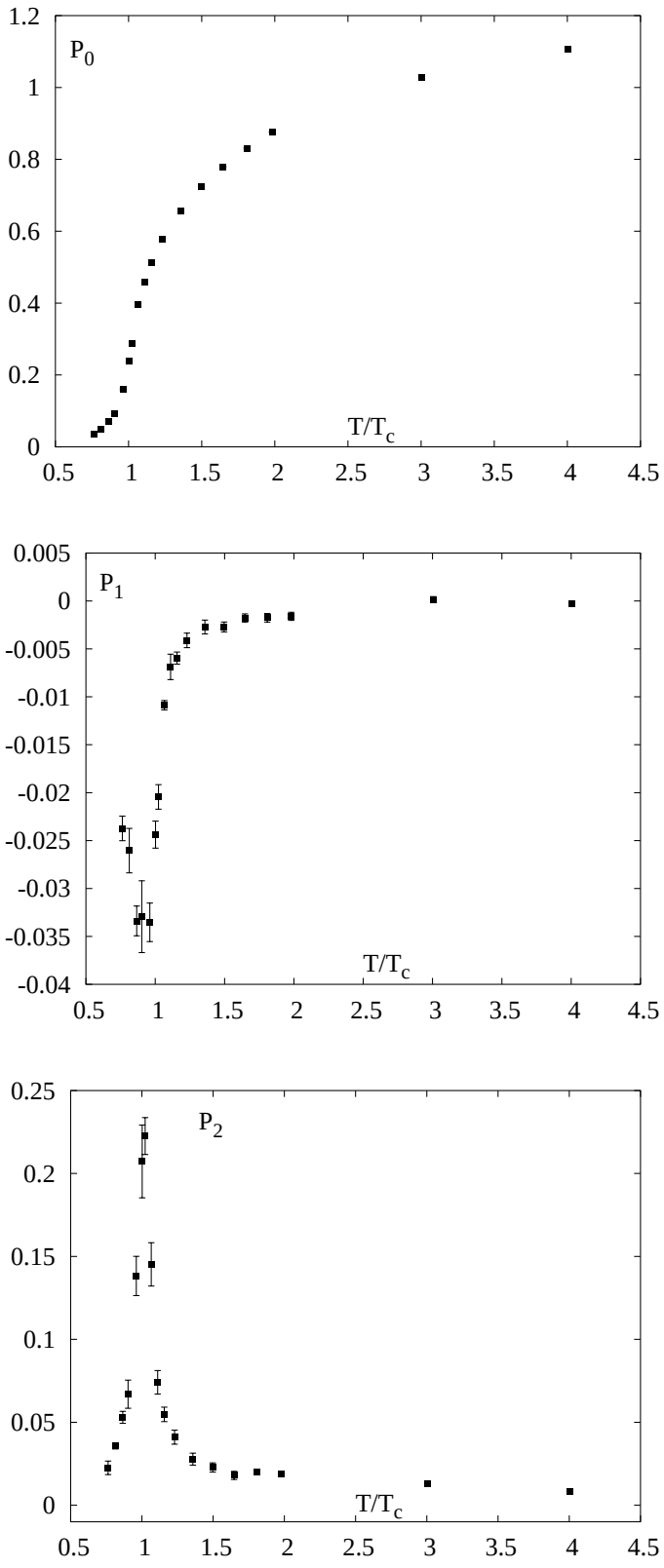

Figure 4.16: Lowest orders of the renormalized Polyakov loop

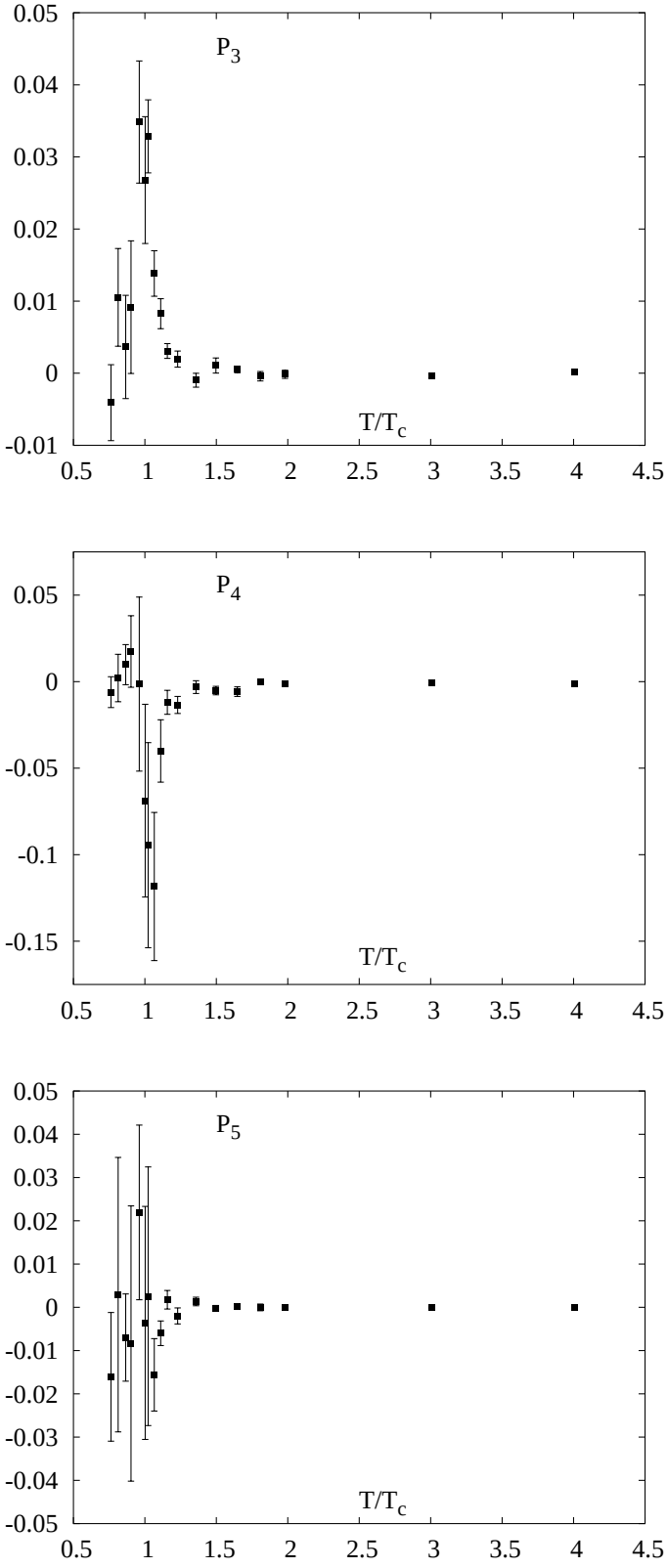

Figure 4.17: 3rd, 4th and 5th order of the Polyakov loop

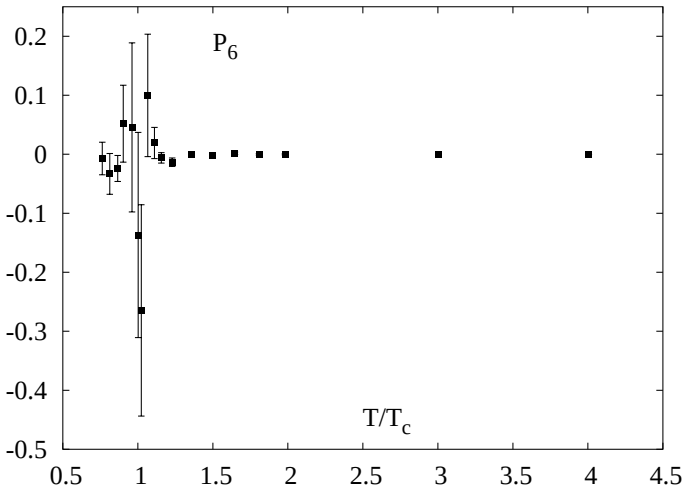

Figure 4.18: 6th order of the Polyakov loop

The logarithm of the expectation value of the renormalized Polyakov loop is related to the free energy of a single heavy quark.

$$F_Q(T,\mu) = -T \ln \left(\langle \, \mathrm{tr} L \, \rangle_\mu \right) . \tag{4.42}$$

We insert the expansion of the Polyakov loop (4.41) into this equation. Then the free energy has the form

$$\begin{aligned} F_Q(T,\mu) &= f_{Q,0}(T) + f_{Q,1}\frac{\mu}{T} + f_{Q,2}\left(\frac{\mu}{T}\right)^2 + f_{Q,3}\left(\frac{\mu}{T}\right)^3 + f_{Q,4}\left(\frac{\mu}{T}\right)^4 \\ &\quad + f_{Q,5}\left(\frac{\mu}{T}\right)^5 + f_{Q,6}\left(\frac{\mu}{T}\right)^6 + \mathcal{O}\left(\left(\frac{\mu}{T}\right)^7\right) , \end{aligned} \tag{4.43}$$

where

$$\begin{aligned} \frac{f_{Q,0}(T)}{T} &= -\ln P_0 \, , \\ \frac{f_{Q,1}(T)}{T} &= -\frac{P_1}{P_0} \, , \\ \frac{f_{Q,2}(T)}{T} &= -\frac{P_2 P_0 - \frac{1}{2} P_1^2}{P_0^2} \, , \\ \frac{f_{Q,3}(T)}{T} &= -\frac{P_3 P_0^2 - P_2 P_1 P_0 + \frac{1}{3} P_1^3}{P_0^3} \, , \\ \frac{f_{Q,4}(T)}{T} &= -\frac{P_4 P_0^3 - P_3 P_1 P_0^2 - \frac{1}{2} P_2^2 P_0^2 + P_2 P_1^2 P_0 - \frac{1}{4} P_1^4}{P_0^4} \, , \\ \frac{f_{Q,5}(T)}{T} &= -\frac{\begin{array}{c} P_5 P_0^4 - P_4 P_1 P_0^3 - P_3 P_2 P_0^3 + P_3 P_1^2 P_0^2 \\ + P_2^2 P_1 P_0^2 - P_2 P_1^3 P_0 + \frac{1}{5} P_1^5 \end{array}}{P_0^5} \, , \\ \frac{f_{Q,6}(T)}{T} &= -\frac{\begin{array}{c} P_6 P_0^5 - P_5 P_1 P_0^4 - P_4 P_2 P_0^4 + P_4 P_1^2 P_0^3 - \frac{1}{2} P_3^2 P_0^4 - \frac{1}{6} P_1^6 \\ + 2 P_3 P_2 P_1 P_0^3 - P_3 P_1^3 P_0^2 + \frac{1}{3} P_2^3 P_0^3 - \frac{3}{2} P_2^2 P_1^2 P_0^2 + P_2 P_1^4 P_0 \end{array}}{P_0^6} \, . \end{aligned} \tag{4.44}$$

For a heavy anti-quark we have

$$\langle \, \mathrm{tr} L^\dagger \, \rangle_\mu = \langle \, \mathrm{tr} L \, \rangle^*_{-\mu} . \tag{4.45}$$

We conclude that the expansion coefficients of the quark free energy $F_Q(T,\mu)$ and the anti-quark free energy $F_{\bar{Q}}(T,\mu)$ are equal for even orders and have opposite sign for odd orders

$$f_{\bar{Q},n}(T) = (-1)^n f_{Q,n}(T) \, . \tag{4.46}$$

Results for the $f_{Q,n}(T)$ are shown in fig. 4.19 to 4.21. We also compare them to the infinite distance limit of the QQ-free energies which are discussed in

the next section. Namely for infinite separation of two heavy quarks we should have twice the free energy of a single quark

$$F^x_{QQ}(\infty, T, \mu) = 2F_Q(T, \mu) \; . \tag{4.47}$$

We confirm that this relation holds to all orders. The infinite distance values were determined in the same way as in the $Q\bar{Q}$ case. Deviations from (4.47) occur because the asymptotic values are not always reached within the accessible distance range. In general the sextet free energies are more consistent with the single heavy quark free energies, because they show only little dependence on the distance.
We also note that the asymptotic values of the free energies $F^x_{Q\bar{Q}}(\infty, T, \mu)$ are consistent with the corresponding relation

$$F^x_{Q\bar{Q}}(\infty, T, \mu) = F_Q(T, \mu) + F_{\bar{Q}}(T, \mu) \tag{4.48}$$

This holds for all orders in μ. So for all values of T and μ we have that the asymptotic values of the free energies of heavy quarks and/or anti-quarks in some color state are equal to the free energies of the corresponding single quarks and anti-quarks.

From (4.1) we can see that for the net number of light sea quarks N_q, i.e. the difference of quarks and anti-quarks, we have

$$\frac{\partial \Delta F^x_{n,m}}{\partial \mu} = -\left(\langle N_q \rangle^x_{n,m} - \langle N_q \rangle_{0,0} \right) \; , \tag{4.49}$$

where $\langle \cdots \rangle^x_{n,m}$ is the ensemble average of a system containing n heavy quarks and m heavy anti-quarks in the state x. Then

$$\Delta N_q = N_q - \langle N_q \rangle_{0,0} \; . \tag{4.50}$$

can be understood as the change in the light quark number that is caused by the presence of the heavy quarks. For one single heavy quark the ensemble average of N_q is

$$\langle \Delta N_q \rangle_\mu = -\frac{\partial F_Q}{\partial \mu} = -f_{Q,1}\frac{1}{T} - 2f_{Q,2}\frac{\mu}{T^2} - \mathcal{O}(\mu^2) \; . \tag{4.51}$$

Because $f_{Q,1}$ is positive we expect the light anti-quarks to dominate the quarks for small values of μ,

$$\langle \Delta N_q \rangle_\mu < 0 \; . \tag{4.52}$$

Thus the presence of a heavy test quark will induce the supply with anti-quarks from the particle reservoir.
The lowest order of the light quark number susceptibility $f_{Q,2}$ is related

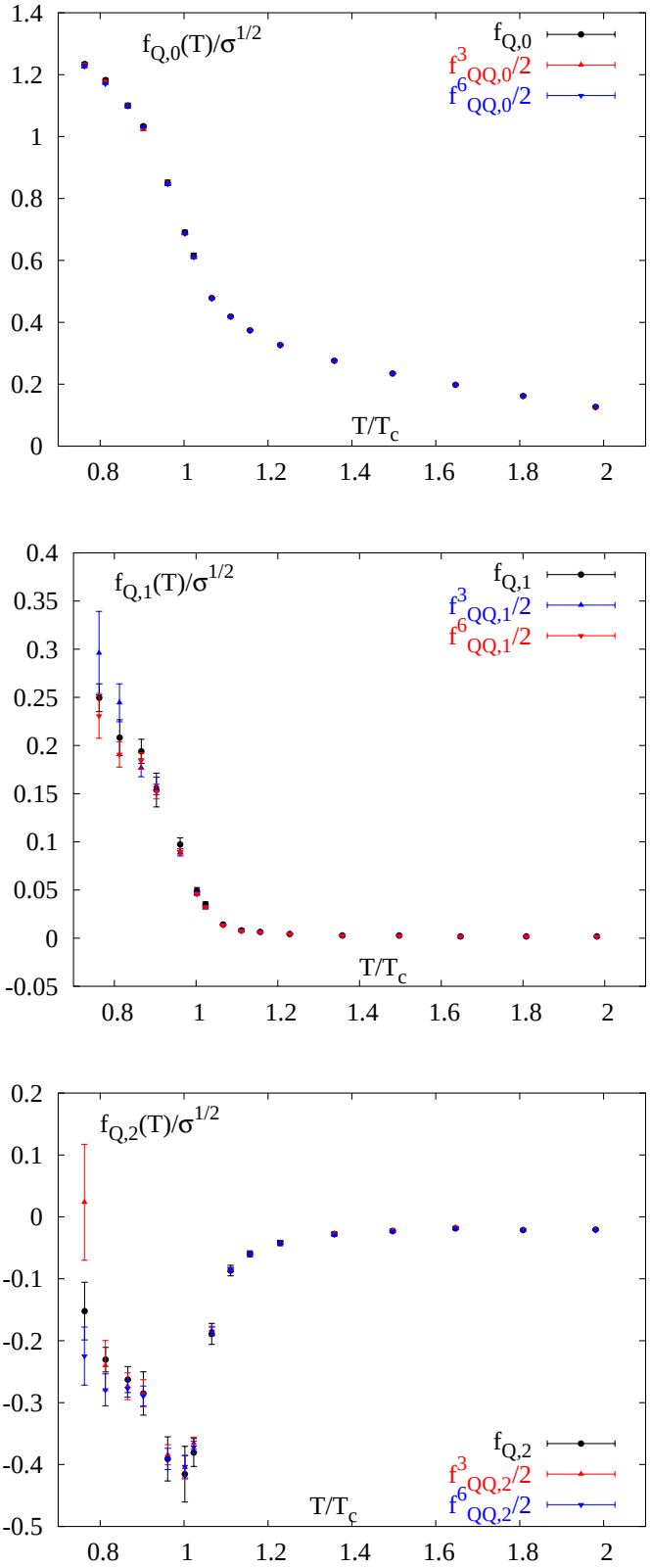

Figure 4.19: 0th, 1st and 2nd order coefficients of the free energy of a single heavy quark calculated from the Polyakov loop (black circles) and from anti-triplet (red triangles) and sextet (blue triangles) free energies of a QQ-pair at infinite distance.

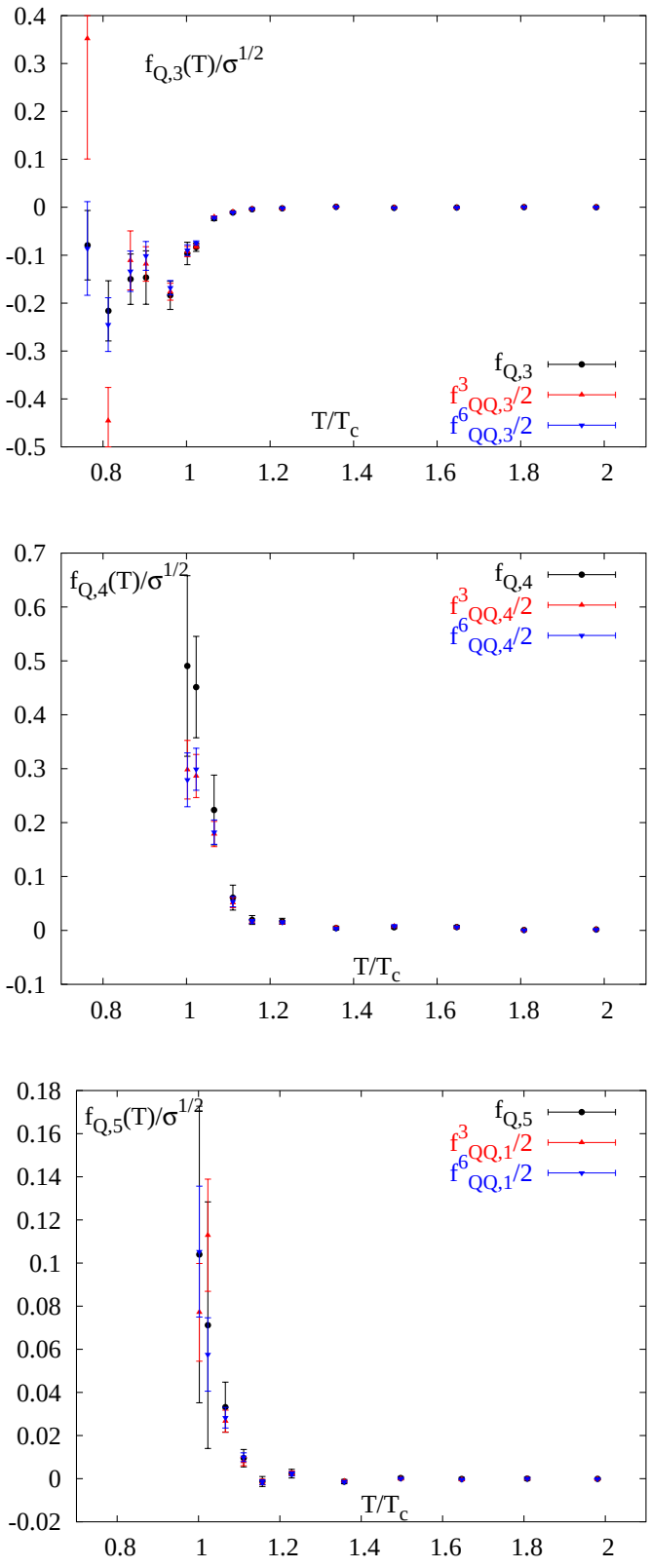

Figure 4.20: 3rd, 4th and 5th order coefficients of the free energy of a single heavy quark.

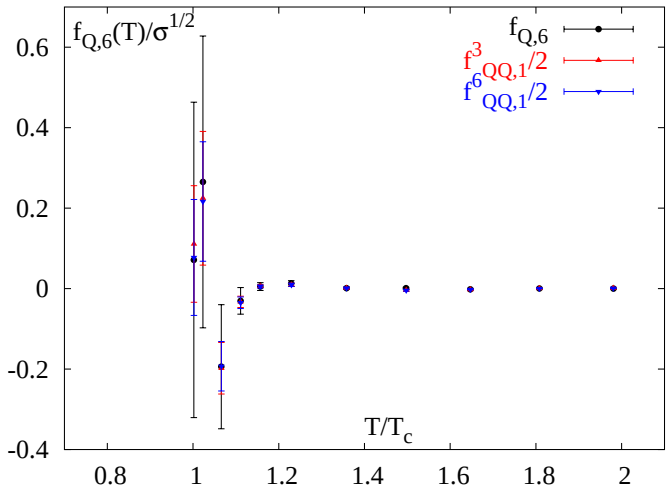

Figure 4.21: 6th order coefficients of the free energy of a single heavy quark.

to the fluctuations in the light quark number which become large at the transition point, namely we have

$$\left\langle \Delta N_q^2 \right\rangle_\mu - \left\langle \Delta N_q \right\rangle^2 = -\frac{1}{T}\frac{\partial^2 F_Q}{\partial \mu^2} = -2\,\frac{f_{Q,2}}{T^3} - \mathcal{O}(\mu)\ . \tag{4.53}$$

Looking at the higher order coefficients, we observe that the diagrams of $f_{Q,0}$ and $f_{Q,1}$ (fig. 4.19) are similar in sign and shape. The same is true for $f_{Q,2}$ and $f_{Q,3}$ (figs. 4.19 and 4.20) as well as for $f_{Q,4}$ and $f_{Q,5}$ (fig. 4.20). In general the signs of the coefficients seem to change every two orders.
From perturbation theory we expect that the free energy of a single heavy quark is proportional to the product of the Debye mass and the square of the coupling [50].

$$F_Q(T,\mu) \propto -m(T,\mu)\cdot g(T)^2\ , \tag{4.54}$$

where we assume only a small or no dependence of the coupling g on μ. Hence the coefficients $f_{Q,n}(T)$ should show a similar asymptotic behavior as a function of T as the corresponding screening mass coefficients. A comparison of figs. 4.12 and 4.13 to the even orders in 4.19, 4.20 and 4.21 supports this picture. Namely the 0th orders are both monotonically decreasing. The 2nd orders are decreasing very slowly and still show a finite value even at large temperatures and the 4th and 6th orders are both consistent with zero for $T > 2T_c$.

4.6 Free energies of two heavy quarks

In the absence of a quark reservoir any state of a medium with two heavy quarks has got the triality

$$t \equiv N \bmod 3 = 2 \; . \tag{4.55}$$

Here N is the total quark number which is the difference of the number of quarks and anti-quarks. Therefore no bound states exist and the partition function is $Z_{QQ} = 0$. Nevertheless in the grand-canonical case the two heavy quarks may take up additional light quarks or anti-quarks from the quark reservoir to form triality zero states. Then the partition function is non-zero $Z_{QQ} \neq 0$ and the free energy is finite.
I.e. we will consider the free energy calculated from the color averaged Polyakov loop correlation function

$$C^{\rm av}(r) = \frac{1}{\mathcal{N}} \sum_{\boldsymbol{x},\boldsymbol{y}} {\rm tr} L(\boldsymbol{x}) {\rm tr} L(\boldsymbol{y}) \; , \tag{4.56}$$

where the sum refers to all pairs of sites with distance r.
Furthermore the decomposition of the color states of heavy diquarks into irreducible representations leads to an anti-triplet and a sextet part. The corresponding Polyakov loop correlation functions are

$$C^{\bar{3}}(r) = \frac{1}{\mathcal{N}} \sum_{\boldsymbol{x},\boldsymbol{y}} \frac{3}{2} {\rm tr} L(\boldsymbol{x}) {\rm tr} L(\boldsymbol{y}) - \frac{1}{2} {\rm tr} \left(L(\boldsymbol{x}) L(\boldsymbol{y}) \right) \; , \tag{4.57}$$

$$C^{6}(r) = \frac{1}{\mathcal{N}} \sum_{\boldsymbol{x},\boldsymbol{y}} \frac{3}{4} {\rm tr} L(\boldsymbol{x}) {\rm tr} L(\boldsymbol{y}) + \frac{1}{4} {\rm tr} \left(L(\boldsymbol{x}) L(\boldsymbol{y}) \right) \; , \tag{4.58}$$

These correlation functions are related via

$$C^{\rm av}(r) = \frac{1}{3} C^{\bar{3}}(r) + \frac{2}{3} C^{6}(r) \; . \tag{4.59}$$

The corresponding free energies are calculated and expanded in powers of μ/T in the same way as for the Polyakov loop.

$$\begin{aligned} F_{QQ}^{{\rm av},\bar{3},6}(r,T,\mu) &= -T \ln \left\langle C^{{\rm av},\bar{3},6}(r) \right\rangle_{T,\mu} \\ &= f_{QQ,0}^{{\rm av},\bar{3},6}(r,T) + f_{QQ,1}^{{\rm av},\bar{3},6}(r,T) \frac{\mu}{T} + \cdots \end{aligned} \tag{4.60}$$

In figs. 4.22 and 4.23 we show the r-dependent 0th order coefficients of the free energies. Figs. 4.24 to 4.32 contain the higher orders of the free energies $F_{QQ}^{\bar{3}}$ and F_{QQ}^{6} up to 6th order in μ/T. We do not show the higher orders of the color averaged free energy explicitly here. In fact they are all very similar to the anti-triplet coefficients.

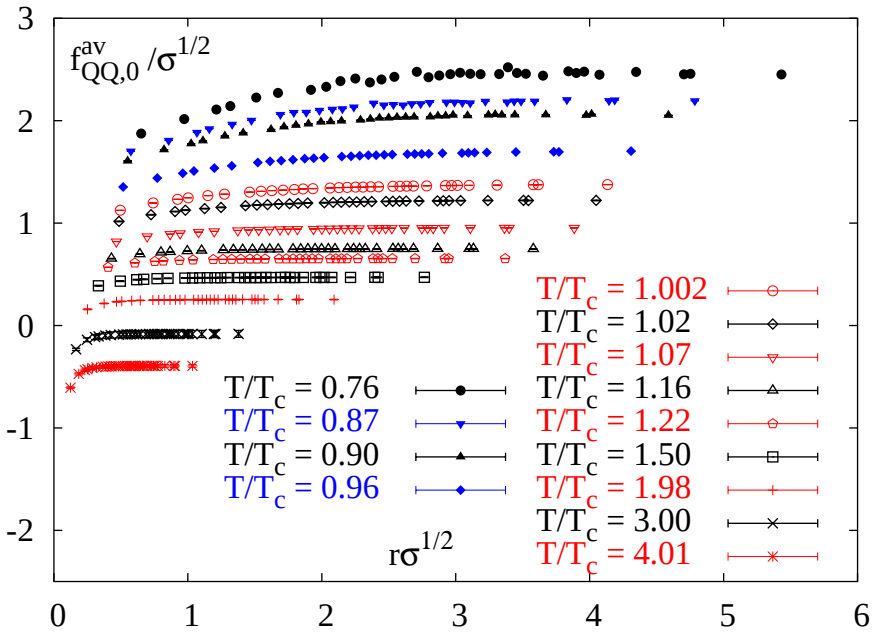

Figure 4.22: 0th order coefficient of the color averaged free energy calculated from the Polyakov loop correlations.

The 0th order shows that the potential between heavy quarks is attractive in the color averaged or anti-triplet and repulsive in the sextet state.
As in the case of a single heavy quark we also see a non-vanishing 1st order contribution to the heavy diquark free energies. The amplitude of the coefficients $f^{3,6}_{QQ,1}$ get smaller with increasing temperature. While the sextet coefficient $f^{6}_{QQ,1}$ is always positive and approaches the asymptotic cluster value very quickly, the anti-triplet coefficient is negative for very small distances and changes the sign at some intermediate distance r_* between $r\sigma^{1/2} = 1$ and $r\sigma^{1/2} = 1.5$. The position of the null $r_*\sigma^{1/2}$ shows only little dependence on the temperature. If at all then the data suggest that $r_*\sigma^{1/2}$ tends to smaller values with increasing temperature.
According to (4.49) we may interpret this change of sign in the following way. If μ is small or even zero and if the two heavy quarks are very close to each other, the particle reservoir provides the system with additional light quarks such that

$$\left\langle \Delta N_q^{\mathrm{av},3} \right\rangle_\mu = -\frac{f^{\mathrm{av},3}_{QQ,1}}{T} + \mathcal{O}(\mu) > 0 \,. \tag{4.61}$$

Here $\Delta N_q^{\mathrm{av},3}$ is the number of light quarks in the color averaged and anti-triplet case respectively. This behavior is different from the $\bar{Q}Q$-system

where $\left\langle \Delta N_q^x \right\rangle_\mu = 0$ for $\mu = 0$ with $x = \mathrm{av}, 1$.
The two heavy quarks try to form a triality zero state with one of the provided light quarks. If on the other hand the QQ-separation becomes very large, the formation of a baryon is unlikely. In this case the two heavy quarks try to build two mesonic states with anti-quarks from the particle reservoir. This is why we observe a negative total light quark number in the system even if the value of μ is positive but small.

$$\left\langle \Delta N_q^{\mathrm{av},3} \right\rangle_\mu < 0 \,. \tag{4.62}$$

In fig. 4.34 the first order coefficients of the color averaged free energies are shown in units of the temperature. Because of eq. (4.61) $-f_1/T$ is just the light quark number at $\mu = 0$. In fig. 4.35 we show the light quark number at $\mu = 0$ for the smallest available separation r_0 and for the infinite separation of the QQ-pair. We see, that the light quark number is consistent with the assumption that in the limit $T \to 0$, the QQ-pair in a color averaged or anti-triplet state picks up exactly one light quark if r is small and picks up exactly two light anti-quarks if r becomes infinite.
For a diquark in a sextet state this consideration does not hold. At least for temperatures above T_c the sextet free energy is not only repulsive in the 0th order but a medium with anti-quarks is always preferred by the sextet QQ-pair. The reason is, that the formation of a color singlet state made up of a diquark in a sextet and a third quark in a triplet state is impossible. This is due to the reduction rule

$$\mathbf{3} \otimes \mathbf{6} = \mathbf{8} \oplus \mathbf{10} \,. \tag{4.63}$$

On the other hand a color singlet does exist if the diquark is a color anti-triplet

$$\mathbf{3} \otimes \bar{\mathbf{3}} = \mathbf{1} \oplus \mathbf{8} \,. \tag{4.64}$$

The question of the binding properties of the sextet QQ-pair below T_c remains still open.
Because the absolute value of $f_{QQ,2}^{3,6}$ is maximum at T_c we conclude that the fluctuations in the light quark number are largest at T_c, namely we have

$$\begin{aligned} \left\langle \left(\Delta N_q^{\mathrm{av},3,6}\right)^2 \right\rangle_\mu - \left\langle \Delta N_q^{\mathrm{av},3,6} \right\rangle^2 &= -\frac{1}{T} \frac{\partial^2 F_{QQ}^{\mathrm{av},3,6}}{\partial \mu^2} \,, \\ &= -2\, \frac{f_{QQ,2}^{\mathrm{av},3,6}}{T^3} - \mathcal{O}(\mu) \,, \end{aligned} \tag{4.65}$$

which is always positive for small μ.
The third order coefficients $f_{QQ,3}^{3,6}$ have the opposite sign of the first order coefficients and the fourth order coefficients $f_{QQ,4}^{3,6}$ have the opposite sign of

the second order ones. This holds both for anti-triplet and sextet coefficients. 5th and 6th order result have the same signs as the 1st and 2nd order respectively. The coefficients of order greater than one seem to follow the rule of thumb that the sign flips whenever the order is increased by two.
The large distance asymptotic values of the coefficients are determined by fitting the values over the five largest distances to a constant. The results are included in figs. 4.19 to 4.21. They are consistent with the free energies of two single heavy quarks.
In fig. 4.33 we show the free energies at T_c for typical values of $\mu = 0.4$ and $\mu = -0.4$ compared to the $\mu = 0$ case. We include all available orders from 0 to 6 in this calculation. For other temperatures than T_c the μ-effects are smaller. We see that the free energy gets lowered as in the $Q\bar{Q}$-case because the main contribution stems from the second order in μ/T. Nevertheless the first order leads to a significant difference between positive and negative quark chemical potential.

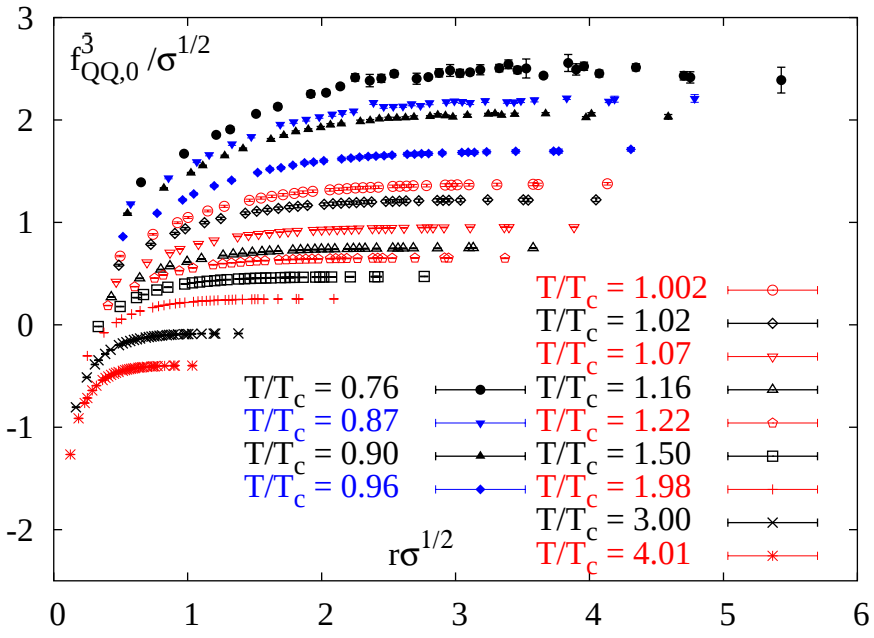

(a)

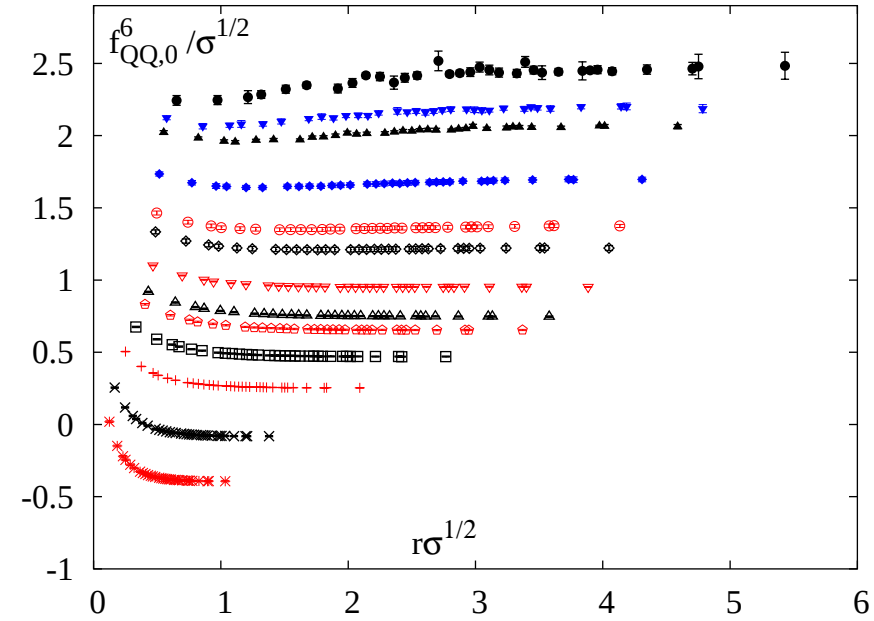

(b)

Figure 4.23: 0th order coefficients of the antitriplet and sextet color free energy calculated from the Polyakov loop correlations.

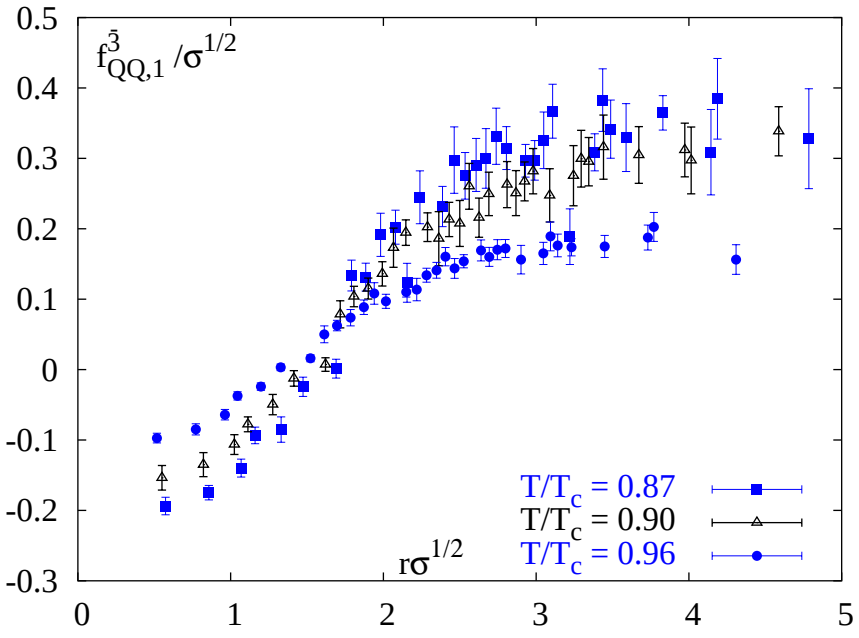

(a)

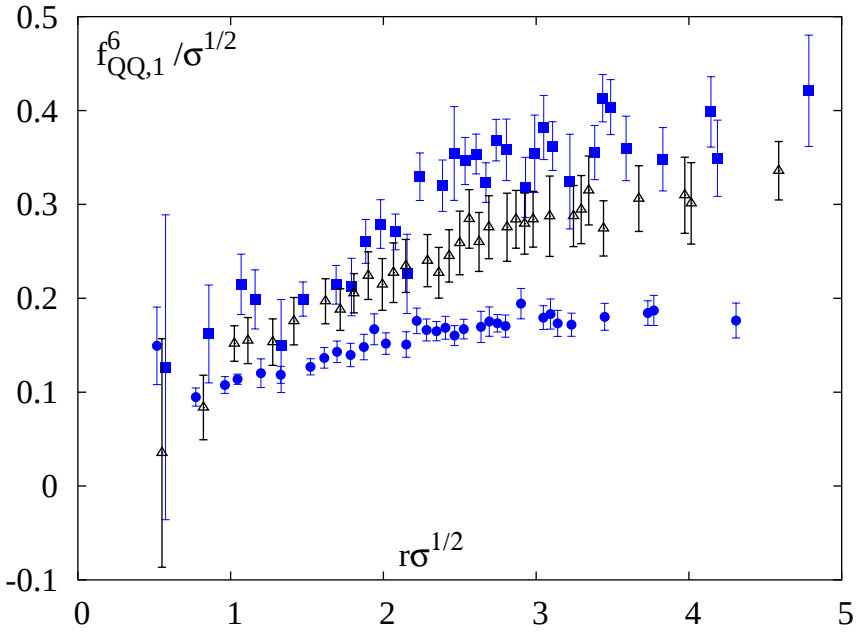

(b)

Figure 4.24: First order correction of heavy quark-quark free energies below T_c.

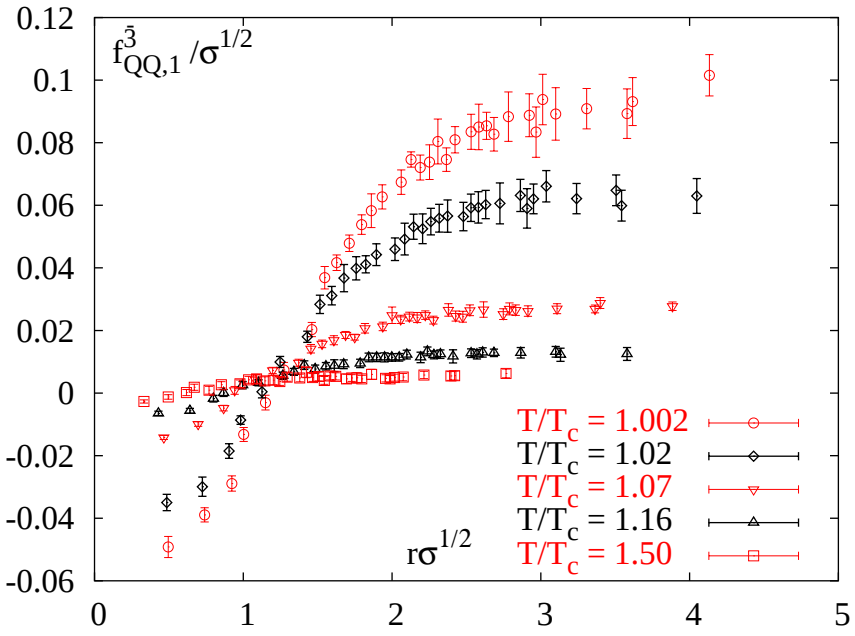

(a)

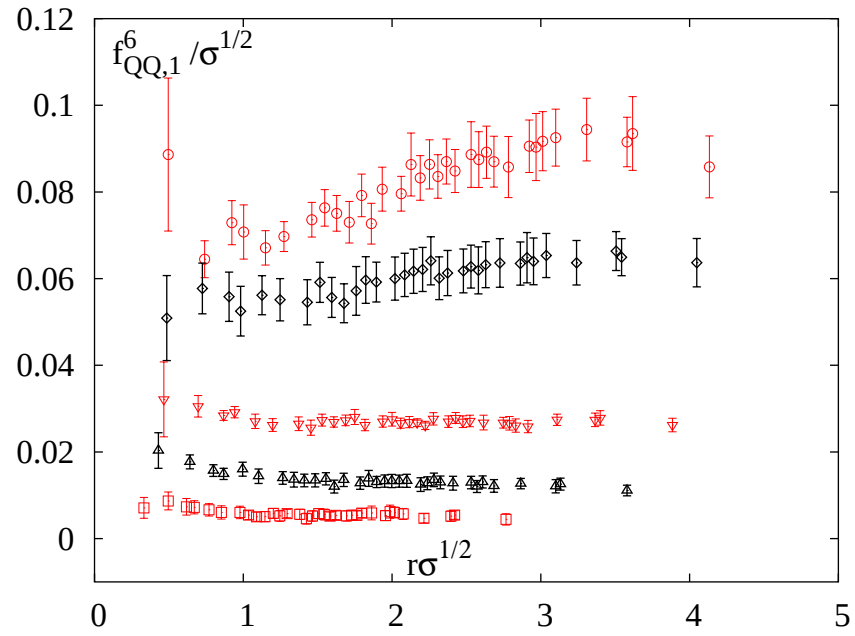

(b)

Figure 4.25: First order correction of heavy quark-quark free energies above T_c.

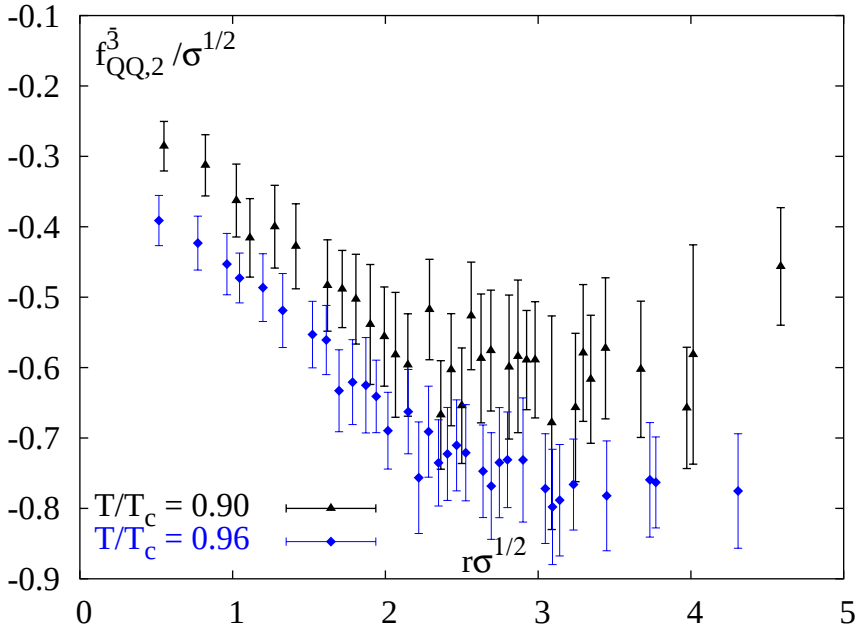

(a)

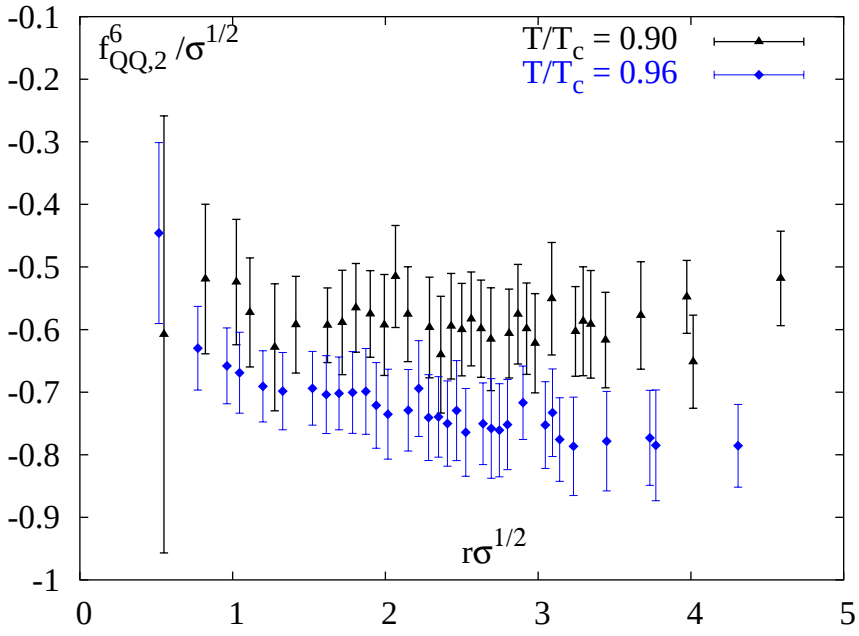

(b)

Figure 4.26: Second order correction of heavy quark-quark free energies below T_c.

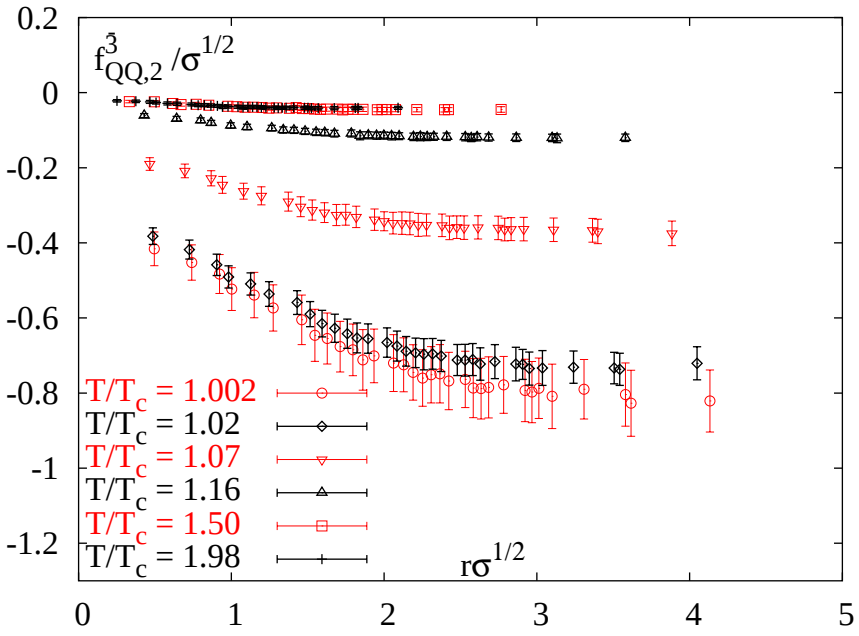

(a)

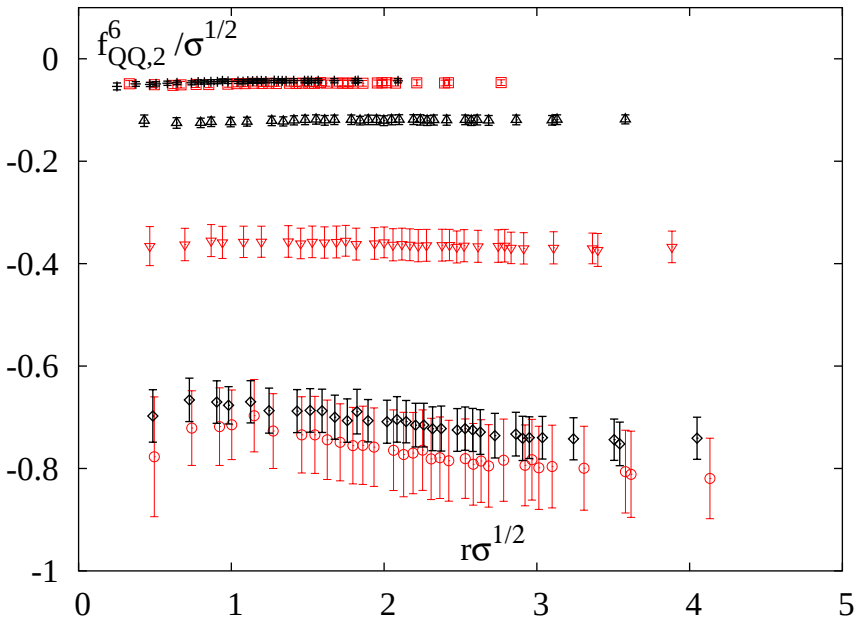

(b)

Figure 4.27: Second order correction of heavy quark-quark free energies above T_c.

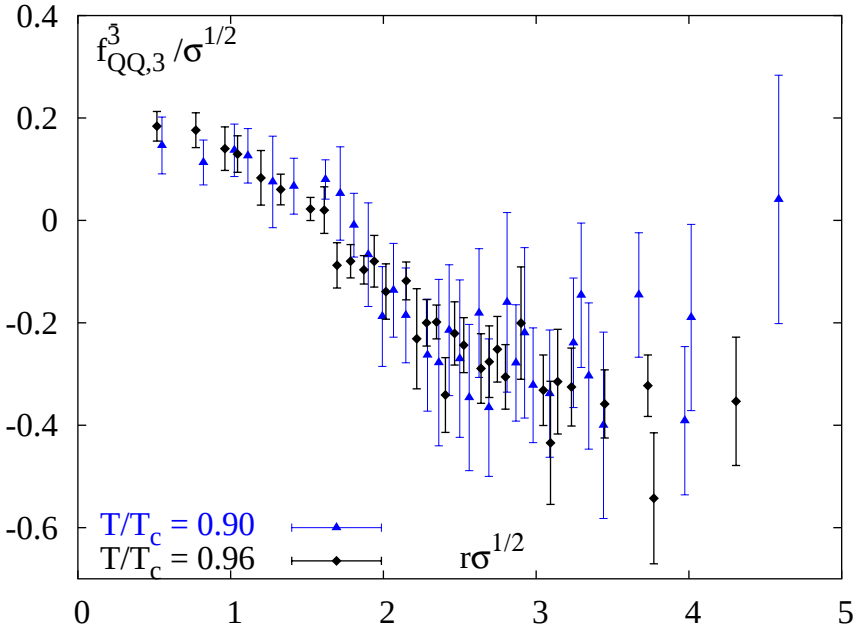

(a)

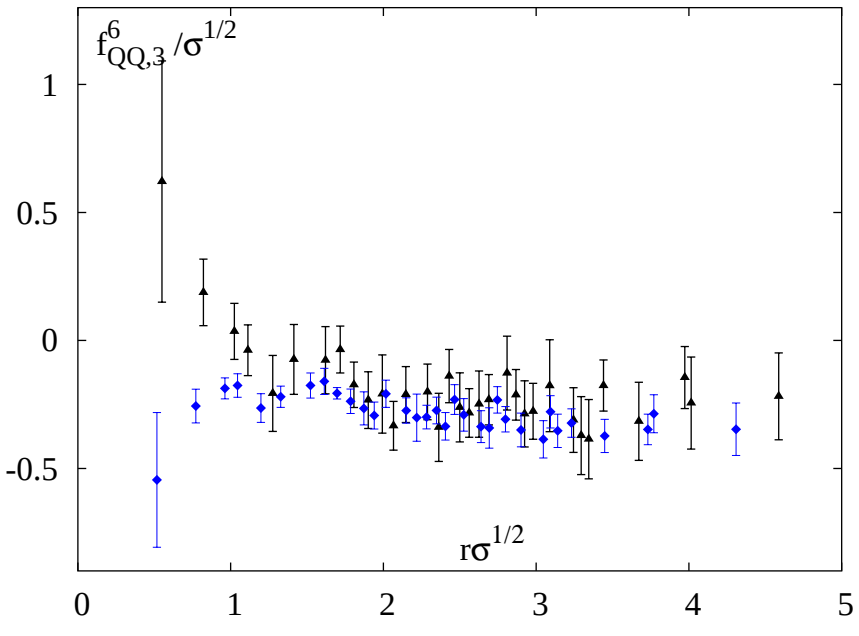

(b)

Figure 4.28: 3rd order correction of heavy quark-quark free energies below T_c.

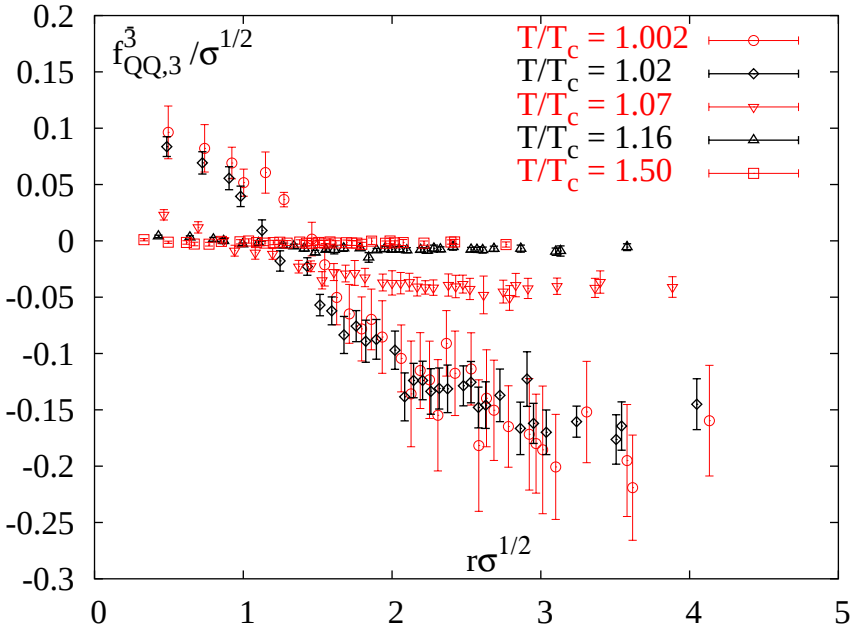

(a)

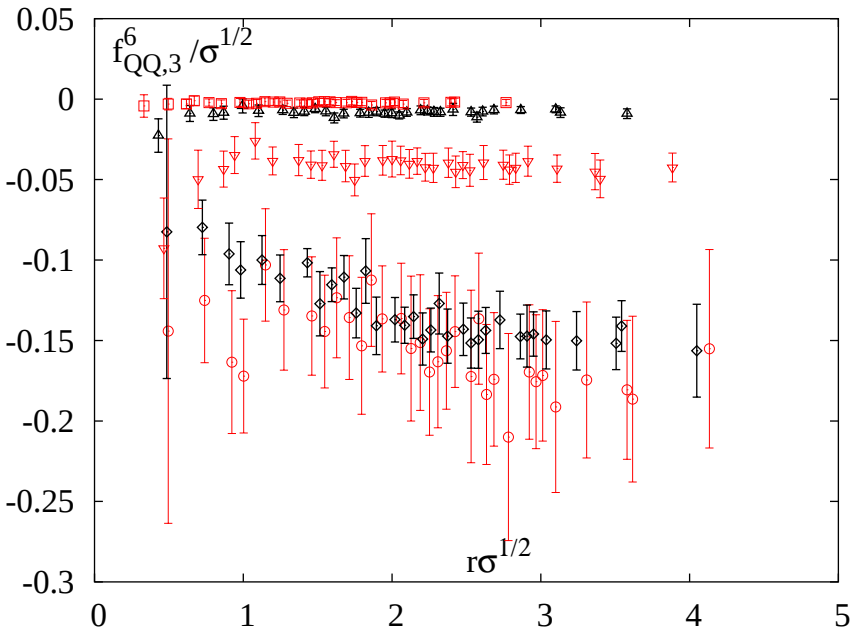

(b)

Figure 4.29: 3rd order correction of heavy quark-quark free energies above T_c.

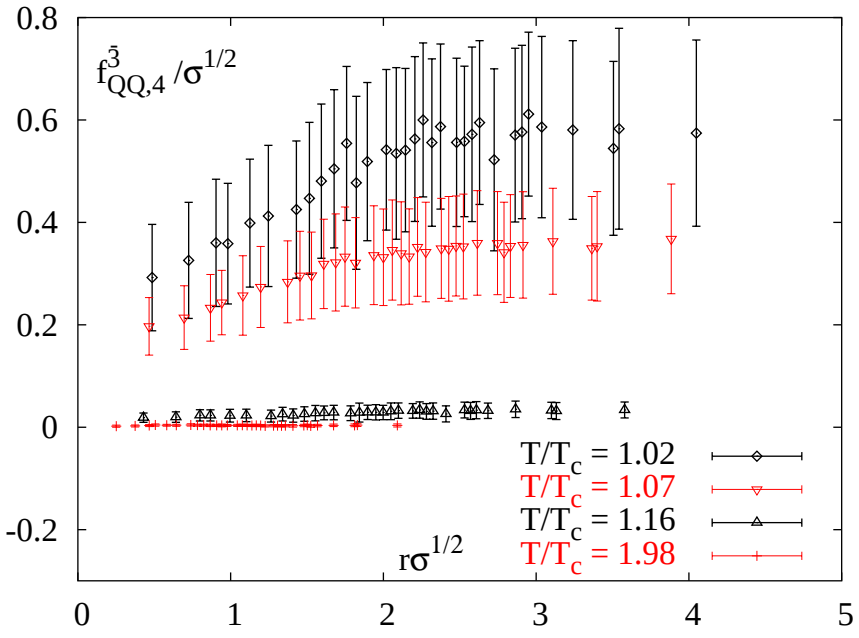

(a)

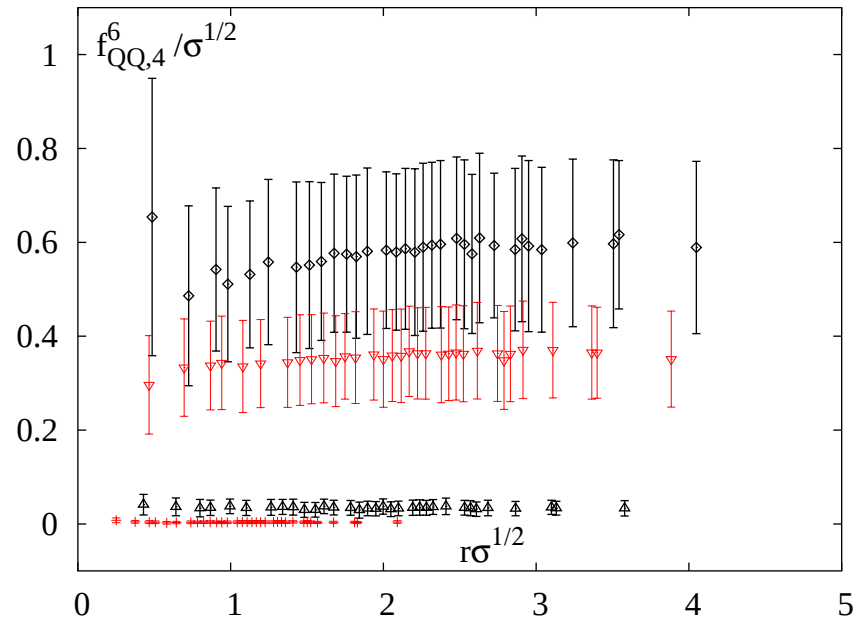

(b)

Figure 4.30: 4th order correction of heavy quark-quark free energies above T_c.

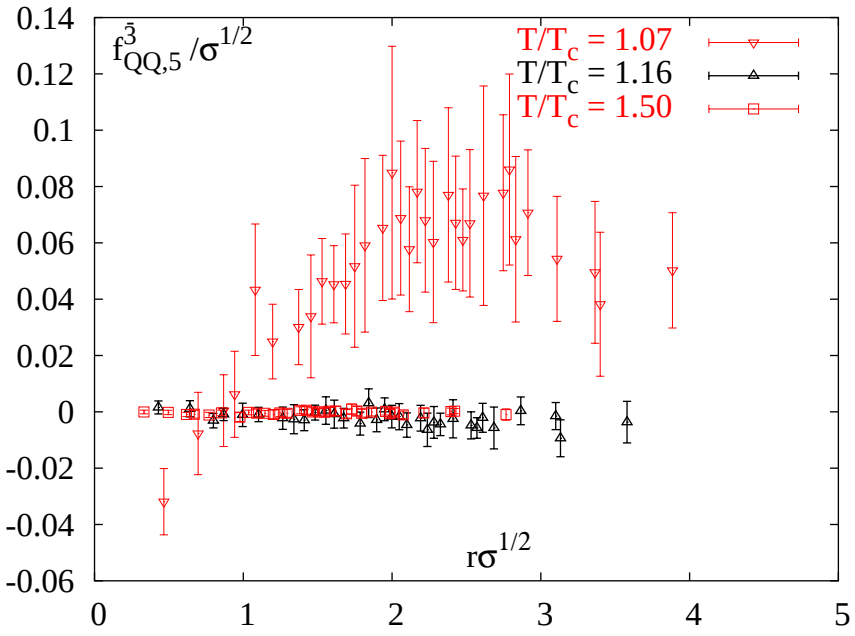

(a)

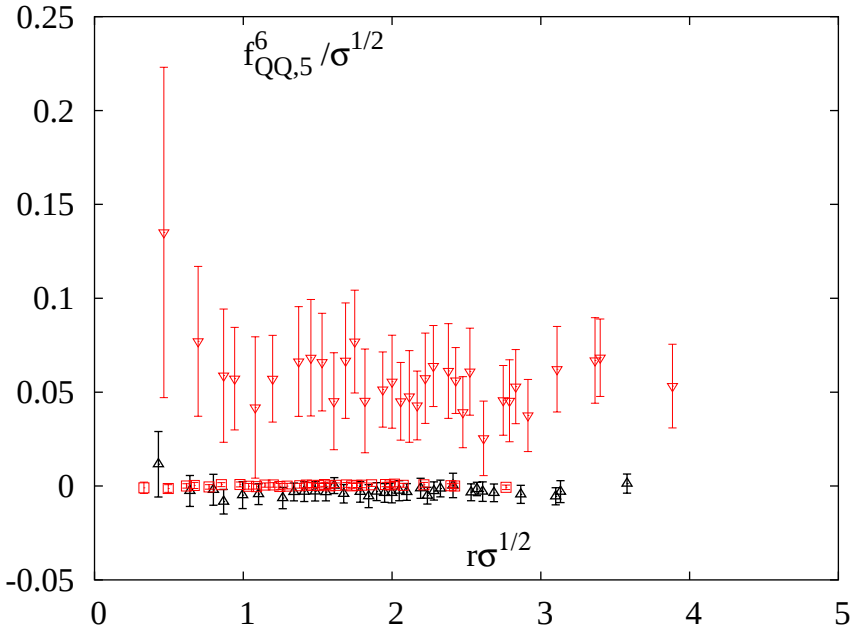

(b)

Figure 4.31: 5th order correction of heavy quark-quark free energies above T_c.

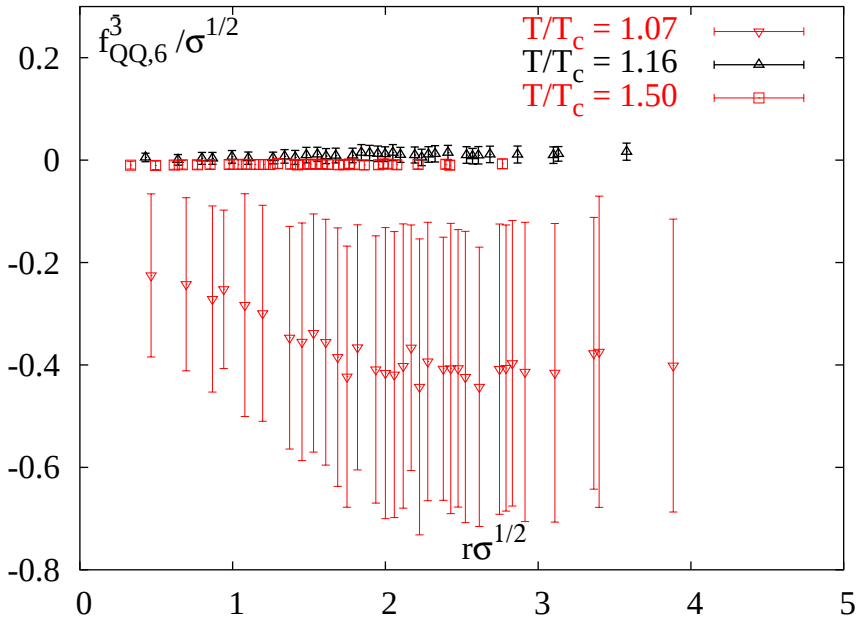

(a)

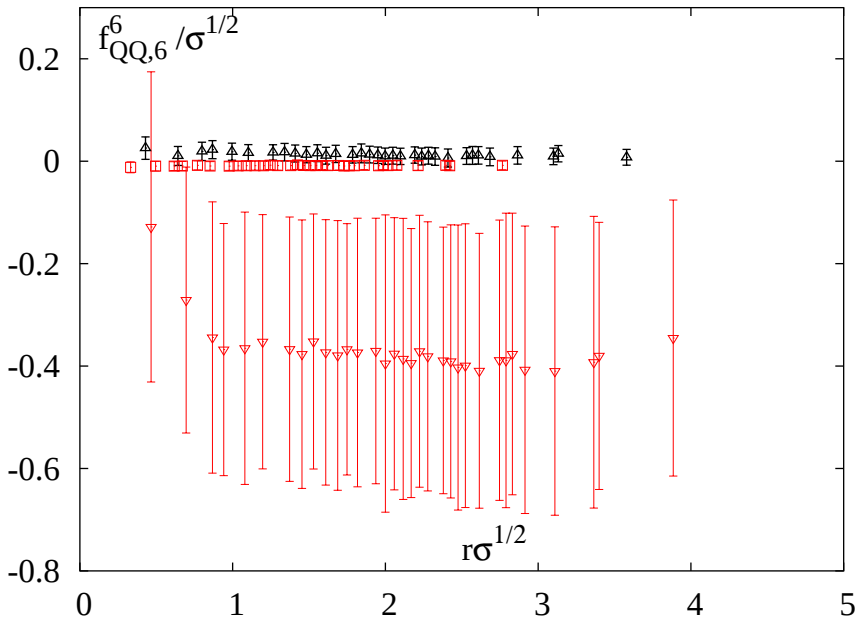

(b)

Figure 4.32: 6th order correction of heavy quark-quark free energies above T_c.

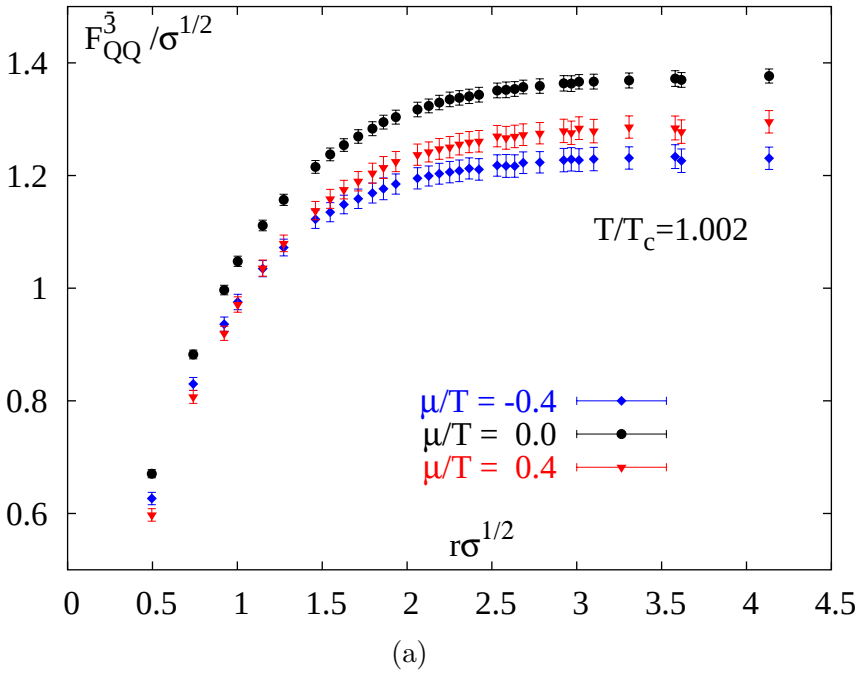

(a)

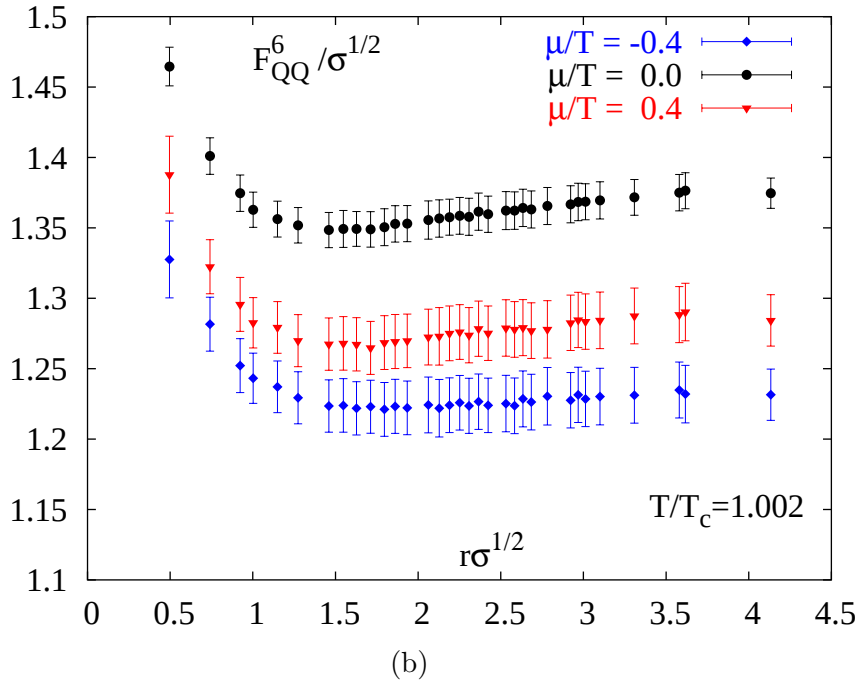

(b)

Figure 4.33: Example of the anti-triplet (a) and sextet (b) free energy at $T = 1.002T_c$ and finite values of μ.

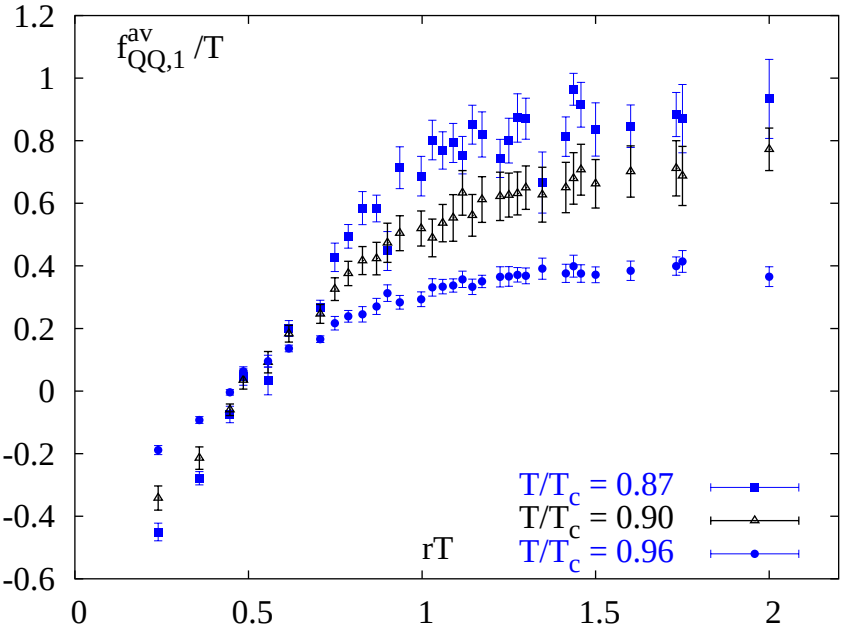

(a)

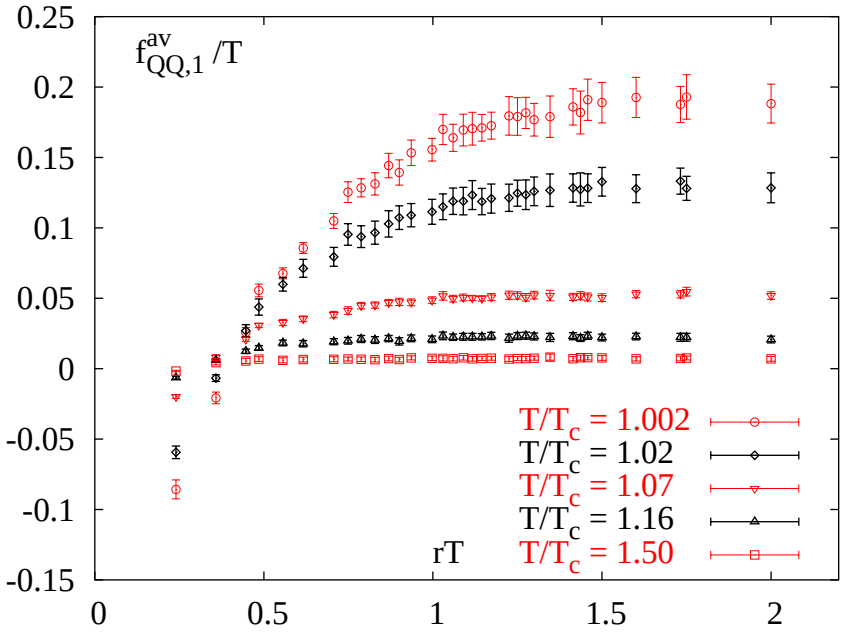

(b)

Figure 4.34: The 1st order correction of the color averaged free energy in units of the temperature.

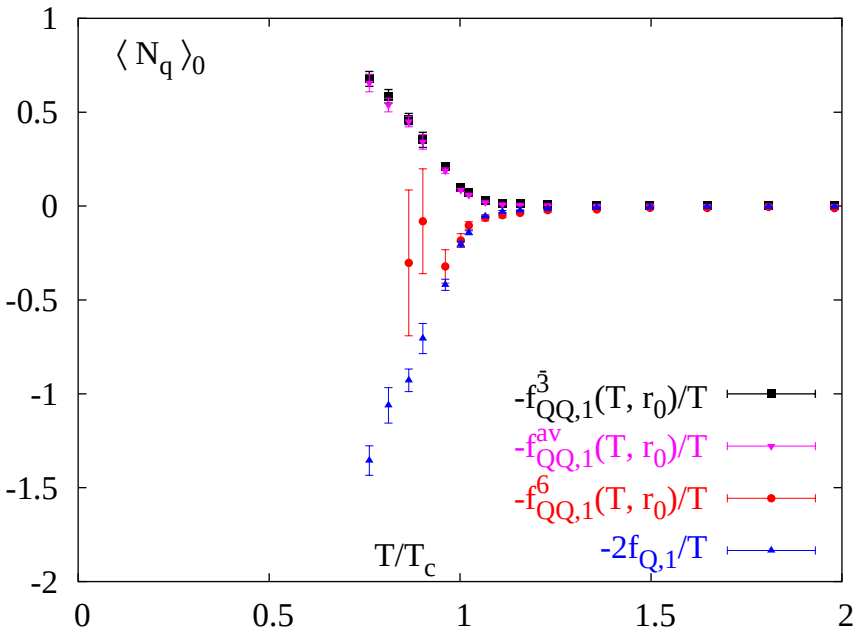

Figure 4.35: The light quark number $\langle N_q \rangle_\mu$ at $\mu = 0$ for the smallest separation r_0 of a heavy QQ-pair in a color averaged (magenta triangles), in a triplet (black squares) and in a sextet state (red circles) and for infinite separation (blue triangles). The latter is calculated from the corresponding cluster value. The $T \to 0$ limits are expected to be $+1$ for the color averaged and anti-triplet states and -2 for infinite distance.

4.7 Screening of diquark free energies

In analogy to the heavy quark anti-quark free energy the anti-triplet diquark free energy fulfills a screening law of the form

$$\begin{aligned} \Delta F^{\bar{3}}_{QQ}(r,T,\mu) &= F^{\bar{3}}_{QQ}(\infty,T,\mu) - F^{\bar{3}}_{QQ}(r,T,\mu) \ , \\ &\sim \frac{1}{r} e^{-m^{\bar{3}}(T,\mu),r} \ . \end{aligned} \tag{4.66}$$

Because $F^{\bar{3}}_{QQ}(r,T,\mu)$ also contains odd orders in μ/T we expect the screening mass $m^{\bar{3}}(T,\mu)$ to be of the form

$$m^{\bar{3}}(T,\mu) = m^{\bar{3}}_0(T) + m^{\bar{3}}_1(T)\frac{\mu}{T} + m^{\bar{3}}_2(T)\left(\frac{\mu}{T}\right)^2 + \mathcal{O}\left(\left(\frac{\mu}{T}\right)^3\right) \ . \tag{4.67}$$

The 0th order screening mass $m^{\bar{3}}_0(T)$ is equal to the screening mass $m^1_0(T)$ as discussed in [51]. Following section 4.4 we determine the higher order coefficients of $m^{\bar{3}}(T,\mu)$ by solving (4.66) for $m^{\bar{3}}(T,\mu)$ and taking the infinite distance limit. We then have

$$m^{\bar{3}}_n(T) = \lim_{r\to\infty} m^{\bar{3}}_{\mathrm{eff},n}(r,T) \ . \tag{4.68}$$

The expressions for the effective masses $m^{\bar{3}}_{\mathrm{eff},n}(r,T)$ are similar to those in the $Q\bar{Q}$ case, apart from contributions of odd orders which are zero in (4.31).

$$m^{\bar{3}}_{\mathrm{eff},1}(r,T) = -\frac{1}{r}\frac{\Delta f^{\bar{3}}_{QQ,1}(r,T)}{\Delta f^{\bar{3}}_{QQ,0}(r,T)} \ , \tag{4.69}$$

$$m^{\bar{3}}_{\mathrm{eff},2}(r,T) = -\frac{1}{r}\left[\frac{\Delta f^{\bar{3}}_{QQ,2}(r,T)}{\Delta f^{\bar{3}}_{QQ,0}(r,T)} - \frac{1}{2}\left(\frac{\Delta f^{\bar{3}}_{QQ,1}(r,T)}{\Delta f^{\bar{3}}_{QQ,0}(r,T)}\right)^2\right] \ . \tag{4.70}$$

As an example we show the effective masses for $T/T_c = 1.11$ in fig. 4.70. We determine the large distance limit by fitting the ratios in (4.70) to a constant. In comparison to the $Q\bar{Q}$-case the infinite distance limit is reached at larger separations rT. Near T_c we have to choose the left border of our fit window at $rT = 0.9$ for $m^{\bar{3}}_1$ and at $rT = 0.7$ for $m^{\bar{3}}_2$. The right border we always place at the maximum distance. With increasing temperature the left border of the fit window can then be shifted further to the left. For $T/T_c > 1.5$ a fit over the full range of distances is possible for both of the coefficients.

The first order correction to the screening mass is exclusively negative. This means that for small μ the screening length of a QQ-pair increases if the number of light quarks in the medium is increased. At large temperatures $m^{\bar{3}}_1(T)$ approaches very small values. We cannot conclude whether there is an asymptotic value which is significantly different from zero. At $T/T_c = 3$

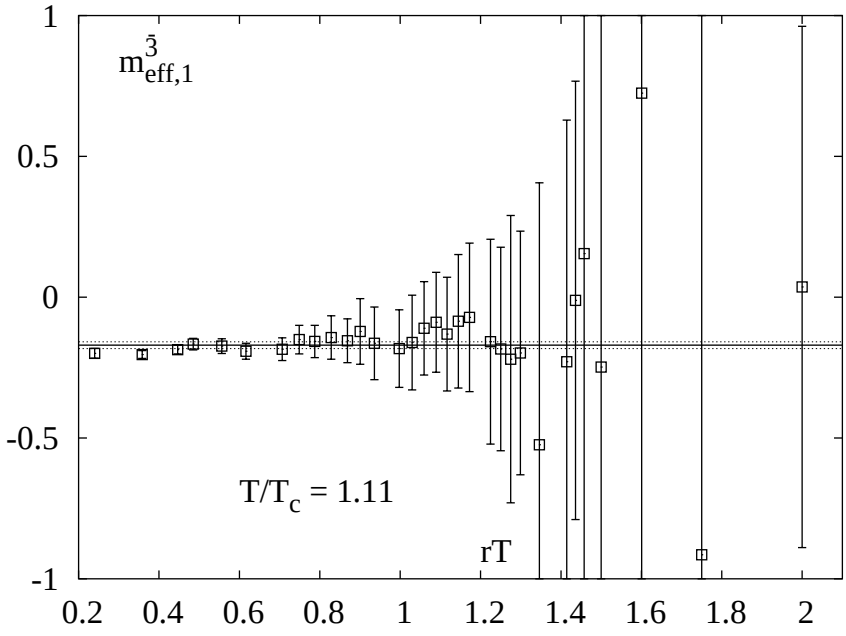

(a)

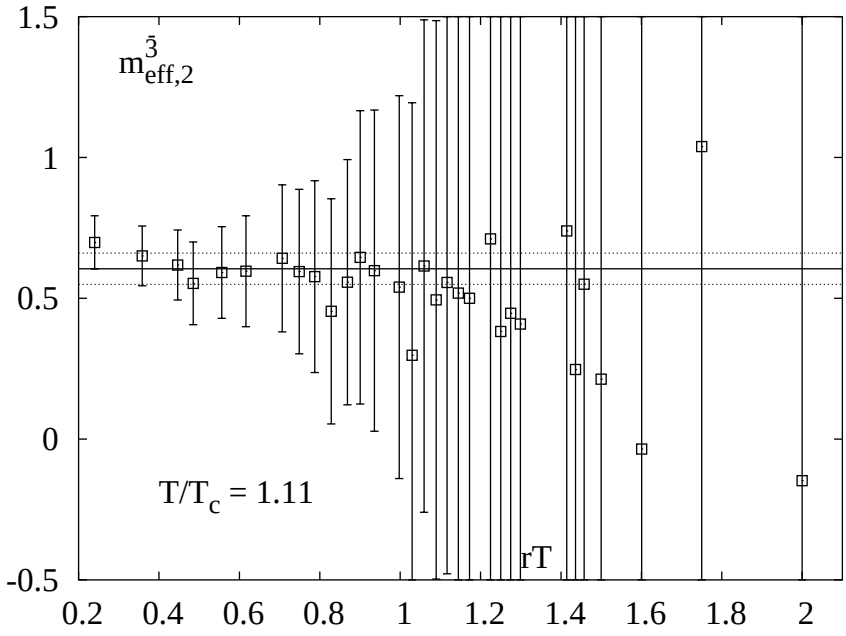

(b)

Figure 4.36: Example for the distance dependent effective masses. The horizontal line represents the infinite distance limit.

we still have $m_1^{\bar{3}} = -0.0020(20)$ but at $T/T_c = 4$ we have $m_1^{\bar{3}} = -0.0156(16)$. To our knowledge perturbative predictions for the screening mass $m^{\bar{3}}(T, \mu)$, which may be gauge dependent, do not exist. Nevertheless we observe that the values for the second order coefficients of QQ and $Q\bar{Q}$ are in almost perfect agreement. This is quite remarkable, because $m_2^{\bar{3}}$ has got contributions from first order corrections in the free energy which were absent in m_2^1.

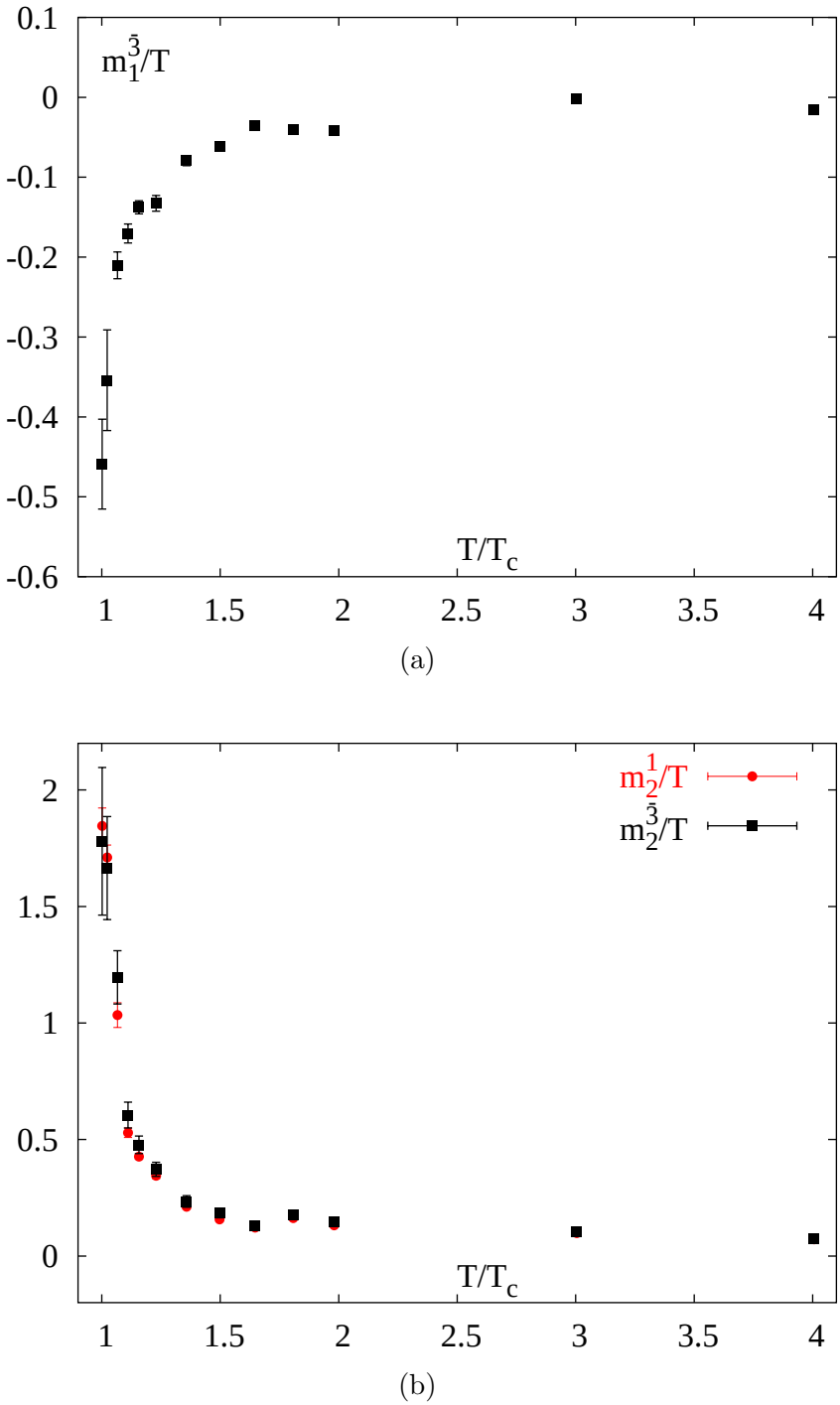

Figure 4.37: 1st and 2nd order correction of the anti-triplet screening mass. The second order is compared to the screening mass of a $Q\bar{Q}$-pair in the singlet state.

4.8 The singlet free energies of three heavy quarks

The singlet free energies F^1_{QQQ} of three heavy quarks in a singlet state are calculated from the correlation function

$$\begin{aligned} C^1_{QQQ}(r_{12}, r_{13}, r_{23}) &= \frac{1}{2\mathcal{N}'} \sum_{\boldsymbol{x},\boldsymbol{y},\boldsymbol{z}} 9\ \mathrm{tr}L(\boldsymbol{x})\mathrm{tr}L(\boldsymbol{y})\mathrm{tr}L(\boldsymbol{z}) \\ &\quad -3\ \mathrm{tr}L(\boldsymbol{x})\mathrm{tr}\left[L(\boldsymbol{y})L(\boldsymbol{z})\right] - 3\mathrm{tr}L(\boldsymbol{y})\mathrm{tr}\left[L(\boldsymbol{x})L(\boldsymbol{z})\right] \\ &\quad -3\mathrm{tr}L(\boldsymbol{z})\mathrm{tr}\left[L(\boldsymbol{x})L(\boldsymbol{y})\right] + \mathrm{tr}\left[L(\boldsymbol{x})L(\boldsymbol{y})L(\boldsymbol{z})\right] \\ &\quad +\mathrm{tr}\left[L(\boldsymbol{x})L(\boldsymbol{z})L(\boldsymbol{y})\right]\ , \end{aligned} \tag{4.71}$$

$\mathcal{N}'$ extends over all positions $\boldsymbol{x}, \boldsymbol{y}, \boldsymbol{z}$ of the three heavy quarks which lead to the same quark-quark separations r_{12}, r_{13}, r_{23}, where r_{ij} is the distance between the quarks i and j, i.e. $r_{12} = |\boldsymbol{x} - \boldsymbol{y}|$. In the following we will restrict to those singlet free energies in which the three quarks are placed on the corners of an equilateral triangle such that $r_{12} = r_{13} = r_{23}$. Furthermore we will use the perimeter $r_\Delta = r_{12} + r_{13} + r_{23} = 3r_{ij}$ as parameter instead of r_{12}, r_{13} or r_{23}.

As can be seen from fig. 4.38 and 4.39 the 0th order coefficients are T independent at short distances and $f^1_{QQQ,n}$ for $n \geq 1$ approaches zero for $r \to 0$. This behavior could be observed for the $Q\bar{Q}$-singlet free energies, too. In any case we see that the surrounding medium has no influence on small colorless heavy quark states.

Due to the small number of data points per temperature a quantitative estimate of the asymptotic value of $f^1_{QQQ,n}$ is difficult especially for low temperatures and odd n. Nevertheless we see that our coefficients are still consistent with the expansion coefficients of $3F_Q(T, \mu)$, which is the expected cluster value.

At $\mu = 0$ the singlet free energy $F^1_{QQQ}(r_\Delta, T, \mu)$ can be compared to the free energies of two heavy quarks. From the lowest non-vanishing order in perturbation theory the following relation has been proposed at $\mu = 0$ [51].

$$F^1_{QQQ}(3r, T, \mu) = 3F^{\bar{3}}_{QQ}(r, T, \mu) - 3F_{\bar{Q}}(T, \mu)\ . \tag{4.72}$$

In fig. 4.38(a) we compare the left handside (red closed symbols) and the right handside (underlying open grey symbols) of this equality for $\mu = 0$. In fact they are in good agreement. We can verify that this relation seems to hold also for the second order in μ (fig. 4.39(a)), whereas for the 1st order it is violated. Therefore the relation (4.72) does not hold for $\mu \neq 0$.

Although we cannot make a quantitative analysis of the screening mass $m^{1,\mathrm{QQQ}}$ for three heavy quarks, we can still make some statements. The 0th order $m^{1,QQQ}$ should be equal to $m^{\bar{3}}_0$ because (4.72) is fullfilled at $\mu = 0$. The effective mass is calculated in the same way as in the QQ-case.

For the first order of $m_{\text{eff}}^{1,QQQ}$ we have

$$m_{\text{eff},1}^{1,QQQ}(r,T) = -\frac{1}{r}\frac{\Delta f_{QQQ,1}^{1}(r,T)}{\Delta f_{QQQ,0}^{1}(r,T)} \,. \tag{4.73}$$

Because both $f_{QQQ,0}^{1,\text{eq}}$ and $f_{QQQ,1}^{1,\text{eq}}$ approach their asymptotic values from below, the first order correction $m_1^{1,QQQ}$ is negative. This we observed for the heavy diquark, too.

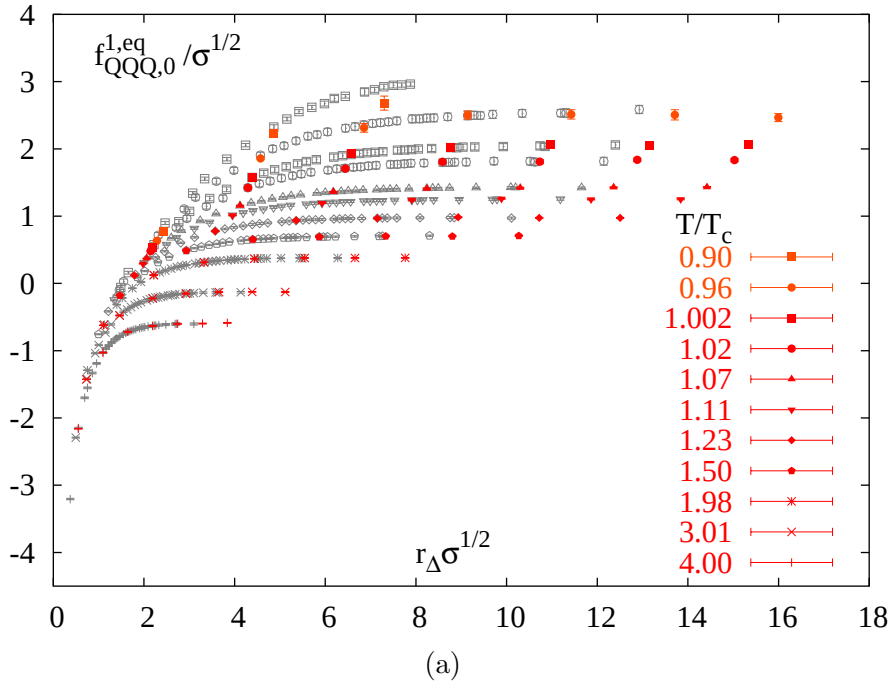

(a)

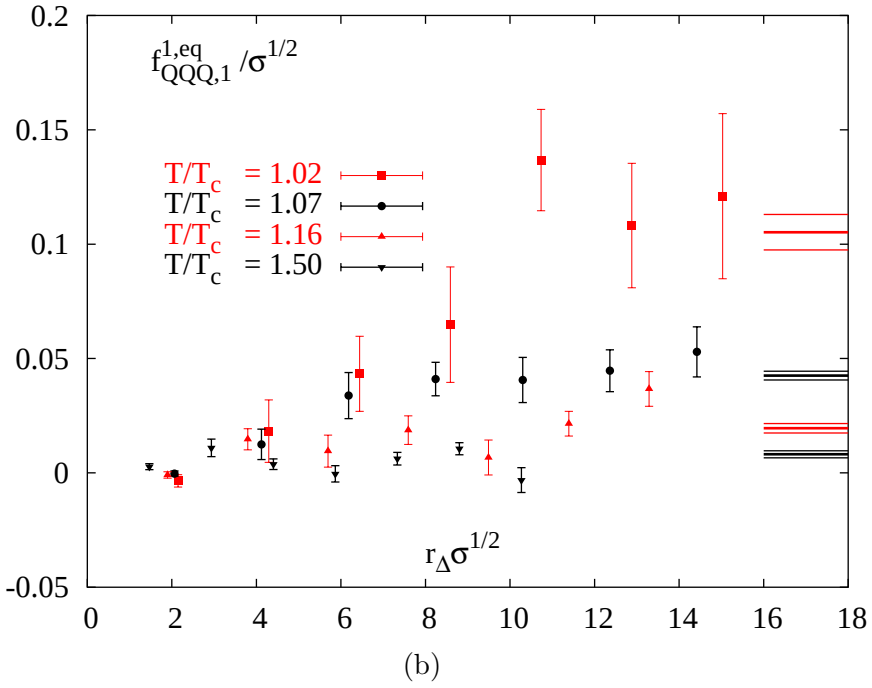

(b)

Figure 4.38: 0th (a) and 1st (b) order of the singlet free energy of three heavy quarks. The underlying grey points in (a) are the data for $3f^3_{QQ,0}$. The horizontal bars on the righthandside of (b) indicate the asymptotic values $3f_{Q,1}$ and corresponding errors, which were determined from the analysis of the Polyakov loop. r_Δ is the perimeter of the equilateral triangle.

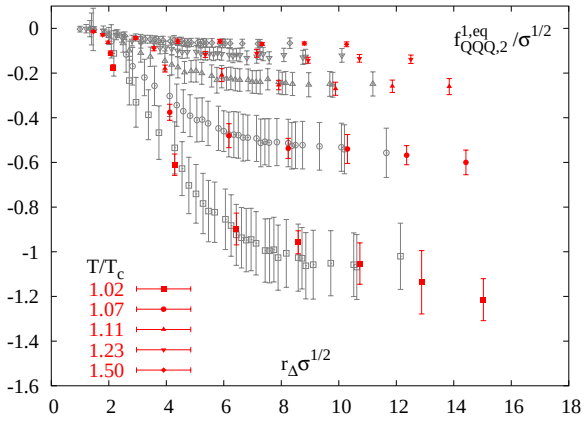

(a)

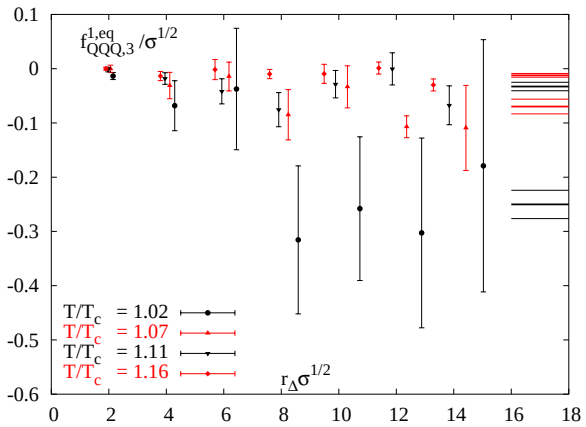

(b)

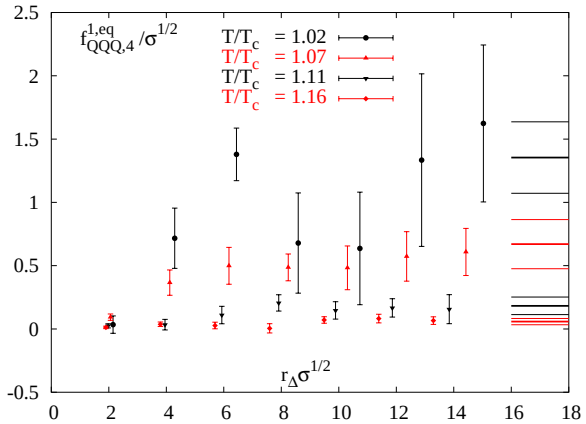

(c)

Figure 4.39: The orders 2,3 and 4 of $F^{1,eq}_{QQQ}$. The grey point in (a) are $3f^{\bar{3}}_{QQ,2}$ and the bars in (b) and (c) are the asymptotic values with errors, as expected from the analysis of the Polyakov loop.

Chapter 5

Hadrons

5.1 Meson correlation functions at finite density

On the lattice of hypercubes with lattice spacing $2a$ the meson operators are defined as

$$\mathcal{M}(n) = \bar{\Psi}(n) \left(\Gamma_D \otimes \Gamma_F\right) \Psi(n) \tag{5.1}$$

where Γ_D and Γ_F are products of γ-matrices which contain the symmetry properties of the corresponding meson. Γ_D acts on the Dirac indices and Γ_F on the flavor part of the fermionic fields. We will restrict the discussion to the case $\Gamma_D = \Gamma_F \equiv \Gamma$. The meson correlation functions are gauge invariant observables.
According to (2.28) the fields $\Psi(n)$ and $\bar{\Psi}(n)$ can be replaced by the staggered fields. Then the local meson operator is

$$\mathcal{M}(n) = \tilde{\phi}(n) \bar{\chi}_n \chi_n \ , \tag{5.2}$$

where $\tilde{\phi}(n)$ is a phase factor depending on the choice of Γ. The meson correlation function in the spatial z-direction and at zero transverse momentum is then obtained as

$$\mathcal{C}(z) = \langle 0| \sum_{n_1,n_2,n_4} \mathcal{M}(n) \mathcal{M}^\dagger(0) \left|0\right\rangle \Big|_{n_3 = z/a} \ . \tag{5.3}$$

It can be shown that the connected part of this correlation function has the form

$$\mathcal{C}_c(z) = - \sum_{n_1,n_2,n_4} \tilde{\phi}(n) G(n,0)_\mu G(0,n)_\mu \ . \tag{5.4}$$

The minus sign originates from the transposition of the fermionic fields. $G(n,0)_\mu$ is the quark propagator

$$G(n,0)_\mu = \langle 0| \chi_n \chi_0 \left|0\right\rangle_\mu = K(\mu)^{-1}_{n,0} \ . \tag{5.5}$$

In this work we use pointlike quark sources for the quark propagators. The meson correlation function is therefore gauge invariant and there is no need to fix the gauge here.
For non-vanishing μ the quark propagator has the property

$$G(n,0)_\mu = \epsilon(n) G(0,n)^\dagger_{-\mu} \,, \tag{5.6}$$

with

$$\epsilon(n) = (-1)^{n_1+n_2+n_3+n_4} \,. \tag{5.7}$$

A proof of the relation (5.6) for vanishing μ can be found in [52]. The generalization to non-vanishing μ is straight forward.
Inserting (5.6) into the meson correlation operator we get

$$\mathcal{C}_c(z) = - \sum_{n_1,n_2,n_4} \phi(n) G(n,0)_\mu G(n,0)^\dagger_{-\mu} \tag{5.8}$$

where $\phi(n) = \epsilon(n)\tilde{\phi}(n)$. The minus sign originates from the transposition of the fermionic fields. The values of $\phi(n)$ for various choices of Γ are listed in table 5.1. We also list the contributing particle states. Further details can be found in [53, 54]. The μ-dependence of hadronic correlation function is much

No.	Γ	$\tilde{\phi}(n)$	particle states
1	$\gamma_1\gamma_3$	$(-)^{n_1}$	a_T, ρ_T
2	$\gamma_2\gamma_3$	$(-)^{n_2}$	a_T, ρ_T
3	$\gamma_4\gamma_3$	$(-)^{n_4}$	a_L, ρ_L
4	1	1	f_0, π
5	γ_1	$(-)^{n_2+n_4}$	b_T, ρ_T
6	γ_2	$(-)^{n_1+n_4}$	b_T, ρ_T
7	γ_4	$(-)^{n_1+n_2}$	b_L, ρ_L
8	γ_5	$(-)^{n_1+n_2+n_4}$	$-, \pi$

Table 5.1: Meson phase factors, the partners of $a_{T,L}$ and $b_{T,L}$ are also referred to as ρ_2 and ρ_1 respectively.

more involved than for the other observables discussed so far. This is because not only the fermion determinant but also the correlation function $C_c(z)$ depends on the quark chemical potential μ. Namely the quark propagator is itself μ-dependent and can be written as a power expansion in μ.

$$G(n,0)_\mu \;=\; G^{(0)}_{n,0} + G^{(1)}_{n,0}\,\mu + G^{(2)}_{n,0}\,\mu^2 + \mathcal{O}\left(\mu^3\right) \,. \tag{5.9}$$

Expanding eq. (5.6) in powers of μ we get an alternating sign.

$$G^{(i)}_{n,0} = (-1)^i \epsilon(n) G^{(i)\dagger}_{0,n} \quad \text{for} \quad i = 0,1,2,\cdots \,. \tag{5.10}$$

Hence the propagator for the anti-quarks contains the corresponding adjoint coefficients and the opposite sign in front of μ.

$$G(n,0)^\dagger_{-\mu} = G^{(0)\dagger}_{n,0} - G^{(1)\dagger}_{n,0}\,\mu + G^{(2)\dagger}_{n,0}\,\mu^2 - \mathcal{O}\left(\mu^3\right) \ . \tag{5.11}$$

Because of eq. (5.5) the expansion coefficients $G^{(i)}_{n,0}$ are calculated from the derivatives of the inverse of the fermion matrix, i.e.

$$\begin{aligned} G^{(0)}_{n,0} &= K^{-1}_{n,0}\Big|_{\mu=0} \ , \\ G^{(1)}_{n,0} &= -\,K^{-1}_{n,m}\frac{\partial K_{m,j}}{\partial\mu}K^{-1}_{j,0}\,\Big|_{\mu=0} \ , \\ G^{(2)}_{n,0} &= K^{-1}_{n,m}\left(\frac{\partial K_{m,l}}{\partial\mu}K^{-1}_{l,k}\frac{\partial K_{k,j}}{\partial\mu} - \frac{1}{2}\frac{\partial^2 K_{m,j}}{\partial\mu^2}\right)K^{-1}_{j,0}\,\Big|_{\mu=0} \ , \end{aligned} \tag{5.12}$$

where K is the fermion matrix and doubly occuring indices on the right hand side are implicitly summed. We then have

$$\mathcal{C}_c(z) = \mathcal{C}_0(z) + \mathcal{C}_1(z)\,\mu + \mathcal{C}_2(z)\,\mu^2 + \mathcal{O}\left(\mu^3\right) \ , \tag{5.13}$$

which corresponds to the expansion (A.14) and where

$$\mathcal{C}_i(z) = -\sum_{n_1,n_2,n_4}\phi(n)\left(\sum_{j=0}^{i}(-1)^{i-j}G^{(j)}_{n,0}G^{(i-j)\dagger}_{n,0}\right) \tag{5.14}$$

for $i = 0, 1, 2, \cdots$. Taking the adjoint of this equation we can immediately see that the coefficient $C_i(z)$ of order i is real for even and imaginary for odd i. Because this also holds for the expansion coefficients D_i of the fermion determinant the μ-expansion of the expectation value $\langle C_c(z)\rangle_\mu$ is also real in the even and imaginary in the odd orders. Moreover because $\langle C_c(z)\rangle_\mu$ is an even function in μ the odd orders vanish and only the real even orders remain.

$$C_c(z) = \langle\mathcal{C}_c(z)\rangle_\mu = C_0(z) + C_2(z)\left(\frac{\mu}{T}\right)^2 + C_4(z)\left(\frac{\mu}{T}\right)^4 + \mathcal{O}\left(\left(\frac{\mu}{T}\right)^6\right) \tag{5.15}$$

In particlular $C_c(z)$ is real and the coefficients $C_i(z)$ can be calculated using eq. (A.18).

5.2 Screening of mesons

On a finite lattice the screening behaviour of meson correlation functions at large distances z can for staggered fermions be parametrized as the sum of an oscillating and a non-oszillating cosh.

$$C_c(z) = A\cosh\left(m_A\tilde{z}\right) + (-)^{\tilde{z}}B\cosh\left(m_B\tilde{z}\right) \ , \tag{5.16}$$

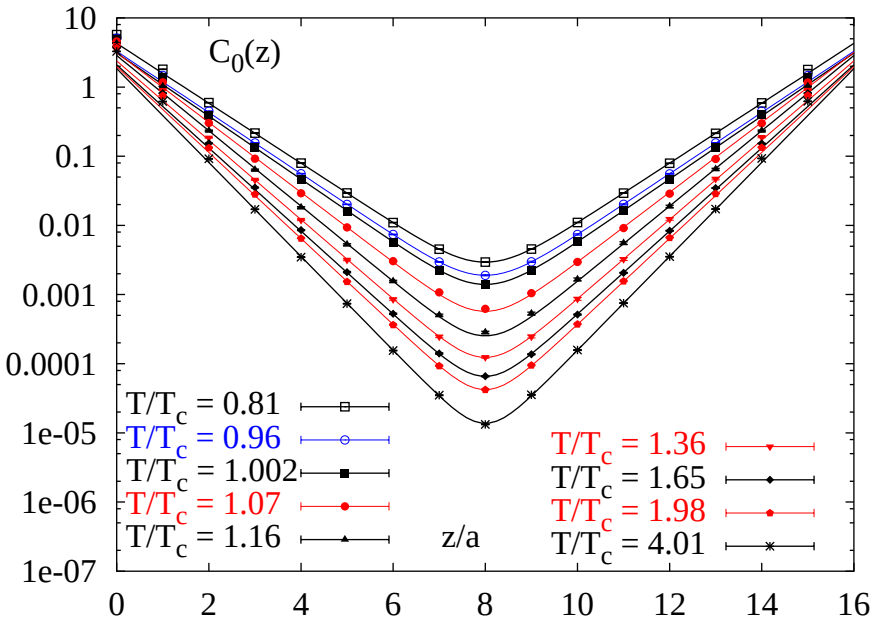

(a)

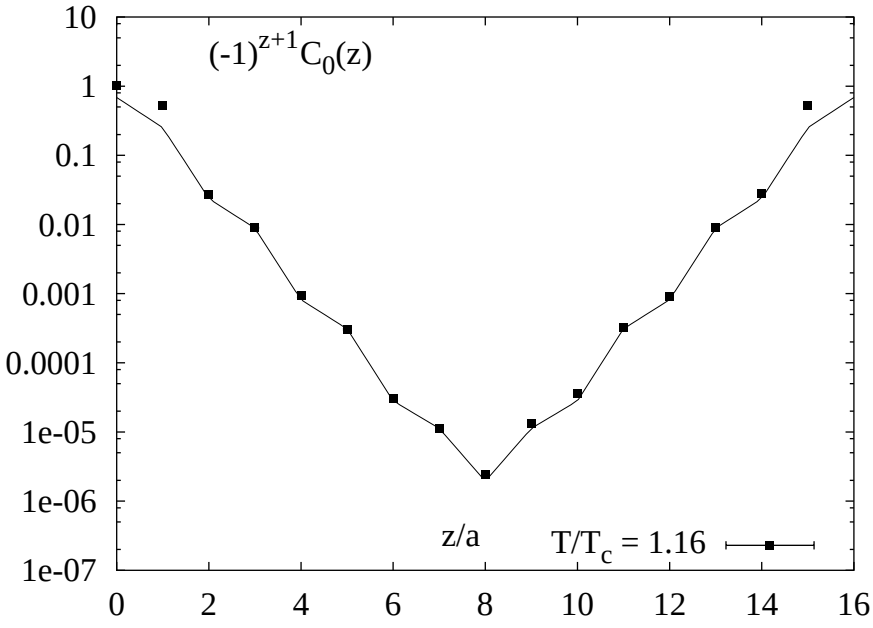

(b)

Figure 5.1: (a): Some examples of the 0th order pion correlation function. (b): Example for the ρ_T, a_T-correlation function (see entry no.1 in table 5.1). The multiplicative factor of $(-1)^{z+1}$ has been added to make the correlation function positive for every value of z. The values of the fitting function at the positions $z/a = 0, 1, 2, \cdots, 16$ are connected via straight lines for convenience.

where $\tilde{z} = z - N_\sigma/2$. m_A and m_B are the screening masses of the contributing particle states. For small z there may in general be corrections to this fit ansatz resulting from contributions of excited states. In this case additional cosh's would have to be taken into account in order to get an improved fit ansatz. Due to the small number of independent data points in the z-direction we cannot proceed in this way here. Therefore we will only consider the fit ansatz (5.16) which is valid in the vicinity of $\tilde{z} = 0$.
Furthermore, for the screening behaviour of the pion (no. 8 in table 5.1) there is only one lowest contributing state and we can put $B = 0$ explicitly. The μ-dependence is included in the ansatz (5.16) by assuming power expansions for the parameters.

$$A(T,\mu) = A_0(T) + A_2(T)\left(\frac{\mu}{T}\right)^2 + \mathcal{O}\left(\left(\frac{\mu}{T}\right)^4\right), \tag{5.17a}$$

$$B(T,\mu) = B_0(T) + B_2(T)\left(\frac{\mu}{T}\right)^2 + \mathcal{O}\left(\left(\frac{\mu}{T}\right)^4\right), \tag{5.17b}$$

$$m_A(T,\mu) = m_{A0}(T) + m_{A2}(T)\left(\frac{\mu}{T}\right)^2 + \mathcal{O}\left(\left(\frac{\mu}{T}\right)^4\right), \tag{5.17c}$$

$$m_B(T,\mu) = m_{B0}(T) + m_{B2}(T)\left(\frac{\mu}{T}\right)^2 + \mathcal{O}\left(\left(\frac{\mu}{T}\right)^4\right). \tag{5.17d}$$

Inserting these expansions into (5.16) we get

$$C_0(z) = A_0\cosh\left(m_{A0}\tilde{z}\right) + (-)^{\tilde{z}} B_0\cosh\left(m_{B0}\tilde{z}\right) \tag{5.18a}$$

$$\begin{aligned} C_2(z) &= A_2\cosh\left(m_{A0}\tilde{z}\right) + A_0 m_{A2}\tilde{z}\sinh\left(m_{A0}\tilde{z}\right) \\ &+ (-)^{\tilde{z}}\left[B_2\cosh\left(m_{B0}\tilde{z}\right) + B_0 m_{B2}\tilde{z}\sinh\left(m_{B0}\tilde{z}\right)\right] \end{aligned} \tag{5.18b}$$

For the 0th order we perform χ^2-fits according to eq. (5.18a) using m_{A0}, A_0, m_{B0} and B_0 as parameters. In case of the pion channel (no.8) we can set m_{B0} and B_0 to zero and the oscillating terms drop out. It turns out that apart from the pion the initial values of our parameters have to be chosen very carefully in order to guarantee the convergence of the Levenberg-Marquardt algorithm [55]. We choose the left and the right borders of our fit windows at $+\tilde{z}_b$ and $-\tilde{z}_b$ symmetric to the point $\tilde{z} = 0$. We then look for plateaus in the fit parameters as a function of the window size $2\tilde{z}_b$. Our plateaus are located in the range $\tilde{z}_b/a \in [2, 6]$.
In fig. 5.1 we show some examples of the 0th order correlation functions for the pion and the rho compared to the corresponding fit results. The middle points around $z/a = 8$ match the fitting function quite well. The higher the temperature the more the border points near $z/a = 0$ and $z/a = 16$ violate our fit ansatz. On the one hand this is a consequence of higher excited states contributing to the outer points. On the other hand it is related to the fact that for small meson-meson separations z and high temperatures the meson correlation function is best described by perturbation theory.

For very large temperatures we eventually see the free propagation of the constituting mesons.
Let $C^f(z)$ the pion correlation function for non-interacting free quarks with a μ-expansion

$$C^f(z) = C_0^f(z) + C_2^f(z)\left(\frac{\mu}{T}\right)^2 + \mathcal{O}\left(\left(\frac{\mu}{T}\right)^4\right) . \tag{5.19}$$

$C^f(z)$ can be calculated on the lattice by calculating the correlation function on a unit configuration where all the links are put to $U_\mu(n) = \mathbf{1}$. In fig. 5.2 (a) we calculated the ratio of $C_0(z)$ for some temperatures and the free correlation $C_0^f(z)$. We see that with increasing temperature $C_0(z)$ converges slowly to the free correlation $C_0^f(z)$. This is especially true for the borders of our z-range where the ratio $C_0(z)/C_0^f(z)$ is closest to one.
Following this consideration especially the border points show only the free propagation of quarks and our fit window becomes narrower if temperature increases.
The coefficients A_0 and B_0 are temperature dependent. For some temperatures and in some channels even for all temperatures one of the coefficients A_0 or B_0 is several orders of magnitude greater than the other one. In this case good plateaus can only be seen for that particle state which corresponds to the greater coefficient. This is why the results shown in fig. 5.4 do not include all particle states.
The lowest screening mass is observed for the pion. Here we see a constant value of $m_0/T \approx 4$ for temperatures below T_c. At T_c the value of m_0/T starts increasing monotonically up to an infinite temperature limit m_0^f/T which is the same for all particle states apart from lattice corrections. In the continuum and chiral limit m_0^f is twice the lowest quark momentum which is twice the lowest Matsubara frequency.

$$m_0^f = 2\pi T . \tag{5.20}$$

In order to determine the 2nd order we fit the data of the 0th and 2nd order to the functional forms (5.18a) and (5.18b) simultaneously. Unfortunately fits including non-vanishing parameters B_0, B_2, m_{B0} and m_{B2} could not be accomplished. The fitting process was not able to find a stable minimum of χ^2. Therefore we always drop the oscillating terms, i.e. we set $B_0 = B_2 = m_{B0} = m_{B2} = 0$ explicitly. For the pion this is correct. For other mesons this only leads to good results if the correct value of B is very small compared to A. In this way we could get reliable estimates for the screening mass coefficient m_2 of the ρ meson.
For convenience we furthermore replace eq. (5.18b) by the ratio

$$\frac{C_2(z)}{C_0(z)} = m_{A2}\tilde{z}\tanh\left(m_{A0}\tilde{z}\right) + \tilde{A}_2 . \tag{5.21}$$

Thereby the exponential factor contained in the 0th and 2nd order drops out. $\tilde{A}_2 = A_2/A_0$ is the offset at $\tilde{z} = 0$ and m_{A2} is basically the slope of $C_2(z)/C_0(z)$ near $\tilde{z} = 0$. We use (5.21) as a fit ansatz for C_2/C_0 in the vicinity of $\tilde{z} = 0$.

The statement that the data points at large temperatures and small meson seperations fit in the picture of free quark propagation carries over to the ratio $C_2(z)/C_0(z)$. In fig. 5.2 (b) we compare this ratio to the free case. Again we see that the border points show the characteristics of a free propagation of the quarks.

Fig. 5.3 (a) shows the ratio C_2/C_0 for the pion at low temperatures $T < 1.2T_c$ and the corresponding fitting functions of the form (5.21). We see that the fitting functions and the data are in good agreement. For higher temperatures the outer points start to deviate from this behaviour as can be seen in fig. 5.3 (b). Generalizing the results for finite T in [56] to finite μ the continuum pseudoscalar meson correlation function for freely propagating quarks in the chiral limit has the form [57]

$$C_c^{cont}(z) = \frac{N_c T}{2\pi z^2 \sinh(2\pi T z)} \{\cos(2z\mu)\,[1 + 2\pi T z \coth(2\pi T z)] + 2z\mu \sin(2z\mu)\} \ . \quad (5.22)$$

Using $T = 1/(N_\tau a)$ and

$$C_2^{cont}(z) = \frac{1}{2!} \frac{\partial^2 \mathcal{C}^{cont}(z)}{\partial (\mu/T)^2}\bigg|_{\mu=0} \ , \quad (5.23)$$

we get

$$\frac{C_2^{cont}(z)}{\mathcal{C}_0^{cont}(z)} = \frac{1}{N_\tau^2} \left(\frac{z}{a}\right)^2 \left[-1 + \frac{2}{1 + \frac{2\pi}{N_\tau}\frac{z}{a} \coth\left(\frac{2\pi}{N_\tau}\frac{z}{a}\right)}\right] \ . \quad (5.24)$$

In fig. 5.3(c) we include this function as the red curve. We see that it is qualitatively in good agreement with the ratio C_2/C_0 for the highest temperature evaluated by us. Hence with increasing temperature we have to restrict our fitting range for the screening ansatz (5.21) to a smaller interval around $\tilde{z} = 0$. We average the obtained values for the screening mass coefficient m_2 over the fit results obtained from symmetric fit windows with left(right) borders between $\tilde{z}/a = -7(+7)$ and $\tilde{z}/a = -6(+6)$ for low temperatures and between $\tilde{z}/a = -5(+5)$ and $\tilde{z}/a = -2(+2)$ for large temperatures.
The results for the screening mass coefficients for higher temperatures have to be treated with care as there is a more distinctive dependence on the fitting range. For $T/T_c < 1.5$ the results are non-ambiguous.

The result for the second order screening mass of the pion m_2^π and the transversal ρ-meson m_2^ρ are shown in fig. 5.4 (b). They are qualitatively in

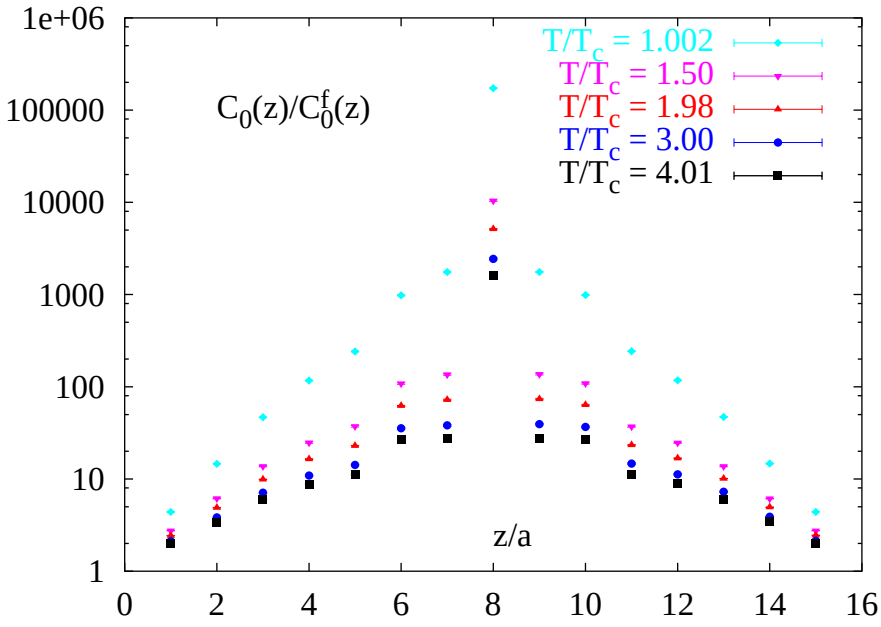

(a)

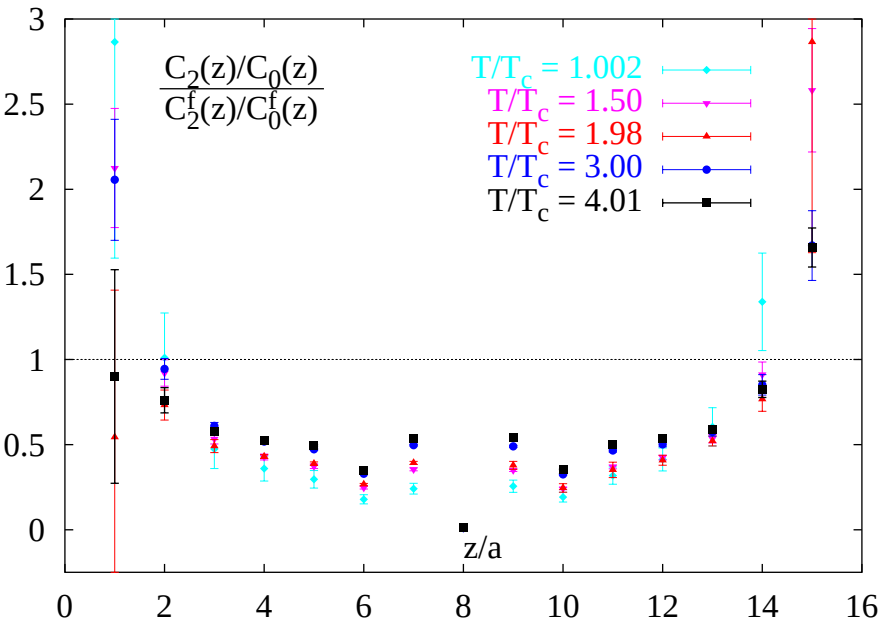

(b)

Figure 5.2: The 0th order pion correlation function $C_0(z)$ (a) and the ratio $C_2(z)/C_0(z)$ (b) compared to the free case calculated on the lattice.

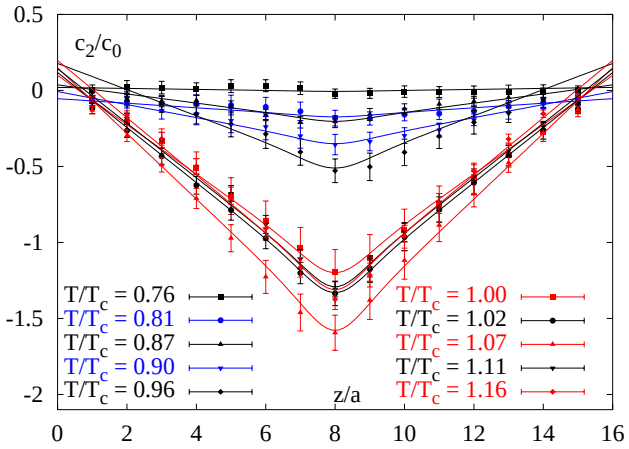

(a)

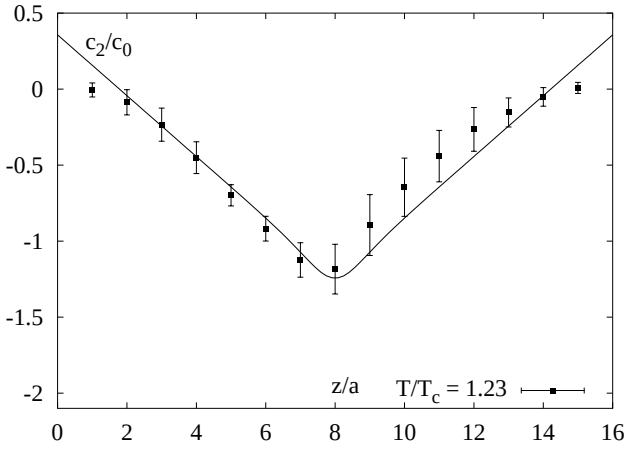

(b)

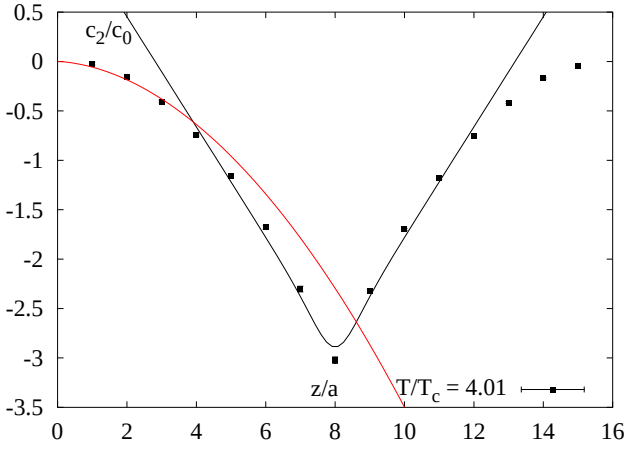

(c)

Figure 5.3: The ratio of C_2/C_0 for the pion at temperatures $T < 1.2T_c$ including the fitting functions (a). For temperatures $T > 1.2T_c$ the screening ansatz becomes more and more misleading especially for large $\tilde{z}$ (b). For very high temperatures (c) the free continuum quark propagator (red line) is in better agreement with the data at large $\tilde{z}$ than the screening ansatz (black line).

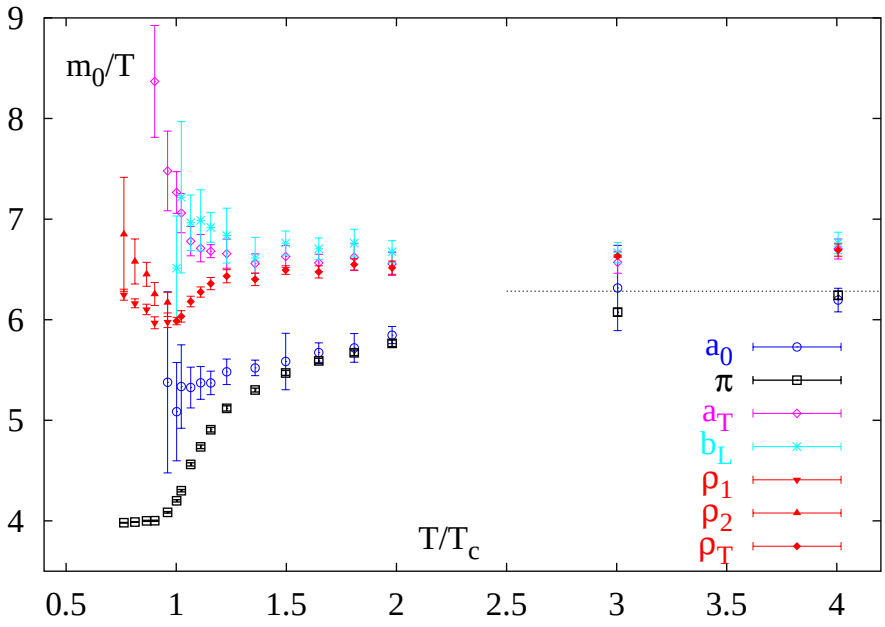

(a)

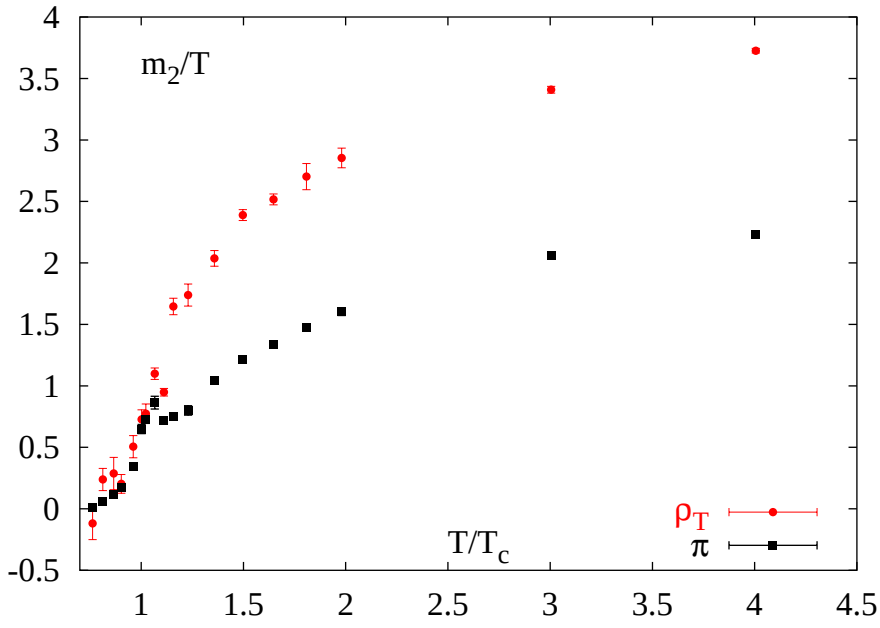

(b)

Figure 5.4: Meson screening masses at $\mu = 0$ (a). The horizontol bar shows the continuum value for massless freely propagating quarks. a_0 corresponds to f_0 in tabular 5.1. (b): The second order responses for the screening mass of the π and the ρ meson.

good agreement with results from QCD-TARO [58].
For both mesons m_2/T starts from zero at low temperatures and rises quickly to higher values especially at T_c. At $T \approx 1.07T_c$ we observe a small bump for both particles which could still be a statistical effect. Below T_c there is no significant difference between m_2^π and m_2^ρ. Above T_c m_2^ρ increases faster than m_2^π such that for temperatures $T > 1.2T_c$ m_2^ρ is almost twice as large as m_2^π.

This picture results from the fit ansatz (5.16) with the assumption of a μ-dependent screening mass. On the other hand in view of eq. (5.22) the concept of a μ-dependent meson screening mass may be misleading at least for the case of free quark propagation. Namely we have for the free correlation at large distances z

$$C_c^{cont}(z) \sim \frac{1}{z} e^{-m_0 z} \left[m_0 \cos(2z\mu) + 2\mu \sin(2z\mu) \right] \tag{5.25}$$

where $m_0 = 2\pi T$. We see that the exponential screening part is independent of μ and that the μ-dependence is contained solely in a factor which is oscillating in z for $\mu \neq 0$. Therefore the screening mass contained in the exponential factor is independent of μ in the infinite temperature limit. On the one hand our fit ansatz (5.16) leads to a good description of our data. On the other hand there is no connection of m_2 to the case of free quark propagation so far.

5.3 Nucleon correlation function

For compound particles like mesons which effectively contain two quarks the total momentum of the constituents is zero in the rest frame. This does not hold for particles made up of more than two constituents like baryons. According to [59] we therefore include the lowest Matsubara frequency for a fermion πT in the staggered nucleon propagator in the following way

$$\mathcal{C}_c(z) = \sum_{n_1,n_2,n_4} \cos(\pi T \tau)\, \epsilon_{ijk}\, G_{1,i}(0,n) G_{2,j}(0,n) G_{3,k}(0,n) \Big|_{\substack{n_4=\tau/a \\ n_3=z/a}} . \tag{5.26}$$

The quark propagator $G_{a,b}(0,n)$ describes the propagation of a quark with color a at position 0 to a quark with color b in n.

5.4 Screening of nucleons

On a finite lattice the screening behaviour of the nucleon correlation function can be parametrized in the form

$$\begin{aligned} C_c(z) = \langle \mathcal{C}_c(z) \rangle &= A \left(e^{-m_A z/a} + (-)^{z/a} e^{-m_A (N_\sigma - z/a)} \right) \\ &+ B \left((-)^{z/a} e^{-m_B z/a} + e^{-m_B (N_\sigma - z/a)} \right) . \end{aligned} \tag{5.27}$$

In contrast to the fit ansatz for temporal nucleon-nucleon separations [54] there are plus signs between the terms inside the brackets due to the periodic boundary conditions in the spatial direction.
In practice we find that B is in general much smaller than A. This prevents our fit algorithm to converge if we take the full ansatz. Therefore we put $B = 0$ explicitly.
Some examples of the $\mu = 0$ correlation function are given in fig. 5.5. We show the absolute value $|C_c(z)|$ of the correlation function in a logarithmic plot multiplied with the sign of $C_c(z)$.
For low temperatures the fitting function matches the data almost perfectly. With increasing temperature the data points oscillate around the fitting function due to a finite value of B which we do not take into account here. Nevertheless we are allowed to assume that the extracted values for A and $m_0 = m_A$ give us good estimates of the correct values although the value of $\chi^2/d.o.f.$ may be quite large. I.e. m_0 is given by the slope of the fitting function in the region of $z/a < N_\sigma/2$. The oscillation of the points does not have a large effect on this slope.

In fig. 5.6 we show the screening energy for the nucleon. For all temperatures we only see small deviations from the free continum limit of $m_0 = 3\pi T$. We also tried to get information about the μ-dependence of the nucleon correlation funcion $C_c(z)$ by assuming μ-dependent parameters A, B, m_A and m_B. The μ-expansion should in general include non-vanishing even and also odd orders in μ/T. The corresponding n'th order correction of the screening mass would then be extracted from the ratios C_n/C_0. We find that all these ratios vanish within statistical errors.

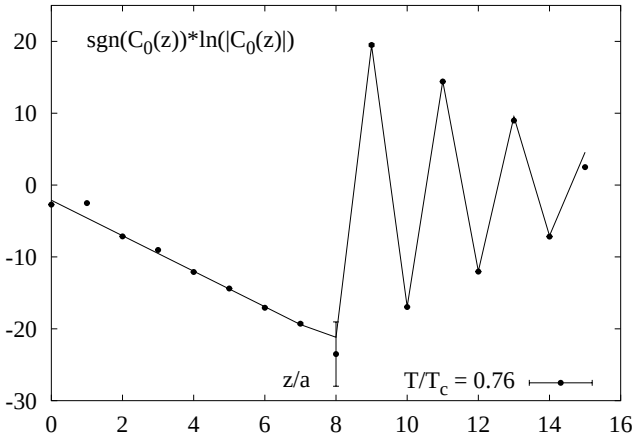

(a)

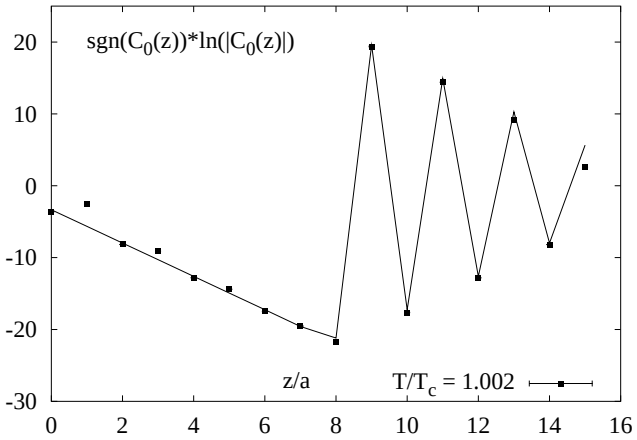

(b)

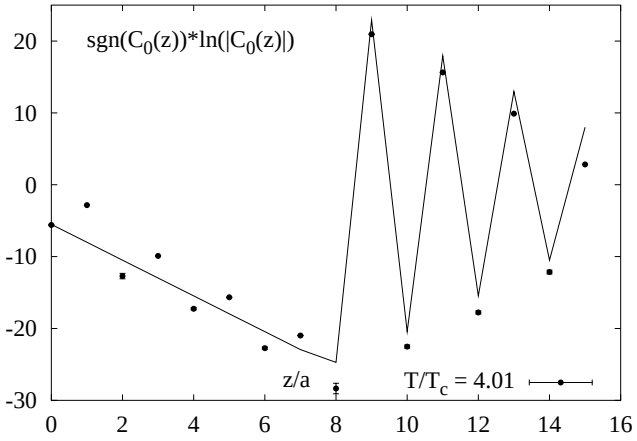

(c)

Figure 5.5: Some examples of nucleon correlation functions for variuos temperatures below (a), at (b) and above (c) T_c. The values of the fitting function at $z/a = 0, 1, 2, \cdots$ are connected via straight lines.

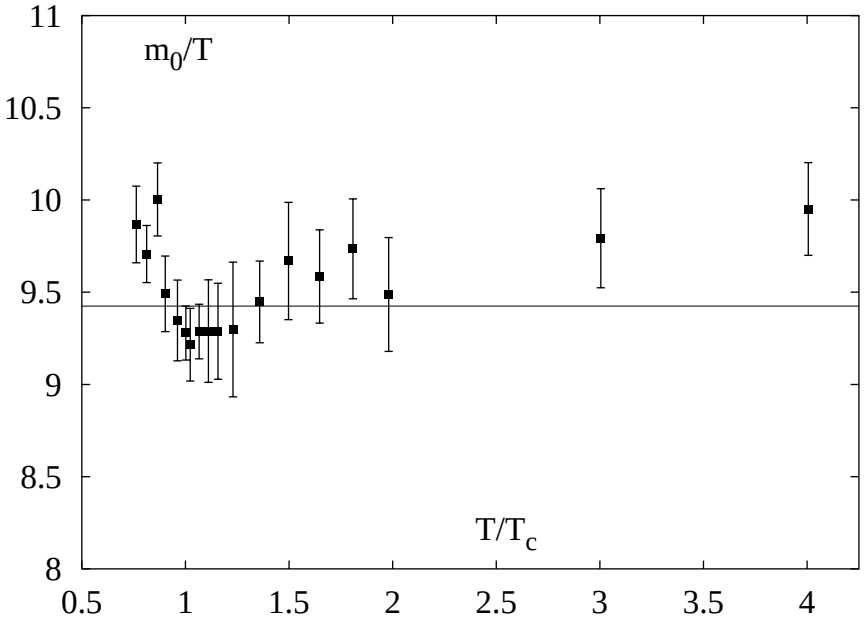

Figure 5.6: The nucleon screening energy at $\mu = 0$. The horizontal bar shows the free continuum value of 3π.

Chapter 6

Conclusions and outlook

This work is devoted to the application of the Taylor expansion in the baryon chemical potential. Using this method we could extend results obtained at finite temperature QCD to the case of non-vanishing baryon densities.
The simplest quantities under investigation are the pressure and particle number densities in a hot and dense medium. Here reliable results could be obtained up to the 6th order in the baryon chemical potential μ.
Introducing a set of static heavy quarks and/or anti-quarks into the medium we could calculate the changes of the free energy in comparison to a medium without any heavy quarks. The free energies were evaluated with respect to the screening properties of the medium. We could give genuine expressions on how to calculate the corresponding screening mass coefficients exactly. For temperatures $T > 2T_c$ the μ-expansion coefficients of the screening mass of a heavy quark-anti-quark pair could be related to results from high temperature perturbation theory. A non-vanishing 1st order appears in the screening mass coefficients of a heavy quark pair. This order is totally absent in high temperature perturbation theory. Nevertheless the observed high temperature limit is zero such that there is no contradiction.
Furthermore we observed that for temperatures $T < T_c$ heavy quarks induce the generation of light quarks and/or anti-quarks from the particle reservoir. This is due to the fact that at temperature $T = 0$ only color singlet states of quarks are stable. Further data at lower temperatures as those studied by us are still desirable. It would also be interesting to investigate the coefficients of the local free energy density in order to localize the induced light quarks.
Finally the screening of hadron correlation functions was studied. For the 0th order screening masses we could get numerous results which are at high temperature in agreement with the free propagation of the constituting quarks. The 2nd order coefficient m_2 of the π- and the ρ-meson show almost the same behaviour below T_c. Above T_c the m_2-value of the ρ becomes significantly larger than the value of the π. On the one hand an explanation for this observation is missing so far. On the other hand the coefficients at

large temperatures have to be treated with care as the free propagation of quarks starts dominating the correlation functions.

Appendix A

Details on the power expansion in μ

A.1 Calculation of μ-expansion coefficients

The μ-dependent expectation value of a complex quantity $\mathcal{O}$ is

$$\langle \mathcal{O} \rangle_\mu = \frac{1}{Z_\mu} \int DU \mathcal{O} \Delta e^{-S} = \frac{\int DU \mathcal{O} \Delta e^{-S}}{\int DU \Delta e^{-S}} \,, \tag{A.1}$$

where Z_μ is the partition function for finite μ and where $\Delta = (\det K(\mu))^{N_f/4}$ is the determinant of the fermion matrix. In the following we denote expectation values for vanishing μ as $\langle \cdots \rangle = \langle \cdots \rangle_0$. We define

$$L_n \equiv \left. \frac{d^n \ln \Delta}{d\mu^n} \right|_{\mu=0} = \frac{N_f}{4} \left. \frac{d^n \ln \det K}{d\mu^n} \right|_{\mu=0} . \tag{A.2}$$

The L_n can be written as traces over the inverse of the fermion matrix and its derivatives

$$L_1 = \frac{N_f}{4}\mathrm{Tr}\left(K^{-1}\frac{\partial K}{\partial\mu}\right)\Big|_{\mu=0}, \tag{A.3a}$$

$$L_2 = \frac{N_f}{4}\mathrm{Tr}\left(K^{-1}\frac{\partial^2 K}{\partial\mu^2} - K^{-1}\frac{\partial K}{\partial\mu}K^{-1}\frac{\partial K}{\partial\mu}\right)\Big|_{\mu=0}, \tag{A.3b}$$

$$\begin{aligned} L_3 = {} & \frac{N_f}{4}\mathrm{Tr}\left(K^{-1}\frac{\partial^3 K}{\partial\mu^3} - 3K^{-1}\frac{\partial K}{\partial\mu}K^{-1}\frac{\partial^2 K}{\partial\mu^2}\right. \\ & + \left. 2K^{-1}\frac{\partial K}{\partial\mu}K^{-1}\frac{\partial K}{\partial\mu}K^{-1}\frac{\partial K}{\partial\mu}\right)\Big|_{\mu=0}, \end{aligned} \tag{A.3c}$$

$$\begin{aligned} L_4 = {} & \frac{N_f}{4}\mathrm{Tr}\left(K^{-1}\frac{\partial^4 K}{\partial\mu^4} - 4K^{-1}\frac{\partial K}{\partial\mu}K^{-1}\frac{\partial^3 K}{\partial\mu^3} - 3K^{-1}\frac{\partial^2 K}{\partial\mu^2}K^{-1}\frac{\partial^2 K}{\partial\mu^2}\right. \\ & + 12K^{-1}\frac{\partial K}{\partial\mu}K^{-1}\frac{\partial K}{\partial\mu}K^{-1}\frac{\partial^2 K}{\partial\mu^2} \\ & - \left. 6K^{-1}\frac{\partial K}{\partial\mu}K^{-1}\frac{\partial K}{\partial\mu}K^{-1}\frac{\partial K}{\partial\mu}K^{-1}\frac{\partial K}{\partial\mu}\right)\Big|_{\mu=0}, \end{aligned} \tag{A.3d}$$

$$\begin{aligned} L_5 = {} & \frac{N_f}{4}\mathrm{Tr}\left(K^{-1}\frac{\partial^5 K}{\partial\mu^5} - 5K^{-1}\frac{\partial K}{\partial\mu}K^{-1}\frac{\partial^4 K}{\partial\mu^4} - 10K^{-1}\frac{\partial^2 K}{\partial\mu^2}K^{-1}\frac{\partial^3 K}{\partial\mu^3}\right. \\ & + 20K^{-1}\frac{\partial K}{\partial\mu}K^{-1}\frac{\partial K}{\partial\mu}K^{-1}\frac{\partial^3 K}{\partial\mu^3} + 30K^{-1}\frac{\partial K}{\partial\mu}K^{-1}\frac{\partial^2 K}{\partial\mu^2}K^{-1}\frac{\partial^2 K}{\partial\mu^2} \\ & - 60K^{-1}\frac{\partial K}{\partial\mu}K^{-1}\frac{\partial K}{\partial\mu}K^{-1}\frac{\partial K}{\partial\mu}K^{-1}\frac{\partial^2 K}{\partial\mu^2} \\ & + \left. 24K^{-1}\frac{\partial K}{\partial\mu}K^{-1}\frac{\partial K}{\partial\mu}K^{-1}\frac{\partial K}{\partial\mu}K^{-1}\frac{\partial K}{\partial\mu}K^{-1}\frac{\partial K}{\partial\mu}\right)\Big|_{\mu=0}, \end{aligned} \tag{A.3e}$$

$$\begin{aligned} L_6 = {} & \frac{N_f}{4}\mathrm{Tr}\left(K^{-1}\frac{\partial^6 K}{\partial\mu^6} - 6K^{-1}\frac{\partial K}{\partial\mu}K^{-1}\frac{\partial^5 K}{\partial\mu^5} - 15K^{-1}\frac{\partial^2 K}{\partial\mu^2}K^{-1}\frac{\partial^4 K}{\partial\mu^4}\right. \\ & - 10K^{-1}\frac{\partial^3 K}{\partial\mu^3}K^{-1}\frac{\partial^3 K}{\partial\mu^3} + 30K^{-1}\frac{\partial K}{\partial\mu}K^{-1}\frac{\partial K}{\partial\mu}K^{-1}\frac{\partial^4 K}{\partial\mu^4} \\ & + 60K^{-1}\frac{\partial K}{\partial\mu}K^{-1}\frac{\partial^2 K}{\partial\mu^2}K^{-1}\frac{\partial^3 K}{\partial\mu^3} + 60K^{-1}\frac{\partial^2 K}{\partial\mu^2}K^{-1}\frac{\partial K}{\partial\mu}K^{-1}\frac{\partial^3 K}{\partial\mu^3} \\ & + 30K^{-1}\frac{\partial^2 K}{\partial\mu^2}K^{-1}\frac{\partial^2 K}{\partial\mu^2}K^{-1}\frac{\partial^2 K}{\partial\mu^2} - 120K^{-1}\frac{\partial K}{\partial\mu}K^{-1}\frac{\partial K}{\partial\mu}K^{-1}\frac{\partial K}{\partial\mu} \\ & K^{-1}\frac{\partial^3 K}{\partial\mu^3} - 180K^{-1}\frac{\partial K}{\partial\mu}K^{-1}\frac{\partial K}{\partial\mu}K^{-1}\frac{\partial^2 K}{\partial\mu^2}K^{-1}\frac{\partial^2 K}{\partial\mu^2} - 90K^{-1}\frac{\partial K}{\partial\mu} \\ & K^{-1}\frac{\partial^2 K}{\partial\mu^2}K^{-1}\frac{\partial K}{\partial\mu}K^{-1}\frac{\partial^2 K}{\partial\mu^2} + 360K^{-1}\frac{\partial K}{\partial\mu}K^{-1}\frac{\partial K}{\partial\mu}K^{-1}\frac{\partial K}{\partial\mu} \\ & K^{-1}\frac{\partial K}{\partial\mu}K^{-1}\frac{\partial^2 K}{\partial\mu^2} - 120K^{-1}\frac{\partial K}{\partial\mu}K^{-1}\frac{\partial K}{\partial\mu}K^{-1}\frac{\partial K}{\partial\mu}K^{-1}\frac{\partial K}{\partial\mu} \\ & \left. K^{-1}\frac{\partial K}{\partial\mu}K^{-1}\frac{\partial K}{\partial\mu}\right)\Big|_{\mu=0}. \end{aligned} \tag{A.3f}$$

From

$$K^\dagger(\mu) \;=\; \gamma_5 K(-\mu)\gamma_5 \tag{A.4}$$

it follows that L_n is real for even and imaginary for odd n. Using $\Delta = e^{\ln \Delta}$ we find

$$\Delta(\mu) \;=\; \Delta(0)\left(1 + D_1\mu + D_2\mu^2 + \cdots + D_6\mu^6 + \mathcal{O}(\mu^7)\right) \;, \tag{A.5}$$

where

$$\begin{aligned}
D_0 &= 1 \;, && \text{(A.6a)}\\
D_1 &= L_1 \;, && \text{(A.6b)}\\
D_2 &= \frac{1}{2}\left(L_1^2 + L_2\right) \;, && \text{(A.6c)}\\
D_3 &= \frac{1}{6}\left(L_1^3 + 3L_1L_2 + L_3\right) \;, && \text{(A.6d)}\\
D_4 &= \frac{1}{24}\left(L_1^4 + 6L_1^2L_2 + 3L_2^2 + 4L_1L_3 + L_4\right) , && \text{(A.6e)}\\
D_5 &= \frac{1}{120}\left(L_1^5 + 10L_1^3L_2 + 15L_1L_2^2 + 10L_1^2L_3\right.\\
&+ \left. 10L_2L_3 + 5L_1L_4 + L_5\right) \;, && \text{(A.6f)}\\
D_6 &= \frac{1}{720}\left(L_1^6 + 15L_1^4L_2 + 45L_1^2L_2^2 + 15L_2^3 + 20L_1^3L_3 + 60L_1L_2L_3\right.\\
&\left. +10L_3^2 + 15L_1^2L_4 + 15L_2L_4 + 6L_1L_5 + L_6\right) \;. && \text{(A.6g)}
\end{aligned}$$

We immediately see that D_n is real for even and imaginary for odd n. Because

$$Z_\mu = Z_0 \cdot \left\langle 1 + D_1\mu + \cdots D_6\mu^6 \right\rangle + \mathcal{O}(\mu^7) \tag{A.7}$$

is real one has $\langle D_n \rangle = 0$ for odd n. We consider the case where the observable $\mathcal{O}$ is independent of μ. The expectation value (A.1) then becomes

$$\langle \mathcal{O} \rangle_\mu \;=\; \frac{\langle \mathcal{O} \rangle + \langle \mathcal{O} D_1 \rangle \, \mu + \cdots + \langle \mathcal{O} D_6 \rangle \, \mu^6}{1 + \langle D_2 \rangle \, \mu^2 + \cdots + \langle D_6 \rangle \, \mu^6} + \mathcal{O}(\mu^7) \;. \tag{A.8}$$

Expanding in powers of μ we get

$$\begin{aligned}
\langle \mathcal{O} \rangle_\mu \;=\; & \langle \mathcal{O} \rangle \left(1 + \mathcal{O}_1\mu + (-\mathcal{D}_2 + \mathcal{O}_2)\,\mu^2 + (-\mathcal{D}_2\mathcal{O}_1 + \mathcal{O}_3)\,\mu^3 + \left(\mathcal{D}_2^2 - \mathcal{D}_4\right.\right.\\
& \left. - \mathcal{D}_2\mathcal{O}_2 + \mathcal{O}_4\right)\mu^4 + \left(\mathcal{D}_2^2\mathcal{O}_1 - \mathcal{D}_4\mathcal{O}_1 - \mathcal{D}_2\mathcal{O}_3 + \mathcal{O}_5\right)\mu^5 + \left(-\mathcal{D}_2^3\right.\\
& \left.\left. +2\mathcal{D}_2\mathcal{D}_4 - \mathcal{D}_6 + \mathcal{D}_2^2\mathcal{O}_2 - \mathcal{D}_4\mathcal{O}_2 - \mathcal{D}_2\mathcal{O}_4 + \mathcal{O}_6\right)\mu^6\right) + \mathcal{O}(\mu^7)
\end{aligned} \tag{A.9}$$

where we use the notation

$$\begin{aligned}
\mathcal{O}_i &= \frac{\langle \mathcal{O} D_i \rangle}{\langle \mathcal{O} \rangle} \;, && \text{(A.10a)}\\
\mathcal{D}_i &= \langle D_i \rangle \;. && \text{(A.10b)}
\end{aligned}$$

In the case that $\mathcal{O}$ is strictly real on every configuration $\mathcal{O}D_n$ is imaginary for odd n. In order to keep $\langle\mathcal{O}\rangle_\mu$ real $\langle\mathcal{O}D_n\rangle$ has to vanish for odd n and the preceding expansion simplifies to

$$\begin{aligned}\langle\mathcal{O}\rangle_\mu &= \langle\mathcal{O}\rangle\left(1+(-\mathcal{D}_2+\mathcal{O}_2)\,\mu^2+\left(\mathcal{D}_2^2-\mathcal{D}_4-\mathcal{D}_2\mathcal{O}_2+\mathcal{O}_4\right)\mu^4\right.\\ &\quad+\left(-\mathcal{D}_2^3+2\mathcal{D}_2\mathcal{D}_4-\mathcal{D}_6+\mathcal{D}_2^2\mathcal{O}_2\right.\\ &\quad\left.\left.-\mathcal{D}_4\mathcal{O}_2-\mathcal{D}_2\mathcal{O}_4+\mathcal{O}_6\right)\mu^6\right)+\mathcal{O}(\mu^8)\,, \qquad (A.11)\end{aligned}$$

i.e. this formula is applicable to the correlation function in (4.20). Because free energies are calculated from logarithms of correlation functions we give here the expansion coefficients of the logarithm of an observable $\mathcal{O}$ which can be obtained by inserting the above expansion into the expansion of the logarithm. For a generic, not necessarily real observable the expansion is

$$\begin{aligned}\ln\langle\mathcal{O}\rangle_\mu &= \ln\langle\mathcal{O}\rangle+\mathcal{O}_1\mu+\left(-\mathcal{D}_2-\frac{1}{2}\mathcal{O}_1^2+\mathcal{O}_2\right)\mu^2+\left(\frac{1}{3}\mathcal{O}_1^3-\mathcal{O}_1\mathcal{O}_2+\right.\\ &\quad\left.\mathcal{O}_3\right)\mu^3+\left(\frac{1}{2}\mathcal{D}_2^2-\mathcal{D}_4-\frac{1}{4}\mathcal{O}_1^4+\mathcal{O}_1^2\mathcal{O}_2-\frac{1}{2}\mathcal{O}_2^2-\mathcal{O}_1\mathcal{O}_3\right.\\ &\quad\left.+\mathcal{O}_4\right)\mu^4+\left(\frac{1}{5}\mathcal{O}_1^5-\mathcal{O}_1^3\mathcal{O}_2+\mathcal{O}_1\mathcal{O}_2^2+\mathcal{O}_1^2\mathcal{O}_3-\mathcal{O}_2\mathcal{O}_3\right.\\ &\quad\left.-\mathcal{O}_1\mathcal{O}_4+\mathcal{O}_5\right)\mu^5+\left(-\frac{1}{3}\mathcal{D}_2^3+\mathcal{D}_2\mathcal{D}_4-\mathcal{D}_6-\frac{1}{6}\mathcal{O}_1^6+\mathcal{O}_1^4\mathcal{O}_2\right.\\ &\quad-\frac{3}{2}\mathcal{O}_1^2\mathcal{O}_2^2+\frac{1}{3}\mathcal{O}_2^3-\mathcal{O}_1^3\mathcal{O}_3+2\mathcal{O}_1\mathcal{O}_2\mathcal{O}_3-\frac{1}{2}\mathcal{O}_3^2+\mathcal{O}_1^2\mathcal{O}_4\\ &\quad\left.-\mathcal{O}_2\mathcal{O}_4-\mathcal{O}_1\mathcal{O}_5+\mathcal{O}_6\right)\mu^6+\mathcal{O}(\mu^7)\,. \qquad (A.12)\end{aligned}$$

For observables which are real on every configuration and have a real expectation value at every value of μ this reduces to

$$\begin{aligned}\ln\langle\mathcal{O}\rangle_\mu &= \ln\langle O\rangle+(-\mathcal{D}_2+\mathcal{O}_2)\,\mu^2+\left(\frac{1}{2}\mathcal{D}_2^2-\mathcal{D}_4-\frac{1}{2}\mathcal{O}_2^2+\mathcal{O}_4\right)\mu^4\\ &\quad+\left(-\frac{1}{3}\mathcal{D}_2^3+\mathcal{D}_2\mathcal{D}_4-\mathcal{D}_6+\frac{1}{3}\mathcal{O}_2^3-\mathcal{O}_2\mathcal{O}_4+\mathcal{O}_6\right)\mu^6+\mathcal{O}(\mu^8)\,. \qquad (A.13)\end{aligned}$$

Finally we can consider the case where $\mathcal{O}=\mathcal{O}(\mu)$ is depending on μ explicitly. Assuming that we have a Taylor expansion

$$\mathcal{O}(\mu)=O_0\left(1+O_1\mu+O_2\mu^2+\cdots\right), \qquad (A.14)$$

and inserting this into (A.8) we get

$$\begin{aligned}\langle\mathcal{O}\rangle_\mu &= \langle O_0\rangle\big(1+(\mathcal{O}_{01}+\mathcal{O}_{10})\,\mu+(-\mathcal{D}_2+\mathcal{O}_{02}+\mathcal{O}_{11}+\mathcal{O}_{20})\,\mu^2\\ &+(-\mathcal{D}_2\,(\mathcal{O}_{01}+\mathcal{O}_{10})+\mathcal{O}_{03}+\mathcal{O}_{12}+\mathcal{O}_{21}+\mathcal{O}_{30})\,\mu^3+\big(-\mathcal{D}_4+\mathcal{D}_2^2\\ &-\mathcal{D}_2\,(\mathcal{O}_{02}+\mathcal{O}_{11}+\mathcal{O}_{20})+\mathcal{O}_{04}+\mathcal{O}_{13}+\mathcal{O}_{22}+\mathcal{O}_{31}+\mathcal{O}_{40})\,\mu^4\\ &+\big(\big(\mathcal{D}_2^2-\mathcal{D}_4\big)\,(\mathcal{O}_{01}+\mathcal{O}_{10})-\mathcal{D}_2\,(\mathcal{O}_{03}+\mathcal{O}_{12}+\mathcal{O}_{21}+\mathcal{O}_{30})+\mathcal{O}_{05}\\ &+\mathcal{O}_{14}+\mathcal{O}_{23}+\mathcal{O}_{32}+\mathcal{O}_{41}+\mathcal{O}_{50})\,\mu^5+\big(-\mathcal{D}_2^3+2\mathcal{D}_2\mathcal{D}_4-\mathcal{D}_6\\ &+\big(\mathcal{D}_2^2-\mathcal{D}_4\big)\,(\mathcal{O}_{02}+\mathcal{O}_{11}+\mathcal{O}_{20})-\mathcal{D}_2\,(\mathcal{O}_{04}+\mathcal{O}_{13}+\mathcal{O}_{22}+\mathcal{O}_{31}\\ &+\mathcal{O}_{40})+\mathcal{O}_{06}+\mathcal{O}_{15}+\mathcal{O}_{24}+\mathcal{O}_{33}+\mathcal{O}_{42}+\mathcal{O}_{51}+\mathcal{O}_{60})\,\mu^6\\ &+\mathcal{O}(\mu^7)\big)\ , \end{aligned} \tag{A.15}$$

where

$$\mathcal{O}_{ij}=\frac{\langle O_i D_j\rangle}{\langle O_0\rangle} \tag{A.16}$$

If $\langle\mathcal{O}\rangle_\mu$ as well as all the coefficients O_i are real $\mathcal{O}_{ij}$ is vanishing for odd j and we are left with

$$\begin{aligned}\langle\mathcal{O}\rangle_\mu &= \langle O_0\rangle\big(1+\mathcal{O}_{10}\mu+(-\mathcal{D}_2+\mathcal{O}_{02}+\mathcal{O}_{20})\,\mu^2+(-\mathcal{D}_2\mathcal{O}_{10}+\mathcal{O}_{12}\\ &+\mathcal{O}_{30})\,\mu^3+\big(-\mathcal{D}_4+\mathcal{D}_2^2-\mathcal{D}_2\,(\mathcal{O}_{02}+\mathcal{O}_{20})+\mathcal{O}_{04}+\mathcal{O}_{22}+\mathcal{O}_{40}\big)\,\mu^4\\ &+\big(\big(\mathcal{D}_2^2-\mathcal{D}_4\big)\,\mathcal{O}_{10}-\mathcal{D}_2\,(\mathcal{O}_{12}+\mathcal{O}_{30})+\mathcal{O}_{14}+\mathcal{O}_{32}+\mathcal{O}_{50}\big)\,\mu^5\\ &+\big(-\mathcal{D}_2^3+2\mathcal{D}_2\mathcal{D}_4-\mathcal{D}_6+\big(\mathcal{D}_2^2-\mathcal{D}_4\big)\,(\mathcal{O}_{02}+\mathcal{O}_{20})-\mathcal{D}_2\,(\mathcal{O}_{04}\\ &+\mathcal{O}_{22}+\mathcal{O}_{40})+\mathcal{O}_{06}+\mathcal{O}_{24}+\mathcal{O}_{42}+\mathcal{O}_{60})\,\mu^6+\mathcal{O}(\mu^8)\big)\ . \end{aligned} \tag{A.17}$$

In chapter 5 we are faced with the special case that O_i is real for even and imaginary for odd i. Then $\mathcal{O}_{ij}$ is real if and only if both i and j are even or both are odd. In particular $\mathcal{O}_{ij}$ is imaginary if only i or only j is even and the other index is odd. If we demand now that $\langle\mathcal{O}\rangle_\mu$ is real for every value of μ the imaginary $\mathcal{O}_{ij}$ have to cancel in some way. Because the odd orders of $\langle\mathcal{O}\rangle_\mu$ in the expansion (A.15) are made up of imaginary $\mathcal{O}_{ij}$ only these orders must vanish. We are then left with

$$\begin{aligned}\langle\mathcal{O}\rangle_\mu &= \langle O_0\rangle\big(1+(-\mathcal{D}_2+\mathcal{O}_{02}+\mathcal{O}_{11}+\mathcal{O}_{20})\,\mu^2+\big(-\mathcal{D}_4+\mathcal{D}_2^2-\mathcal{D}_2\,(\mathcal{O}_{02}\\ &+\mathcal{O}_{11}+\mathcal{O}_{20})+\mathcal{O}_{04}+\mathcal{O}_{13}+\mathcal{O}_{22}+\mathcal{O}_{31}+\mathcal{O}_{40})\,\mu^4+\big(-\mathcal{D}_2^3\\ &+2\mathcal{D}_2\mathcal{D}_4-\mathcal{D}_6+\big(\mathcal{D}_2^2-\mathcal{D}_4\big)\,(\mathcal{O}_{02}+\mathcal{O}_{11}+\mathcal{O}_{20})-\mathcal{D}_2\,(\mathcal{O}_{04}+\mathcal{O}_{13}\\ &+\mathcal{O}_{22}+\mathcal{O}_{31}+\mathcal{O}_{40})+\mathcal{O}_{06}+\mathcal{O}_{15}+\mathcal{O}_{24}+\mathcal{O}_{33}+\mathcal{O}_{42}+\mathcal{O}_{51}\\ &+\mathcal{O}_{60})\,\mu^6+\mathcal{O}(\mu^8)\big)\ . \end{aligned} \tag{A.18}$$

Appendix B

Tabulated results

B.1 Screening mass coefficients

Table B.1: **Screening mass coefficients of the heavy $Q\bar{Q}$ pair in a singlet state:**

T/T_c	m_0^1/T	m_2^1/T	m_4^1/T	m_6^1/T
1.002	3.03(32)	1.846(77)	-1.28(22)	-0.38(59)
1.02	2.95(46)	1.710(53)	-0.50(19)	-1.70(71)
1.07	3.14(17)	1.034(53)	-0.57(18)	-0.09(48)
1.11	3.24(26)	0.529(21)	-0.32(5)	0.043(81)
1.16	3.39(28)	0.427(12)	-0.072(18)	-0.056(23)
1.23	3.16(26)	0.345(12)	-0.117(14)	-0.022(17)
1.35	3.08(24)	0.211(9)	-0.038(10)	-0.0052(71)
1.50	2.90(17)	0.157(7)	-0.0255(64)	-0.0013(66)
1.65	2.84(11)	0.122(5)	-0.0233(56)	0.0120(48)
1.81	2.85(19)	0.162(5)	0.0176(33)	0.0031(37)
1.98	2.57(7)	0.131(3)	-0.0006(34)	0.0042(24)
3.00	2.46(8)	0.098(3)	-0.0013(35)	-0.0025(15)
4.01	2.34(9)	0.071(2)	-0.0084(8)	-0.0012(3)

Table B.2: **Screening mass coefficients of the heavy $Q\bar{Q}$ pair in a color averaged state:**

T/T_c	$m_2^{\rm av}/T$	$m_4^{\rm av}/T$	$m_6^{\rm av}/T$
1.002	2.72(36)	-1.15(1.17)	0.44(3.39)
1.02	2.90(33)	-0.56(1.24)	-2.26(4.59)
1.07	1.91(44)	-1.04(1.56)	-0.22(4.26)
1.11	1.13(22)	-0.63(57)	-0.01(92)
1.16	1.02(11)	-0.21(19)	-0.07(24)
1.23	0.80(13)	-0.24(16)	-0.05(23)
1.35	0.46(13)	-0.02(14)	-0.00(11)
1.50	0.38(10)	-0.13(10)	-0.02(10)
1.65	0.25(11)	-0.07(12)	0.00(9)
1.81	0.32(8)	-0.01(5)	0.00(7)
1.98	0.28(7)	-0.01(5)	0.00(5)
3.00	0.23(7)	-0.02(9)	-0.00(4)
4.01	0.15(6)	-0.01(2)	-0.00(1)

Table B.3: **Screening mass coefficients of the heavy QQ pair in a anti-triplet state:**

T/T_c	m_1^3/T	m_2^3/T
1.002	-0.459(56)	1.78(32)
1.02	-0.354(63)	1.66(22)
1.07	-0.210(17)	1.20(11)
1.11	-0.170(12)	0.60(55)
1.16	-0.138(8)	0.48(38)
1.23	-0.133(10)	0.37(30)
1.35	-0.079(6)	0.23(25)
1.50	-0.062(4)	0.18(19)
1.65	-0.035(3)	0.13(14)
1.81	-0.040(4)	0.17(11)
1.98	-0.042(3)	0.15(14)
3.00	-0.002(2)	0.10(7)
4.01	-0.016(2)	0.08(6)

Table B.4: **0th order screening masses m_0/T of mesons:**

T/T_c	π	a_0	ρ_1	ρ_2	ρ_T	b_L	a_T
0.76	3.983(3)		6.248(55)	6.85(57)			
0.81	3.989(3)		6.163(44)	6.58(22)			
0.87	4.001(5)		6.101(52)	6.45(12)			
0.90	4.001(5)		5.970(59)	6.25(11)			8.37(56)
0.96	4.085(8)	5.38(90)	5.977(55)	6.17(10)			7.48(40)
1.002	4.199(11)	5.09(49)			5.986(37)	6.51(52)	7.26(21)
1.02	4.300(12)	5.34(41)			6.032(57)	7.22(75)	7.06(19)
1.07	4.562(16)	5.33(20)			6.181(53)	6.96(28)	6.78(15)
1.11	4.736(18)	5.37(16)			6.276(51)	6.99(30)	6.71(14)
1.16	4.906(22)	5.37(12)			6.359(60)	6.92(15)	6.681(65)
1.23	5.119(26)	5.48(13)			6.432(66)	6.84(27)	6.66(14)
1.35	5.301(20)	5.521(77)			6.401(62)	6.61(20)	6.559(97)
1.50	5.471(24)	5.58(28)			6.493(42)	6.76(12)	6.63(11)
1.65	5.590(27)	5.673(97)			6.475(61)	6.71(11)	6.565(86)
1.81	5.671(28)	5.72(14)			6.550(56)	6.76(14)	6.62(13)
1.98	5.765(32)	5.847(85)			6.516(65)	6.68(11)	6.55(11)
3.00	6.075(37)	6.32(42)			6.632(11)	6.67(10)	6.57(11)
4.01	6.243(40)	6.19(12)			6.692(61)	6.76(11)	6.70(10)

Table B.5: **2nd order screening masses m_2/T of mesons:**

T/T_c	π	ρ
0.76	0.013(13)	-0.11(13)
0.81	0.060(11)	0.238(90)
0.87	0.120(8)	0.28(13)
0.90	0.171(15)	0.203(76)
0.96	0.344(26)	0.505(89)
1.002	0.649(37)	0.727(78)
1.02	0.724(29)	0.773(79)
1.07	0.864(52)	1.098(47)
1.11	0.717(19)	0.948(30)
1.16	0.754(24)	1.646(67)
1.23	0.800(38)	1.738(90)
1.35	1.044(24)	2.037(64)
1.50	1.216(16)	2.389(44)
1.65	1.334(7)	2.517(45)
1.81	1.472(20)	2.70(10)
1.98	1.603(31)	2.853(80)
3.00	2.058(11)	3.409(28)
4.01	2.228(17)	3.726(19)

Table B.6: **2nd order screening masses m_2/T of mesons:**

T/T_c	π	ρ
0.76	0.013(13)	-0.11(13)
0.81	0.060(11)	0.238(90)
0.87	0.120(8)	0.28(13)
0.90	0.171(15)	0.203(76)
0.96	0.344(26)	0.505(89)
1.002	0.649(37)	0.727(78)
1.02	0.724(29)	0.773(79)
1.07	0.864(52)	1.098(47)
1.11	0.717(19)	0.948(30)
1.16	0.754(24)	1.646(67)
1.23	0.800(38)	1.738(90)
1.35	1.044(24)	2.037(64)
1.50	1.216(16)	2.389(44)
1.65	1.334(7)	2.517(45)
1.81	1.472(20)	2.70(10)
1.98	1.603(31)	2.853(80)
3.00	2.058(11)	3.409(28)
4.01	2.228(17)	3.726(19)

Table B.7: **0th order screening masses m_0/T of the nucleon:**

T/T_c	N
0.76	9.86(21)
0.81	9.70(15)
0.87	10.00(20)
0.90	9.49(20)
0.96	9.34(22)
1.002	9.28(15)
1.02	9.22(20)
1.07	9.29(15)
1.11	9.29(28)
1.16	9.29(26)
1.23	9.30(37)
1.35	9.45(22)
1.50	9.67(32)
1.65	9.59(25)
1.81	9.73(27)
1.98	9.49(31)
3.00	9.79(27)
4.01	9.95(25)

Bibliography

[1] **BRAHMS** Collaboration, I. Arsene *et al.*, "Quark gluon plasma and color glass condensate at rhic? the perspective from the brahms experiment", *Nucl. Phys.* **A757** (2005) 1–27, `nucl-ex/0410020`.

[2] B. Muller and J. L. Nagle, "Results from the relativistic heavy ion collider", `nucl-th/0602029`.

[3] U. W. Heinz and M. Jacob, "Evidence for a new state of matter: An assessment of the results from the cern lead beam programme", `nucl-th/0002042`.

[4] P. Braun-Munzinger, D. Magestro, K. Redlich, and J. Stachel, "Hadron production in au au collisions at rhic", *Phys. Lett.* **B518** (2001) 41–46, `hep-ph/0105229`.

[5] **PHENIX** Collaboration, K. Adcox *et al.*, "Formation of dense partonic matter in relativistic nucleus nucleus collisions at rhic: Experimental evaluation by the phenix collaboration", *Nucl. Phys.* **A757** (2005) 184–283, `nucl-ex/0410003`.

[6] **STAR** Collaboration, J. Adams *et al.*, "Experimental and theoretical challenges in the search for the quark gluon plasma: The star collaboration's critical assessment of the evidence from rhic collisions", *Nucl. Phys.* **A757** (2005) 102–183, `nucl-ex/0501009`.

[7] **MILC** Collaboration, C. Bernard *et al.*, "Qcd thermodynamics with three flavors of improved staggered quarks", *Phys. Rev.* **D71** (2005) 034504, `hep-lat/0405029`.

[8] V. G. Bornyakov *et al.*, "Critical temperature in qcd with two flavors of dynamical quarks", *PoS* **LAT2005** (2005) 157, `hep-lat/0509122`.

[9] M. Cheng *et al.*, "The transition temperature in qcd", `hep-lat/0608013`.

[10] C. R. Allton *et al.*, "Thermodynamics of two flavor qcd to sixth order in quark chemical potential", *Phys. Rev.* **D71** (2005) 054508, `hep-lat/0501030`.

[11] M. E. Peskin and D. V. Schroeder, *An introduction to quantum field theory*. Perseus Books, 1995.

[12] J. I. Kapusta, *Finite Temperature Field Theory*. Cambridge Univ. Press, 2000.

[13] M. Le Bellac, *Thermal Field Theory*. Cambridge Univ. Press, 1996.

[14] P. Hasenfratz and F. Karsch, "Chemical potential on the lattice", *Phys. Lett.* **B125** (1983) 308.

[15] J. B. Kogut and L. Susskind, "Hamiltonian formulation of wilson's lattice gauge theories", *Phys. Rev.* **D11** (1975) 395.

[16] I. Montvay and G. Munster, *Quantum fields on a lattice*. Cambridge University Press, 1997.

[17] H. J. Rothe. World Scientific Publishing, 2005.

[18] K. Symanzik, "Continuum limit and improved action in lattice theories. 1. principles and phi**4 theory", *Nucl. Phys.* **B226** (1983) 187.

[19] K. Symanzik, "Continuum limit and improved action in lattice theories. 2. o(n) nonlinear sigma model in perturbation theory", *Nucl. Phys.* **B226** (1983) 205.

[20] T. Blum *et al.*, "Improving flavor symmetry in the kogut-susskind hadron spectrum", *Phys. Rev.* **D55** (1997) 1133–1137, `hep-lat/9609036`.

[21] U. M. Heller, F. Karsch, and B. Sturm, "Improved staggered fermion actions for qcd thermodynamics", *Phys. Rev.* **D60** (1999) 114502, `hep-lat/9901010`.

[22] S. Naik, "On-shell improved lattice action for qcd with susskind fermions and asymptotic freedom scale", *Nucl. Phys.* **B316** (1989) 238.

[23] C. Schmidt, "The phase diagram and equation of state of improved lattice qcd for high temperatures and small chemical potentials", *PhD thesis*.

[24] S. A. Gottlieb, W. Liu, D. Toussaint, R. L. Renken, and R. L. Sugar, "Hybrid molecular dynamics algorithms for the numerical simulation of quantum chromodynamics", *Phys. Rev.* **D35** (1987) 2531–2542.

[25] **JLQCD** Collaboration, S. Aoki *et al.*, "An exact algorithm for any-flavor lattice qcd with kogut- susskind fermion", *Comput. Phys. Commun.* **155** (2003) 183–208, `hep-lat/0208058`.

[26] M. A. Clark and A. D. Kennedy, "The rhmc algorithm for 2 flavors of dynamical staggered fermions", *Nucl. Phys. Proc. Suppl.* **129** (2004) 850–852, `hep-lat/0309084`.

[27] C. R. Allton *et al.*, "The qcd thermal phase transition in the presence of a small chemical potential", *Phys. Rev.* **D66** (2002) 074507, `hep-lat/0204010`.

[28] C. Aubin *et al.*, "Light hadrons with improved staggered quarks: Approaching the continuum limit", *Phys. Rev.* **D70** (2004) 094505, `hep-lat/0402030`.

[29] C. W. Bernard *et al.*, "The qcd spectrum with three quark flavors", *Phys. Rev.* **D64** (2001) 054506, `hep-lat/0104002`.

[30] A. Gray *et al.*, "The upsilon spectrum and m(b) from full lattice qcd", *Phys. Rev.* **D72** (2005) 094507, `hep-lat/0507013`.

[31] O. Kaczmarek and F. Zantow, "Static quark anti-quark interactions in zero and finite temperature qcd. i: Heavy quark free energies, running coupling and quarkonium binding", *Phys. Rev.* **D71** (2005) 114510, `hep-lat/0503017`.

[32] C. R. Allton, "Lattice monte carlo data versus perturbation theory", `hep-lat/9610016`.

[33] F. Karsch, E. Laermann, and A. Peikert, "Quark mass and flavor dependence of the qcd phase transition", *Nucl. Phys.* **B605** (2001) 579–599, `hep-lat/0012023`.

[34] A. Peikert, "Qcd thermodynamics with 2+1 quark flavours in lattice simulations", *PhD thesis* (2000).

[35] Z. Fodor and S. D. Katz, "A new method to study lattice qcd at finite temperature and chemical potential", *Phys. Lett.* **B534** (2002) 87–92, `hep-lat/0104001`.

[36] M. G. Alford, A. Kapustin, and F. Wilczek, "Imaginary chemical potential and finite fermion density on the lattice", *Phys. Rev.* **D59** (1999) 054502, `hep-lat/9807039`.

[37] O. Philipsen, "The qcd phase diagram at zero and small baryon density", *PoS* **LAT2005** (2005) 016, `hep-lat/0510077`.

[38] S. Ejiri *et al.*, "Aspects of the thermal phase transition of qcd with small chemical potential", *Nucl. Phys. Proc. Suppl.* **106** (2002) 459–461, `hep-lat/0110080`.

[39] F. Karsch, E. Laermann, and A. Peikert, "The pressure in 2, 2+1 and 3 flavour qcd", *Phys. Lett.* **B478** (2000) 447–455, `hep-lat/0002003`.

[40] C. R. Allton *et al.*, "The equation of state for two flavor qcd at non-zero chemical potential", *Phys. Rev.* **D68** (2003) 014507, `hep-lat/0305007`.

[41] P. Braun-Munzinger, K. Redlich, and J. Stachel, "Particle production in heavy ion collisions", `nucl-th/0304013`.

[42] L. D. McLerran and B. Svetitsky, "Quark liberation at high temperature: A monte carlo study of su(2) gauge theory", *Phys. Rev.* **D24** (1981) 450.

[43] K. Hübner, "Freie energien schwerer quarks in su(3)-reiner eichtheorie", *Diploma thesis* (2003).

[44] S. Nadkarni, "Nonabelian debye screening. 2. the singlet potential", *Phys. Rev.* **D34** (1986) 3904.

[45] J. E. Mandula and M. Ogilvie, "Efficient gauge fixing via overrelaxation", *Phys. Lett.* **B248** (1990) 156–158.

[46] O. Kaczmarek, F. Karsch, P. Petreczky, and F. Zantow, "Heavy quark anti-quark free energy and the renormalized polyakov loop", *Phys. Lett.* **B543** (2002) 41–47, `hep-lat/0207002`.

[47] S. Necco and R. Sommer, "The n(f) = 0 heavy quark potential from short to intermediate distances", *Nucl. Phys.* **B622** (2002) 328–346, `hep-lat/0108008`.

[48] S. Nadkarni, "Nonabelian debye screening. 1. the color averaged potential", *Phys. Rev.* **D33** (1986) 3738.

[49] P. Arnold and L. G. Yaffe, "The nonabelian debye screening length beyond leading order", *Phys. Rev.* **D52** (1995) 7208–7219, `hep-ph/9508280`.

[50] E. Gava and R. Jengo, "Perturbative evaluation of the thermal wilson loop", *Phys. Lett.* **B105** (1981) 285.

[51] K. Hübner, "The polyakov loop and its correlators in higher representations of su(3) at finite temperature", *PhD thesis*.

[52] G. W. Kilcup and S. R. Sharpe, "A tool kit for staggered fermions", *Nucl. Phys.* **B283** (1987) 493.

[53] M. F. L. Golterman, "Staggered mesons", *Nucl. Phys.* **B273** (1986) 663.

[54] **MT(c)** Collaboration, R. Altmeyer *et al.*, "The hadron spectrum in qcd with dynamical staggered fermions", *Nucl. Phys.* **B389** (1993) 445–512.

[55] W. Press, B. Flannery, S. Teukolsky, and W. Vetterling, "Numerical recipes", *Cambridge Univ. Press* (1986).

[56] W. Florkowski and B. L. Friman, "Spatial dependence of the finite temperature meson correlation function", *Z. Phys.* **A347** (1994) 271–276.

[57] E. Laermann *priv. comm.* (2006).

[58] **QCD-TARO** Collaboration, I. Pushkina, "Lattice qcd with chemical potential: The properties of hadrons at the extreme conditions", *PoS* **LAT2005** (2006) 169.

[59] **MT(c)** Collaboration, K. D. Born *et al.*, "Hadronic correlation functions in the qcd plasma phase", *Phys. Rev. Lett.* **67** (1991) 302–305.

Acknowledgments

I thank my supervisor Prof. Dr. Frithjof Karsch for giving me the possibility to work on one of the most ambitious and inspiring research subjects in today's theoretical physics. His guidance and support were indispensable.
I thank Prof. Dr. Edwin Laermann for many very fruitful discussions and hints and for the professional attendance especially during the hadron correlation project.
I thank Dr. Olaf Kaczmarek and Dr. Shinji Ejiri for their help to introduce me into the physical and technical details of our physics, for their hard work on our projects and for their patience when answering most of my silly questions.
I thank Dipl. Phys. Kay Hübner for his contributions to the heavy quark project, for the good friendship over the last years and for the great time we had in Paris.
Furthermore I thank all the people from the theoretical particle physics group in Bielefeld for the good mood and companionship over the last years.
I thank the people from the theoretical physics group in Orsay especially Prof. Dr. Olivier Pène and Dr. Philippe Boucaud for their excellent hospitality and teaching me so much about our APE computers.
I thank the DFG for supporting this work by funding the graduate school GRK 881 "Quantum fields and strongly interacting matter".
Finally a special thanks goes to my mother Dr. Margareta Döring, my girlfriend Silvia and my friends for their mental support.

Matthias Döring
Bielefeld in October 2006